ADVANCED MASTERS IN STRUCTURAL ANALYSIS
OF MONUMENTS AND HISTORICAL CONSTRUCTIONS

Master's Thesis

Aleksandra Kosykh

Computational Modeling of the Arch Stone Bridge in Rabstejn, Czech Republic.

This Masters Course has been funded with support from the European Commission. This publication reflects the views only of the author, and the Commission cannot be held responsible for any use which may be made of the information contained therein.

Czech Republic | 2016

CZECH TECHNICAL UNIVERSITY IN PRAGUE
Faculty of Civil Engineering
Thákurova 7, 166 29 Prague 6, Czech Republic

MASTER'S THESIS PROPOSAL

study programme: Civil Engineering
study branch: Advanced Masters in Structural Analysis of Monuments and Historical Constructions
academic year: 2015/2016

Student's name and surname: Aleksandra Kosykh
Department: Department of Mechanics
Thesis supervisor: Petr Havlasek
Thesis title: Computational modeling of the arch stone bridge in Rabštejn, Czech Republic
Thesis title in English See above

Framework content: The stone arch bridge in Rabštejn is one of the oldest structures in the Czech Republic. It is still in use, and the goal of current thesis is to the evaluate load bearing capacity of the bridge in its current state. For this purpose simplified assessment methods and Finite Element Modeling using Atena software are employed.

Assignment date: 16/04/2016 Submission date: 03/07/2016

If the student fails to submit the Master's thesis on time, they are obliged to justify this fact in advance in writing, if this request (submitted through the Student Registrar) is granted by the Dean, the Dean will assign the student a substitute date for holding the final graduation examination (2 attempts for FGE remain). If this fact is not appropriately excused or if the request is not granted by the Dean, the Dean will assign the student a date for retaking the final graduation examination, FGE can be retaken only once. (Study and Examination Code, Art 22, Par 3, 4.)

The student takes notice of the obligation of working out the Master's thesis on their own, without any outside help, except for consultation. The list of references, other sources and names of consultants must be included in the Master's thesis.

Master's thesis supervisor

Head of department

Date of Master's thesis proposal take over: July 2016

Student

This form must be completed in 3 copies – 1x department, 1x student, 1x Student Registrar (sent by department)

DECLARATION

Name:	Aleksandra Kosykh
Email:	Alexa1990@list.ru
Title of the Msc Dissertation:	Computational modeling of the arch stone bridge in Rabstejn, Czech Republic
Supervisor(s):	Petr Havlasek
Year:	2016

I hereby declare that all information in this document has been obtained and presented in accordance with academic rules and ethical conduct. I also declare that, as required by these rules and conduct, I have fully cited and referenced all material and results that are not original to this work.

I hereby declare that the MSc Consortium responsible for the Advanced Masters in Structural Analysis of Monuments and Historical Constructions is allowed to store and make available electronically the present MSc Dissertation.

University:	Czech Technical University
Date:	21.07.2016
Signature:	

This page is left blank on purpose.

ACKNOWLEDGEMENTS

I would like to express my sincere gratitude to my supervisor, Petr Havlasek for sharing his knowledge, availability and enthusiasm. His guidance helped me in all the time of my research and writing of this thesis. Besides my supervisor, I would like to thank Dusan Drahos from Pudis a.s. for granting me technical and historical data on the Rabstejn bridge. This base data were indispensible for the development of my graduation work. Also, I offer my sincere appreciation to Jan Cervenka and Cervenka Consulting for providing me with ATENA software as also kind guidance and support.

I am particularly grateful to all the professors and lectures of the SAHC program for sharing their knowledge and experience. Very special thanks should be given to program coordinators, Paulo Lourenco and Petr Kabele. Completion of this course would not have been possible without their guidance and support.

I would also like to express my deepest gratitude to the SAHC consortium for their financial support, which made my participation in this program possible.

Finally, I wish to thank my family, fiancé, colleagues and friends for their continuous support, patience and encouragement.

This page is left blank on purpose.

ABSTRACT

The arch stone bridge in Rabstejn is one of the oldest structures of its kind in the Czech Republic. It was probably built in the 14th century, and it is still in use. Recent engineering survey has shown that, despite having moderate damages, the bridge is safe for use. Nevertheless, numerical modeling of the structure was required in order to evaluate its load bearing capacity.

In this work a numerical assessment of the load bearing capacity of the Rabstejn bridge was carried out using nonlinear Finite Element Analysis (FEA) as also two simplified techniques available in Czech building standards.

Adoption of the simplified approaches allowed for a straightforward evaluation of the bearing strength of the bridge, but the obtained results were too conservative in comparison with the FEA outcomes. The nonlinear FEA, on the other hand, provided more accurate and extensive data but required more time and effort. Six computational models were created in ATENA software; these models combined various approaches to simplify representation of masonry materials (homogenized macro level and two variants of micro level) and different continuum approaches (plane stress and plane strain).

Results obtained from the FEA indicate that the highest value of permissible load is reached for the micro-model tested in plane strain continuum state, whereas the lowest capacity is obtained in the simplified approach on a macro level. The results are summarized in the last sections of this work, where the pros and cons of each assessment method are discussed.

Keywords: historical constructions, masonry structures, arch stone bridges, finite element modeling, nonlinear analysis.

This page is left blank on purpose.

ABSTRAKT

Výpočetní modelování obloukového kamenného mostu v Rabštejně

Kamenný obloukový most v Rabštejně je jedna z nejstarších staveb svého druhu v České republice. Most byl pravděpodobně postaven ve 14. století a svou funkci plní i v současné době. Navzdory střednímu stupni poškození, který byl zjištěn při nedávném inženýrském průzkumu, zůstává most v bezpečném stavu pro užívání. Skutečnou únosnost mostu bylo nicméně potřeba podložit numerickým výpočtem.

V této práci bylo provedeno numerické posouzení únosnosti jednak nelineární metodou konečných prvků (MKP) a dále dvěma zjednodušenými postupy dle českých technických norem pro stavitelství.

Použití zjednodušených postupů umožnilo rychlé a přímočaré vyhodnocení únosnosti mostu, ale obdržené výsledky byly příliš konzervativní v porovnání s výsledky z MKP. Na druhou stranu za cenu vyšší pracnosti a výpočetního času poskytla MKP přesnější a rozsáhlejší informace. V programu ATENA bylo vytvořeno šest výpočetních modelů. Tyto modely kombinují různé zjednodušující přístupy pro modelování zdiva (homogenizovaný model na makroúrovni a dvě varianty na mikroúrovni) se dvěma přístupy pro popis kontinua ve 2D (rovinná napjatost a rovinná deformace).

Výsledky získané pomocí MKP naznačují, že nejvyšší hodnoty dovoleného zatížení je dosaženo při výpočtu s modelem na mikroúrovni za rovinné napjatosti, zatímco nejnižší únosnosti je dosaženo při použití homogenizovaného modelu na makroúrovni. Výsledky jsou shrnuty v poslední části této práce, kde jsou také probrány klady a zápory jednotlivých výpočetních přístupů.

Klíčová slova: historické stavby, zděné stavby, kamenné obloukové mosty, modelování metodou konečných prvků, nelineární analýza.

This page is left blank on purpose.

АБСТРАКТ

Компьютерное моделирование каменного арочного моста в Рабштейне

Арочный каменный мост в Рабштейне является одним из самых старых мостов в Чешской Республике. Вероятнее всего, он был построен в 14 веке и используется по назначению по сей день. Несмотря на некоторые повреждения, мост находится в рабочем техническом состоянии. Тем не менее, компьютерное моделирование конструкции необходимо для оценки ее грузоподъемности.

В данной работе оценка несущей способности моста в Рабштейне выполнена посредством нелинейного анализа по методу конечных элементов, а также с использованием упрощенных методов, приведенных в строительных нормативах Чешской Республики.

Применение упрощенных методов позволило быстро и просто оценить несущую способность конструкции, но результаты оказались заниженными по сравнению с данными конечно-элементного анализа. С другой стороны, нелинейный расчет по методу конечных элементов позволил более точно и подробно описать поведение конструкции, но потребовал больше времени и усилий. Для конечно-элементого анализа был использован программный комплекс ATENA, в котором были разработаны шесть вычислительных моделей, отличающихся методом моделирования материалов арки моста (макро- и микро-моделирование), а также упрощениями относительно напряженного состояния (плоское напряжение и плоская деформация).

Наибольшая несущая способность моста по результатам конечно-элементого анализа была получена для микро-модели, рассчитанной в условиях плоской деформации, в то время как наименьшая несущая способность была получена для макро-модели, проанализированной в состоянии плоского напряжения. Обзор этих результатов приведен в заключении данной работы, где проанализированы плюсы и минусы каждого метода оценки.

Ключевые слова: исторические конструкции, каменные конструкции, арочные мосты, метод конечных элементов, нелинейный анализ

This page is left blank on purpose.

TABLE OF CONTENTS

1. INTRODUCTION

Arch stone bridges are considered to be one of the most durable and stable historical structures. Built centuries ago with a great reserve in strength, many of them are still in use serving not only as foot but also as roadway bridges. Nevertheless, with the course of time these structures undergo structural changes related to material ageing, atmospheric, anthropogenic and temperature actions. In general, the most significant damages, which historical bridges accumulate, are related to service loads.

Due to considerable age and significant amount of damage historical bridges require comprehensive investigation on their current state. This implies historical and in-situ surveying as well as numerical evaluation required for safety verification and assessment of load bearing capacity. The most complex and responsible task among these procedures is numerical analysis. Based on the data obtained from historical records, surveying and experimental results, it can provide thorough understanding on the structural behavior of historical bridge, explain occurrence of existing damage and serve to propose the solutions for repairing and extending service life of the bridge. One more important goal of numerical analysis is the definition of permissible service load. For this purpose different techniques can be used.

First methods to verify the capacity of arch stone structures were developed centuries ago and were merely geometry based. Then in the middle of 20th century first approaches based on the usage of empirical and semi-empirical formulas were created. Finally, with the advent of computers, use of more complex methods employing theory of nonlinear structural analysis became a frequent practice. As opposed to simplified methods, these approaches provide with more extensive and accurate information but require deep knowledge on structural mechanics and building science in general. Additionally, for detailed and accurate modeling significant amount of input data is needed. Despite that, due to complexity and high costs of in-situ investigations as also undesirability of conducting destructive tests on historical structures, it is not always possible to get required information from surveying or archival records. For this reason analyst should derive data from different recommendations and experimental works. The amount of such sources is large, and searching for reasonable values can be challenging and time-consuming.

Even though all required information will be obtained, created model will never be able to reflect the reality totally. Albeit availability of different theories and approaches allowing for reliable characterization of existing structures, all processes occurring in these structures cannot be captured by numerical modeling. Doubtless, existing theories and methods account for the most significant for structural behavior aspects, but to reflect the reality combination of these methods is required.

2. OVERVIEW OF THE RABSTEJN BRIDGE

2.1 History

The road bridge analyzed in the current work is situated in the village of Rabstejn nad Strelou, which is located in the Western part of the Czech Republic. The village lies on a steep cape surrounded with the river of Strela passing from the southwest to the northeast. The bridge over the river bears the name of the village and is registered in the Czech Republic cultural heritage list.

Historical records reveal that the arch stone bridge was built in the 14th century and was an important trade highway connecting Prague with Rakovník, Zlutice, Bochov and Loket. Nowadays the bridge is still in use and is serving the Municipal road II/ 206.

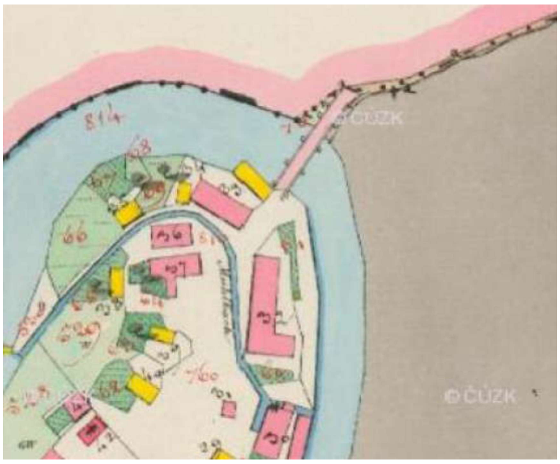

Figure 1: Bridge location. Map of 1839 (archivnimapy.cuzk.cz/, 2016)

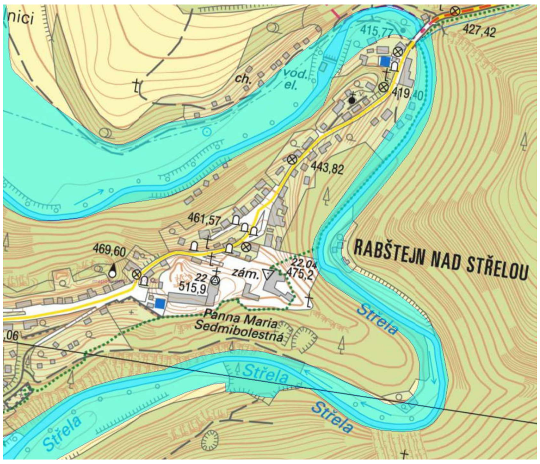

Figure 2: Bridge location. Up-to-date map (Pudis report, 2016)

During its lifetime Rabstejn bridge has suffered several repairs. Nevertheless, an overall appearance and structural configuration remained unchanged. According to archival data, remedial works took place in the years of 1872, 1966-1967 and 1991-1993. Repair works involved rebuilding of retaining walls, replacement of parapets and renewal of the roadway material.

Recently, in order to assess safety of the bridge and evaluate its bearing capacity, an engineering survey was carried out. Inspection works were performed by Pudis a.s. in December of 2014 and resulted in the new repair proposals. Executed works and obtained results are briefly described in the following section.

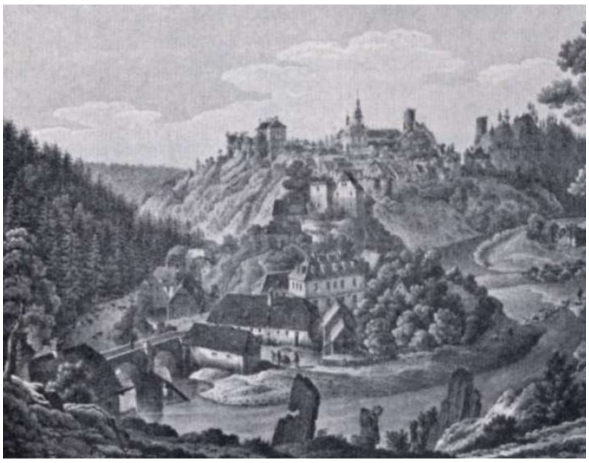

Figure 3: Rabstejn nad Strelou. Year of 1850 (Soupis pamatek historickych a umeleckych v Kralovstvi Ceskem, 1934)

Figure 4: Rabstejn bridge. Year of 1889 (Collection of Pavel Sukl)

2.2 Geometry and materials

According to undertaken investigations (Pudis a.s., 2014), the two-span arch masonry bridge has a span of 21 meters, and its roadway plane is inclined. The width of the bridge is 4.60 meters with a fall-width of the roadway between parapets equal to 3.80 meters. Parapets have a height of 0.90 meters with 0.40 meters width. They were constructed of arkosic blocks with granite top desks in the end of 20th century and are not original.

Figure 5: Rabstejn bridge. Recent photo (Pudis a.s., 2015)

Masonry arches have clear span of 8.40 meters and variable thickness, which is decreasing from 600 mm at the impost to 500 mm at the keystone. The rise is uniform for both arches and is equal to 4.30 meters. Arches and spandrel walls are constructed of irregular thin phyllite stones, which are linked together with thick lime mortar joints. According to the photographical documentation (Pudis a.s., 2015) stone-mortar thickness ratio can be evaluated as 3:1. In some portions of the arch phyllite stones, which have fallen, were substituted with brick.

Arches and spandrel walls are supported by the abutments on the ends and by the pier in the central part. Abutments are made of regular sandstone masonry faced with the arkosic blocks in the bottom part. They connect the bridge with earthen dams. Central pier has 3.90 meters width in the bridge plane direction and is propped in the river flow course with the tapered masonry addition protecting the bearing structure from the ice drift (see Figure 5).

An overall geometry of the bridge can be seen in the drawings prepared by Pudis a.s. (see Annex A).

2.3 Testing

In-situ and laboratory tests were carried out by Pudis a.s. and involved following procedures (Pudis a.s., 2015):

1. Visual inspection and photographic survey have shown that bridge has no significant damages posing a threat to its stability. Nevertheless, stone and mortar weathering, scaling and biological colonization were detected in some parts of the bridge. Accordingly, minor repairing procedures were recommended by Pudis a.s. The proposals included replacement of significantly damaged or lost stones, mortar repointing, removal of vegetation and facing renovation. Rebuilding of parapets using original materials, roadway replacement and drainage repair were also suggested.

Figure 6: Brick portions in phyllite masonry arch (Pudis a.s., 2015)

Figure 7:Weathering and plaster deterioration on the spandrel wall (Pudis a.s., 2015)

Figure 8:Weathering of pier materials (Pudis a.s., 2015)

Figure 9:Weathering and biological growth on the central pier (Pudis a.s., 2015)

2. Inspection of roadway composition. For that two pits (denoted as KS-1 and KS-2) with plan dimensions 0.40 x 0.40 meters were executed. The pits had the depth of 0.50 meters and were dug out till the arch extrados. From the test, the structure of the roadway was identified as shown in the Figure 10.

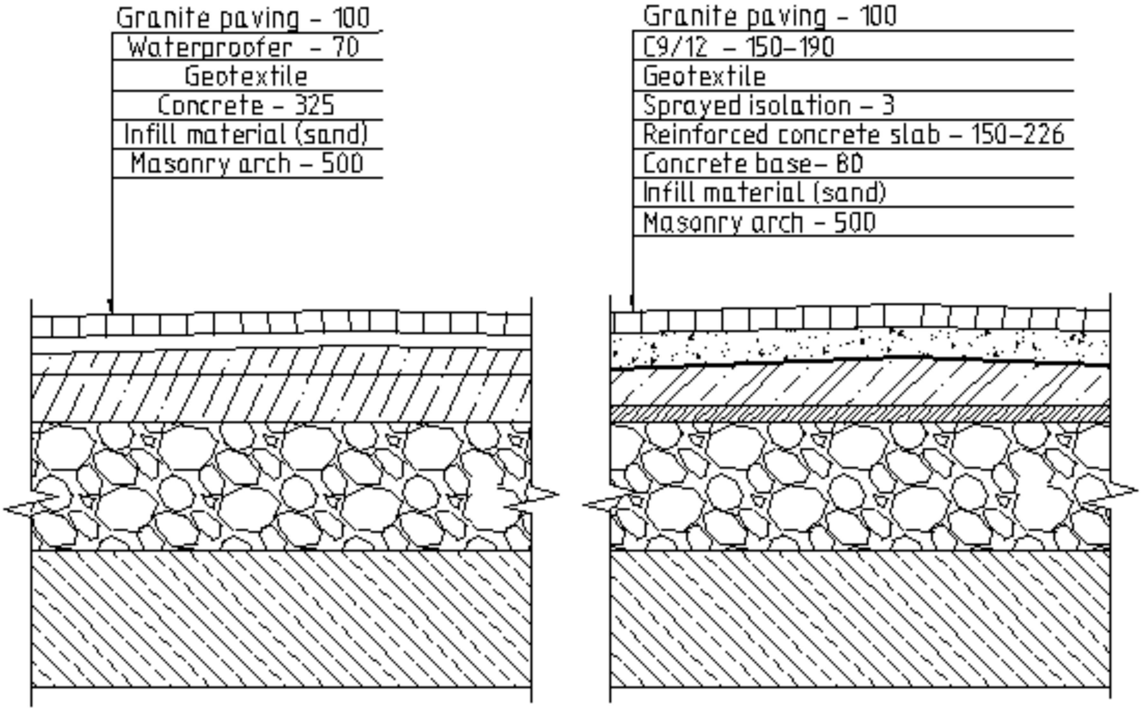

a. Existing roadway composition

b. Proposed roadway composition

Figure 10: Roadway composition of Rabstejn bridge

Relevant roadway structure is composed of thick concrete slab covered with waterproofing material and granite pavement. To ensure better load distribution from roadway to bridge components, new composition of pavement was proposed. It implies casting of reinforced concrete slab, laid upon the concrete base, as well as placing of sprayed isolation. In this wise, new pavement will not only improve structural behavior of the bridge but will also ensure better protection and durability of underneath bearing structures.

3. Inspection of infill material involved drilling of vertical boreholes from the bottom of pit KS-1. Holes with diameter of 80 mm and 3.5 m depth were performed in order to collect samples of infill material and test them in the laboratory conditions.

Figure 11: Roadway pit (Pudis a.s., 2015)

Figure 12: Drilling equipment (Pudis a.s., 2015)

Eventually, it was found that infill material features hard clay sand with material properties presented in the Table 1.

Table 1: Material properties of infill material

Material weight γ, [kN/m^3]	Young's modulus E, [Mpa]	Angle of internal friction φ, [^{o}]	Cohesion c, [kPa]
20.0	20	28	5

4. Inspection of foundations and soil conditions. For this purposes single pit KS-3 was implemented in the ground level. It had the depth of 1.50 meters with planar directions 0.60 ×0.60 m. On the basis of undertaken investigations, it was concluded that soil in the base represents weathered phyllite rock with sandstone bands. Basement structures were observed to be in good conditions, and the supporting ground could be considered as sufficient and rigid.

5. Assessment of composition of masonry piers was implemented by means of horizontal, vertical and diagonal drilling. Four holes with diameter of 20 mm and 1.40 m depth were executed in different directions as shown in the Figure 13.

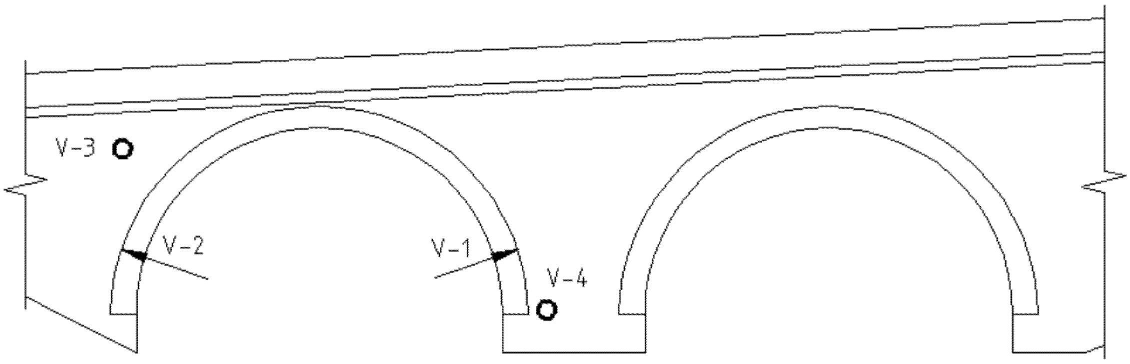

Figure 13: Drilling points and directions

Figure 14:Diagonal drilling in central pier (Pudis report, 2015)

Figure 15:Hole resulted from sampling (Pudis report, 2015)

This test allowed determining thickness of masonry layers and material strength as functions of drilling depth. According to results of drilling in the directions V-1, V-2 and V4, thickness of phyllite masonry was found to be equal to 1 meter. On the basis of that, conclusion on the existence of phyllite haunch in the central support was made. For the sake of simplicity it was assumed to have planar surface as it is shown in the Figure 16. Based on the outcomes of the V-3 test, thickness of spandrel walls was determined to be equal to 0.3 m.

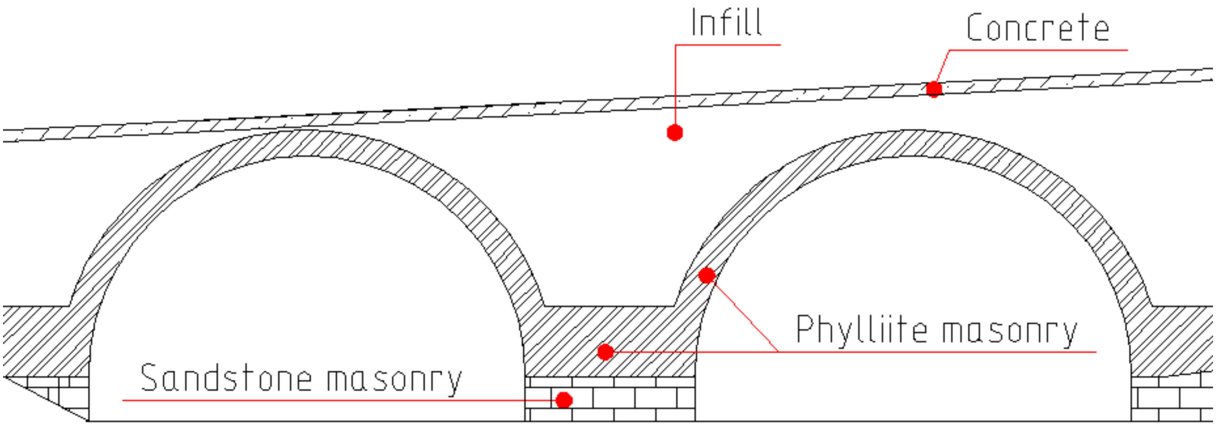

Figure 16: Material composition of the bridge

6. Destructive laboratory tests on masonry units collected from the site served to define mechanical properties of masonry. Despite the availability of stone samples from the bridge, only few tests were of carried out. They allowed defining uniaxial compressive strength of phyllite composing arch vault and spandrel walls to be about 40 MPa with a Poisson's ratio equal to 0.34. Uniaxial compressive strength of sandstone was determined to be up to 80 MPa.

Figure 17:Drilling and sampling equipment (Pudis report, 2015)

Figure 18:Samples collected from the site (Pudis report, 2015)

7. Evaluation of mortar in compression. Compressive strength of mortar was defined as a function of drilling depth obtained during in-situ destructive tests. It was determined to be in the range between 0.40 and 1 MPa.

3. METHODS TO ASSESS ARCH STONE BRIDGES

Practical experience shows that arch stone bridges have considerable reserve in strength and are capable to accumulate significant amount of damage prior to failure. Therefore, for safety assessment of old masonry bridges, evaluation of ultimate limit state (ULS) capacity is not sufficient; not only the load corresponding to the transition of the damaged structure into mechanism should be identified, but also the load level, at which the first damage occurs. This turns out to be challenging due to the large number of bridge topologies and possible failure mechanisms.

The necessity to employ universal methods for the load rating of existing bridges resulted in development of simplified experience-based techniques. They were indispensible in a pre-computer era. These methods addressed different approaches. The best known are middle-third rule, lower and upper bound plastic theorems (Heyman, 1982, Kooharian, 1952) as also different empirical and semi-empirical methods such as MEXE and modified MEXE (Department of Transport, 2001). Most of these methods are geometry-based two-dimensional methods and do not take into account material properties and their variation throughout loading process. These are big simplifications, but they allow for fast evaluation of load bearing capacity with minimal expenses in terms of time and costs. Additionally, assessment procedure does not require strong analytical skills, whereas safety of the structure is ensured due to conservative nature of the approach.

Most of existing simplified methods are derived for specific bridge typology, for example, for structures situated within one country and built within particular time span. In this case, examined bridges can be characterized by identical or similar geometries, materials, construction techniques and even damage patterns. Accordingly, application of these empirical methods is often limited by certain conditions. One more challenge is that most of simplified methods are based on the definition of the Ultimate Load State (ULS) load, and the load for Serviceability Limit State (SLS) is derived as its fraction. Definition of the reduction factor turns out to be complex and subjective. There is no uniform value for this parameter, and it varies in different countries and from method to method. For example, British standard (Department of transport, 2001) recommend the reduction factor for the derivation of service load equal to 3.4, whereas combined factor derived from Eurocode 1(European committee for standardisation, 2002) is equal to 2.17 (Rericha P., Posch M. , 2012). It is evident that results obtained in different methods can vary significantly. Nevertheless, relatively high value of reduction factor is introduced in all techniques, which lead to conservative results in terms of bearing capacity.

Drawbacks related with application of simplified assessment techniques gave rise to the development of more accurate computer-based analysis methods allowing for more thorough investigation of arch stone bridges. The most advanced assessment method is nonlinear finite element modeling (FEM). It enables to evaluate masonry bridges at both ultimate and service limit states as well as to investigate damage formation and propagation. Two-dimensional and three-dimensional modeling can be implemented allowing considering an interaction between structural elements of the bridge as also introducing of different material models and continuum states. Doubtless, nonlinear FE modeling takes precedence over simplified techniques, because more comprehensive and accurate data can be obtained. Nevertheless, this advanced method requires involvement of highly qualified analysts, large computational efforts, time and money expenditures. For this reason, decision on the use of nonlinear FEA use should be based on the significance of the structure, goals of assessment, availability of funds and timing.

Among all existing approaches available for the assessment of arch stone bridges, methods discussed in Czech Standard TP 199 (MD ČR, 2008) were employed in the current work. This code was developed for the population of arch stone bridges situated in Czech Republic, and is applicable for 95% of bridges situated in the Czech Republic (Rericha P., Posch M. , 2012).

Standard TP 199 suggests three approaches: two simplified methods and nonlinear finite-element modeling. Description of these methods is given in the following sections.

4. SIMPLIFIED ASSESMENT TECHNIQUES

As it is mentioned above, standard TP 199 (MD ČR, 2008) drafts two simplified methods: direst semi-empiric formula and elaborate simplified numerical analysis. Their use is hierarchical, and primarily the direct formula is to be used. If this seems to be insufficient, numerical analysis is adopted.

4.1 Assumptions on materials and geometry

Target formulas derived for both methods are geometry based and do not depend on material properties. This assumption seems to be an oversimplification. Nevertheless, this idea is not new, and material independent approach can be employed providing certain level of conservatism as consistent with works of Hogg V., 1997 and Cavicchi A., Gambarotta L., 2005.

Next simplification adopted in proposed methods is that they serve only for the assessment of the arch and do not take into account its interaction with abutments, spandrels and piers as well as their failure. In this wise, for the evaluation of the bridge two-dimensional model is used. It includes arch, infill and roadway material (see Figure 19). Spandrel walls represent the same plane as infill material and are not considered. This seems to be serious omission, but several works, for example, Page J., 1993, recommend neglecting interaction between arch barrel and spandrel walls to evaluate ultimate capacity of the arch. This is reasonable, because spandrel walls make positive impact on the bearing capacity of the bridge. They stiffen the structure and retain infill material. In this wise, elimination of spandrel walls can be employed, because it provides underestimation of the maximum load, which can be carried by the arch. Nevertheless, capability of spandrel walls should be checked, because it might be insufficient to take forces corresponding to the ultimate load defined for the arch barrel. This is additional task and is not addressed in the current methods.

Simplified methods discussed in TP 199 are based on the usage of empirical and semi-empirical formulas. These formulas are calibrated with outputs of numerical modeling and can be implicitly used for the evaluation of arch stone bridges situated in the Czech Republic.

Figure 19 shows two-dimensional model employed in simplified methods. Geometrical characteristics of the bridge used as input parameters for target formulas can be defined as follows:

- l – barrel span;
- h – barrel rise;
- d - barrel thickness;
- s – Infill thickness above the barrel crown.

Parameters referring to the transverse cross section are set ex post and are as follows:

- w – overall width of the bridge;
- w_1 - loading width.

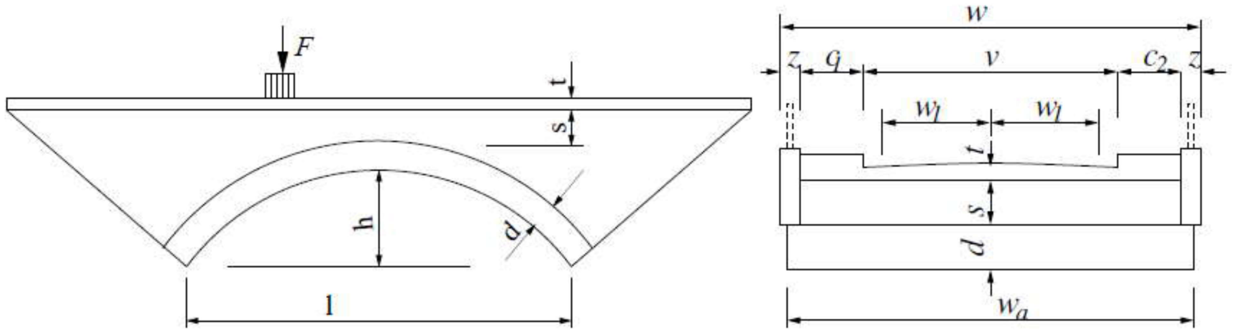

Figure 19: Longitudinal and transverse bridge sections (MD ČR, 2008)

4.2 Load pattern

Roadway bridges are subjected to the variety of actions posing a load to the structure. Considering all of them at the same time is not suitable for simplified assessment. For this reason, TP 199 introduces simplified load pattern, in which only dead load and produced by the moving passage live load are taken into account.

Despite the fact that the load influencing the capacity of the bridge foremost is induced by the moving vehicle, relevant building standard recommends using static axle load. The truck is considered to have two axles, and live load is set up to be transferred only through the rear axle (see Figure 20).

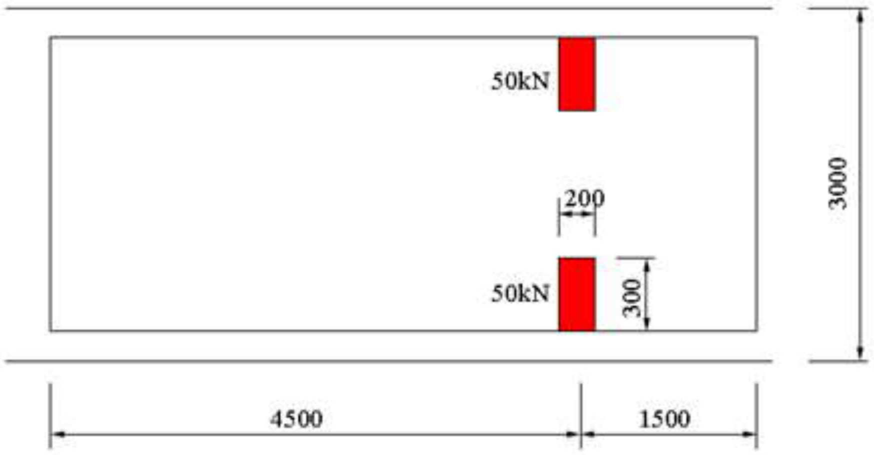

Figure 20: The model of a truck (MD ČR, 2008)

Since the code suggests using 2D model, axle load should be imposed in the point. Accordingly, load from the vehicle distributed along the wheel is set up as a pin load at the quarter span of the bridge (see Figure 19). This live load should be applied to the structure in a stepwise fashion and should be gradually increased from step to step by multiplying factor f_0.

In this wise, load imposed to the bridge can be expressed as a function of self-weight of the bridge Q_g and live load increment Q_n:

$$Q = Q_g + Q_n \cdot f_0 \tag{1}$$

This load pattern does not include any dynamic or moving loads, but, even so, provides conservative results. This is mainly due to the application of live load in the point corresponding to the most unfavorable position or occurrence of highest bending moments within arch barrel.

4.3 Simplified numerical analysis

Simplified numerical analysis is the second method employed by the code and is more sophisticated than the approach using direct formula. The latter is to be primarily used, but, indeed, direct formulation is obtained by idealizing of more general simplified numerical approach. Accordingly, to explain the idea of both methods, simplified numerical analysis is primarily discussed.

First of all, applicability of the method should be checked. For that geometrical parameters of the bridge must be consistent with the following relations:

$$\begin{gathered} 2 < l < 12 \quad [m] \\ 0.07 < d / l < 0.20 \\ 0.15 < h / l < 0.5 \\ 0.08 < s / l < 0.45 \end{gathered} \tag{2}$$

If these conditions are satisfied, simplified numerical analysis can be employed. Brief description of the technique is given below.

It is experimentally proven, that the majority of arch stone masonry bridges are put out of service, when significant damage is accumulated within the arch barrel. This is normally related with the deterioration of mortar and formation of the sufficient number of hinges required to turn the arch structure into the mechanism. The most probable collapse mode in the case, when the load is applied at the quarter span of the arch, is the four hinge mechanism, as it is shown in the Figure 21.

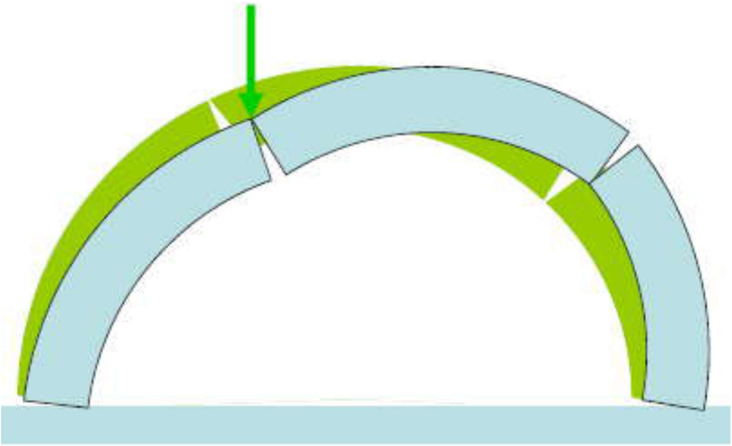

Figure 21: Collapse mechanism of the arch loaded at a quarter span (Roca P., 2007)

The state corresponding to the excessive deterioration of mortar joints can be described by neither ultimate nor service limit states. Accordingly, additional limit state should be introduced. This hypothesis is adopted in the work of Rericha and Posch, 2012. Following their idea, bridge is subjected to the repetitive loading induced by the vehicle passing across the bridge. When the truck moves along the longitudinal section of the bridge, intrados and extrados of the arch are subjected to the reverse tensile and compressive stresses. This action is combined with atmospheric agents and other (chemical, anthropogenic etc) impacts. Under these conditions damage is mainly accumulated in the weak joints, and cracks can open and close. For this reason the new limit state is described in terms of so called relative crack width c_0, which represents the ratio between width of the crack and thickness of the barrel. The limit of this value $c_{0,\lim}$ corresponds to the so called Repeated Load Limit State (RLLS). Accordingly, the criterion adopted for evaluation of RLLS can be written as follows:

$$c_0 < c_{0,\lim} \tag{3}$$

Formula for defining $c_{0,\lim}$ is obtained experimentally depending on the number of loading cycles and is not addressed in the current work. It is also known that formation of hinge is linked to the value of thrust eccentricity within the arch. In this wise, relative thrust eccentricity e, which can be obtained from the linear elastic analysis, can be correlated with the relative crack depth c_0 representing the criterion for RLLS. Accordingly, it is assumed that relation (3) is valid as long as:

$$e < e_{\lim} \tag{4}$$

In this relation $e_{\lim}$ represents ultimate value of relative eccentricity, which can be defined as follows:

$$e_{\lim} = 0.338 + 0.216 \cdot d + 0.0734 \cdot h - 0.0235 \cdot l - 0.00142 \cdot l^2 + 0.00953 \cdot s \tag{5}$$

In this wise, criterion for RLLS load can be established using formula (3). For the assessment, numerical two-dimensional model is used. Structure is loaded with the self-weight and live load, as consistent with section 4.2. Axle live load is gradually increased in each step by means of multiplying factor f_0, Value of eccentricity can be obtained in each step as an absolute value of the ratio between bending moment and axial force acting within arch elements. Divided by the thickness of the barrel, these values represent relative eccentricities e. The maximum value of e along the barrel should be compared with the ultimate value $e_{\lim}$. If the limit value $e_{\lim}$ is reached, corresponding value of axle load represents RLLS load F^{RLLS} . It can be attributed to the Serviceability Limit State (SLS). Therefore, partial safety factor can be taken as 1.

Additionally, ULS load should be evaluated. For that, direct formula and expedient safety factor γ are introduced. In the current code the value of safety factor is set up as 3.4, as consistent with British standard (Department of transport, 2001). This coefficient is introduced into the target formula, and no additional reduction of the load is required.

$$F^{ULS} = w_{1,eff} \cdot (0.177 + 0.207 \cdot d + 0.0074 \cdot h - 0.0237 \cdot l + 0.000117 \cdot l^2 + \\ + 0.0807 \cdot s) \quad [MN] \tag{6}$$

Here $w_{1,eff}$ is effective width of the roadway, which can be defined according to CSN 73 6220 (Český normalizační institut, 1996). For the bridge with one traffic lane across the width it can be set up as:

$$w_{1,eff} = w_1 = 3 \text{ [m]} \tag{7}$$

Eventually, admissible for the bridge axial load is defined as the minimum value between RLLS and ULS load values.

$$F_a = \min(F^{ULS}, F^{RLLS}) \tag{8}$$

4.4 Direct formula

Direct formula represents simplification of the numerical approach discussed in the previous section. The difference with respect to simplified numerical analysis is that for each step permissible service load is defined as a function, and use of numerical model is not required. Approximating formula for the load per unit width of the bridge can be expressed as:

$$F_{cap} = 0.283 + 0.180 \cdot d - 0.0108 \cdot h - 0.102 \cdot l + 0.00868 \cdot l^2 + 0.0456 \cdot s \\ [MN/m] \tag{9}$$

Consequently, admissible axial load can be defined as follows:

$$F_a = w_{1,eff} \cdot F_{cap} \quad [MN] \tag{10}$$

Applicability of direct approach is restricted by conditions (2), but length of the arch span is limited by stricter relation:

$$2 < l < 8 \ [m] \tag{11}$$

4.5 Definition of the load bearing capacity

Once the axial load for service conditions F_a is defined according to direct or simplified numerical analysis, bearing capacity of the bridge can be evaluated in compliance with CSN 73 62226220 (Český normalizační institut, 1996). For the bridge with clear arch span more than 8 m but less than 12 m, capacity for normal service conditions can be expressed as follows:

$$V_n = \frac{4 \cdot F_a [KN]}{3 \cdot g \cdot \delta} \quad [t] \tag{12}$$

Here g is gravity acceleration in m/sec2 and δ is dynamic coefficient, which is determined with respect to the number of lanes. For one traffic lane across the bridge width δ is equal to 1.4.

5. RESULTS OF SIMPLIFIED ASSESSMENT

5.1 Direct formula

As consistent with requirements of TP 199(MD CR, 2008), first, bearing capacity of the bridge was assessed using direct formula. Prior to that, geometrical ratios of both arches were compared with ultimate values set up by the code. Controlled parameters were computed for left and right arches. They are presented in the Table 2 together with the limit values. Since thickness of the arch barrel is not uniform, an average value of 0.55 meters was used for calculations.

Table 2: Geometrical parameters of arches

Parameter	$d,[m]$	$l,[m]$	$h,[m]$	$s,[m]$	h/l	d/l	s/l
Lower limit	-	-	-	-	0.15	0.07	0.08
Right arch	0.55	8.45	4.30	0.68	0.51	0.07	0.08
Left arch	0.55	8.45	4.30	0.08	0.51	0.07	0.01
Upper limit	-	-	-	-	0.50	0.20	0.45

It can be seen from the table that direct formula can hardly be used for the left arch, mainly due to a very small infill thickness above the crown. For the right arch controlled ratios are within established limits, but clear span of the arch exceeds the boundary. Taking into account that method is proved to be applicable for 95% of bridges in the Czech Republic, this minor discrepancy can be neglected.

In this wise, direct formula can be used for the right arch, but for the left arch this approach can provide inaccurate results. Nevertheless, direct method was already employed under the scope of previous investigations. For this reason and for the sake of comparison with results of numerical modeling, calculations were implemented for both left and right arches. Results are presented in the Table 3.

Table 3: Results obtained from direct method

	$F_{cap},[MN]$	$w_{1,eff},[MN]$	$F_a,[MN]$	$V_n,[t]$
Left arch	0.097	3.00	0.291	27.70
Right arch	0.124	3.00	0.373	35.60

From the table, it can be concluded that capacity of the bridge obtained from direct formula is equal to 27.7 tons. This value represents bearing capacity of the left arch. This result is not supposed to be accurate, and for more precise evaluation simplified numerical analysis is employed.

5.2 Simplified numerical analysis

Simplified numerical analysis is the second step in the evaluation of arch stone masonry bridges as consistent with the standard TP 199. This method combines adoption of semi-empirical formulas as well as testing of numerical model. The 2D structural model was created and examined in ATENA software (see section 6.3).

5.2.1 Modeling of geometry in FE model

Creation of simplified numerical model implies adopting of several assumptions regarding geometry, materials and interaction of structural components. This is required due to the lack of information on the structural arrangement of the bridge, its history and material properties. Additionally, in-depth modeling, taking into account all details, can provide erroneous results. In this wise, adopted model should be simplified with respect to available data so that it reflects reality and is consistent with analysis goals.

As consistent with requirements of TP 199, two-dimensional model was created. Longitudinal section of the bridge was modeled, implying that transverse capacity is ensured. Thickness of the structure was set up as input parameter, and section with one meter width was analyzed. Accordingly, outputs of numerical analysis represent average values along one meter width of the transverse cross-section.

Given that out of plane capacity of the bridge was considered to be sufficient, such structural components as pillars and ice-drift protecting addition were not modeled. Also, parapets were not created, since the one meter width was assigned to the longitudinal section.

In this wise, simplified numerical model involves arch barrels, piers, infill, roadway and base. The last is considered to be fully fixed in horizontal and vertical directions. This represents rigid connection to the bridge substructure lying on the low-compressible rock soils, as consistent with surveying results. It is also distilled from the survey report (Pudis a.s., 2016) that arches composing the bridge have uniform geometry. Nevertheless, the bridge is not symmetrical with respect to the centerline, due to the inclined roadway plane resulting in differential thickness of infill along the structure. The height of the cover above the arch extrados is increasing from the left arch side to the right one and is the lowest above the crown of the left arch (see Figure 22).

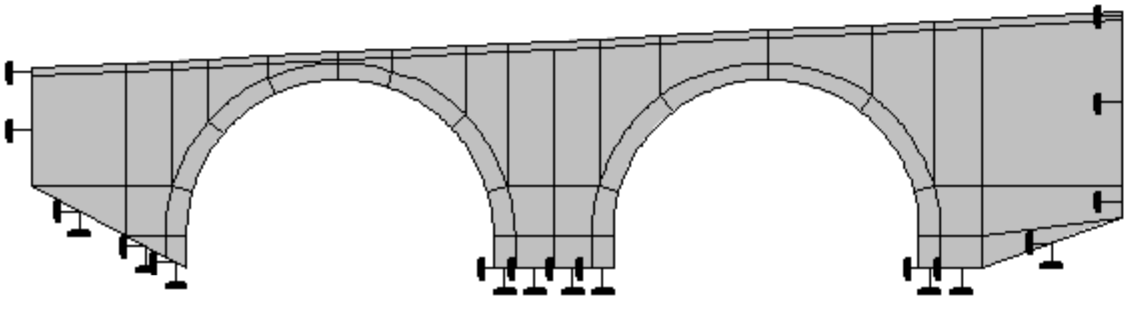

Figure 22: Geometrical model of the bridge

5.2.2 Modeling of materials

As consistent with code requirements, materials were modeled as linear elastic. In this case Young's modulus, Poisson's ratio and material weight serve as input parameters. They were defined for each structural component of the bridge (see Table 4). It is of importance, that experimental data on required parameters was only available for the infill material. In other cases modeling constants were defined mathematically, as will be discussed in the section 7.3.1.

Table 4: Input parameters for linear-elastic model

Parameter	Arch barrel and piers	Sandstone base	Infill	Roadway
Young's Modulus E, [Mpa]	3170	2218	20	17000
Poisson's ratio υ	0.20	0.20	0.30	0.20
Material weight γ, [kN/m^3]	24.00	23.20	20.00	23.50

5.2.3 Modeling of loads

Following the idea of standard TP 199, self-weight and live load were applied to the bridge. The dead load of a modeled structure was applied automatically, and one more simplification was done with respect to the weight of multilayered roadway cover. Sandwich type structure lying above the concrete base was substituted with uniformly distributed load. This allowed avoiding definition of roadway materials and decreased computational efforts without any negative impact to the accuracy of modeling. Accordingly, materials above concrete base were substituted with uniformly distributed load defined across one meter width of the bridge. The resulting load drew up the value of 5.7 kN/m, as it is shown in the Table 5.

Table 5:Self-weight of the roadway cover materials

Layer	Weight, [kN/m^3]	Thickness, [m]	Width, [m]	Load, [kN/m]
Granite	25.0	0.10	1.0	2.5
Hydroisolation	16.0	0.07	1.0	1.1
Concrete	23.0	0.09	1.0	2.1
			Sum	5.7

In this wise, the self-weight of roadway materials was applied as it is shown in the Figure 23. The resultant dead load was imposed to the structure in a stepwise fashion prior to live load application.

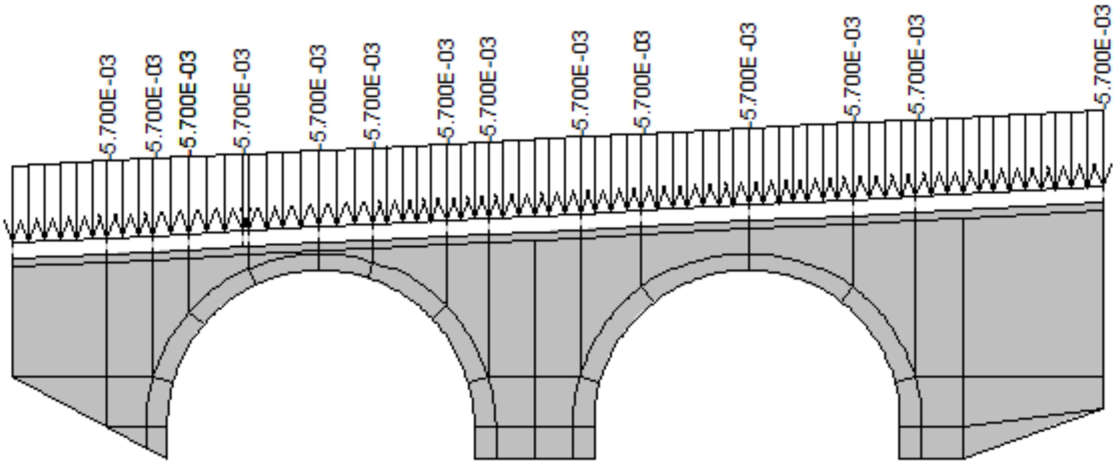

Figure 23: Application of roadway cover self-weight

Next, as discussed in section 4.2, live load was applied as a pin load at the quarter span of the arch. In this wise, live load increment, equal to 10 KN, was imposed in the above mentioned position and was gradually increased in each step by means of multiplying factor f_0.

5.2.4 Analysis procedure

Under the scope of current analysis both, left and right, arches were evaluated. For that, two numerical analyses were run. First, point live load was applied at the quarter span of the left arch, remaining the right arch unloaded. After application of the dead load pin load was imposed at the left quarter span of the arch. In order to control forces within the arch, moment line was introduced in the centerline of the barrel, as shown in the Figure 24.

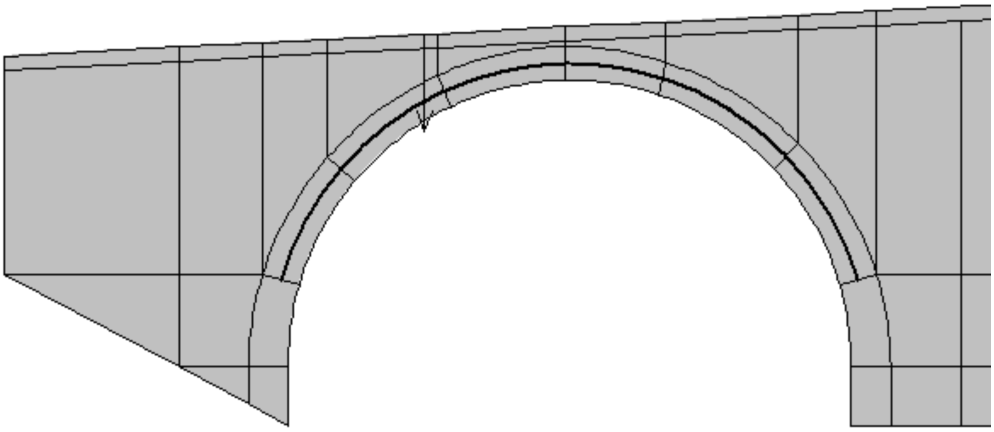

Figure 24: Live load and moment line for the left arch

Values of bending moment and axial force were read for each step, and relative with respect to the barrel width eccentricity was defined. For that, values of bending moment M_i and axial force N_i

within i element of moment line were read. After that maximum within the step eccentricity was defined as follows:

$$e = \frac{\max\left[M_i / N_i\right]}{d} \tag{13}$$

If this value was lower than ultimate relative eccentricity $e_{\lim}$ given by formula (5), live load was increased, and new value of maximum relative eccentricity within arch barrel was defined. Once the limit was reached, corresponding value of live load was set up as Repeated Load Limit State (RLLS) force. To account for the thickness of the bridge, this load was multiplied by the effective width of the roadway $w_{1,eff}$.

Eventually, value of RLLS load was compared with Ultimate Limit State (ULS) load derived from empirical formula (6). Minimum of these two values was set up as allowable axial load F_a . Results of calculations are presented in Table 6.

Table 6: Results of simplified numerical analysis

	$e_{\lim}$	$F^{ULS}, [MN]$	$F^{RLLS}, [MN]$	$F_a, [MN]$	$V_n, [t]$
Left arch	0.40	0.404	1.590	0.404	38.5
Right arch	0.41	0.549	1.566	0.549	52.3

Analogically, in the second analysis pin load was imposed at the left quarter span of the right arch, and analysis procedure was implemented in the same fashion (see Figure 25 and Table 6).

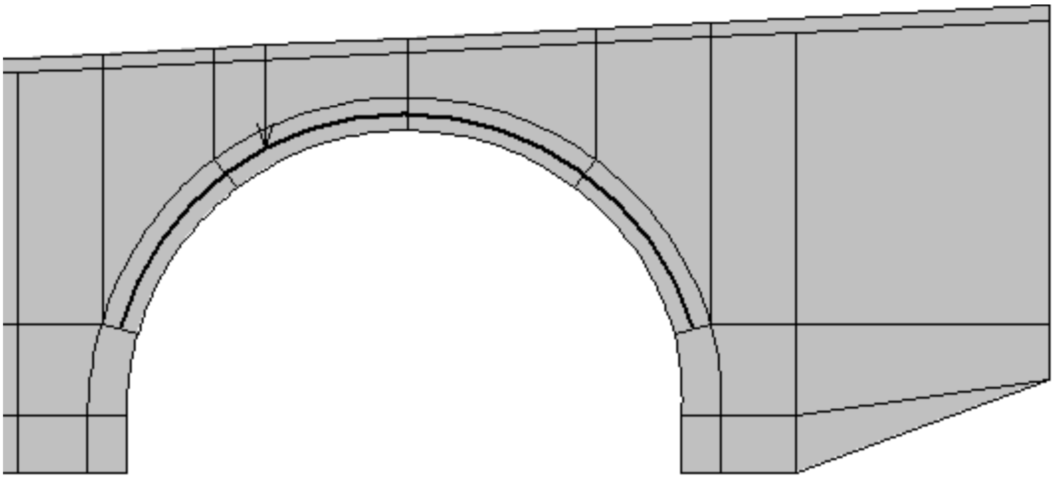

Figure 25: Live load and moment line for the right arch

It is important to note that for both cases live load was applied at the left side of the arch, where thickness of infill was lower. Accordingly, worse live load distribution and higher stresses within the arch took place.

It can be concluded from Table 6 that bearing capacity of the bridge draws the value of 38.5 tons, which is higher than the value obtained in direct method. It is interesting to note that in numerical approach boundaries for geometrical parameters are wider, and right arch fully satisfies geometrical requirements set up by the code. Capacity, computed for the right arch, can be evaluated as 51.4 tons, which is much higher than for the left arch. Nevertheless, capacity of the bridge is related with strength of the left arch, for which ratio between height of infill above the crown s and clear span l is out of range. Accordingly, obtained results should be checked and verified. For that FE modeling is implemented.

6. NONLINEAR FINITE ELEMENT ANALYSIS

The third method for the assessment of arch stone bridges suggested by TP 199 is nonlinear Finite Element Analysis (FEA). This approach is considered to be the most appropriate for evaluation of historical structures. Indeed, linear-elastic analysis can hardly be used for this purpose due its fundamental assumption that stiffness of the structure does not change throughout the loading process. This implies that deformations are always proportional to the load, and material properties are constant throughout analysis procedure. Apparently, these assumptions are inapplicable for old structures, which accumulated significant amount of damage, got permanent deformations and suffered material aging during their service life. Their behavior cannot be governed by liner-elastic law, and for accurate structural assessment nonlinear analysis is to be primarily used. Combined with Finite Element Analysis (FEA), it becomes a powerful tool for the assessment of both, historical and new, structures. It can capture different sources of nonlinearity such as geometry, materials and contacts. Since it is not normally possible to distinguish single source of nonlinear behavior, contemporary FE packages allow considering their combination. In this wise, stiffness becomes variable, which is changing the value, once one or more sources of nonlinearity are activated.

Under the scope of nonlinear FEA studied structure was tested using the same geometrical model and load pattern as described in sections 4.1 and 4.2. Nevertheless, consideration of material nonlinearity implies adoption of specific material models allowing for softening, once the strength limit is reached.

In the current work, nonlinear finite element analysis is required for accurate assessment of bearing strength of the bridge as also for observation of damage propagation process and collapse mechanism. Complex and time-consuming computations, required to obtain these data, are implemented in FE software ATENA, which will be discussed in the section 6.3.

6.1 Modeling strategies for masonry structures

Masonry represents anisotropic material consistent of stone units and mortar joints, which represent planes of weakness and accumulate most of damage. Modeling of masonry components in real scale can be challenging and time consuming. Furthermore, it is not normally required to accurately simulate structural behavior of the structure. Accordingly, for numerical evaluation of composite masonry different strategies can be adopted (Lourenço P.B., 2009).

The roughest idealization of composite masonry can be introduced throughout macro-modeling. In this approach masonry represents homogeneous continuum, since no distinction is made between units and joints (see Figure 26c). This approach can be used in large-scale tasks, where consideration of unit-joint interaction is not of importance towards global structural behavior. It is also significant that due to homogenization of mortar and stone materials, macro-model is unable to reflect accumulation of damage in mortar strips. In other words, shear or tensile failure of mortar joints, which are the most probable to occur, cannot be observed. To account for these masonry failure mechanisms, micro-modeling can be adopted. This strategy is preferable, when thorough investigation on the local behavior of masonry components is required. In this approach units and joints are modeled separately. In the detailed micro-modeling approach they represent continuum elements with discontinuous interfaces in-between (see Figure 26a). This allows accounting for both, stone and mortar, mechanical properties as well as for cracking and slipping along interfaces. Due to this detailing, micro-model can provide more accurate results than macro-model, but creation of this model is more sophisticated and requires more input data. Additionally, explicit description of interfaces performance is needed. Less demanding strategy to evaluate masonry failure is the simplified micro-modeling. In this approach mortar joints and interfaces between units and joints are turned into discontinuous elements, whereas units are expanded to preserve initial geometry (see Figure 26b). In this case, masonry represents set of stone blocks bonded by mortar lines, along which slipping and fracturing are possible.

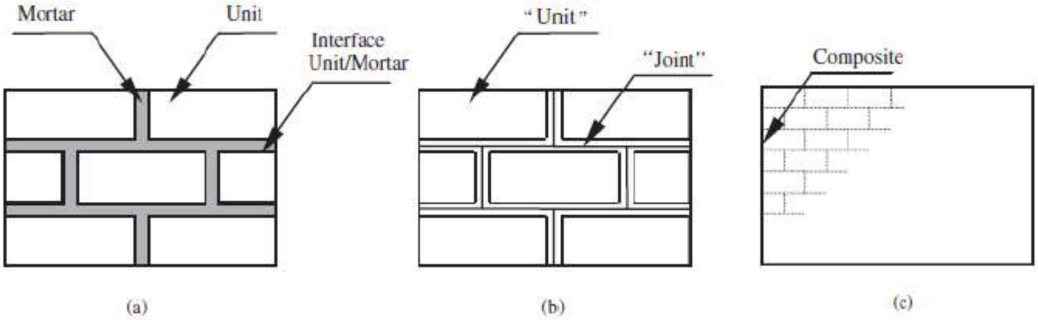

Figure 26: Numerical modeling strategies: (a) detailed micro-modeling; (b) simplified micro-modeling; (c) macro-modeling (Lourenço P.B., 2009)

The choice on the approach depends on the goals of analysis and availability of experimental. In this case study both, micro- and macro-modeling, are implemented. First, macro-model was adopted as the most convenient and optimized to evaluate global behavior of the bridge. Further, micro-scale models were developed in order to define the most probable failure mechanism and assess the capacity more precisely.

6.2 Stress state idealized configurations

In the current work two simplifications with respect to continuum state of studied model were adopted. These simplifications are plane stress and plane strain continuum states.

Plane stress state is typical for thin plates, when in plane dimension of the structure significantly exceeds its thickness in the transverse direction, and the load is only applied in the structural plane (see Figure 27). In this case stresses across thickness of the structure can be considered to be equal to zero. Accordingly, stress and strain tensors in three-dimensional continuum can be expressed as follows:

$$\boldsymbol{\sigma}(y,z)=\begin{bmatrix}0 & 0 & 0\\ 0 & \sigma_y(y,z) & \tau_{yz}(y,z)\\ 0 & \tau_{yz}(y,z) & \sigma_z(y,z)\end{bmatrix}\quad \boldsymbol{\varepsilon}(y,z)=\begin{bmatrix}\varepsilon_x(y,z) & 0 & 0\\ 0 & \varepsilon_y(y,z) & \dfrac{\gamma_{yz}(y,z)}{2}\\ 0 & \dfrac{\gamma_{yz}(y,z)}{2} & \varepsilon_z(y,z)\end{bmatrix} \tag{14}$$

Another continuum state used for simplification of real conditions is plane strain state. In this case structure is considered to have one of its dimensions much larger than others. This is typical for elongated in the transverse direction thick structures, for example, retaining walls. For these structures loads act in the plane parallel to the cross section, and they are considered to be uniform throughout the thickness (see Figure 28).

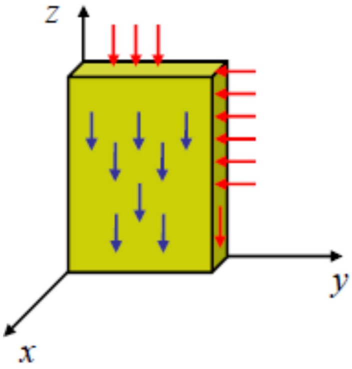

Figure 27: Plane stress state
(Kabele P., 2011)

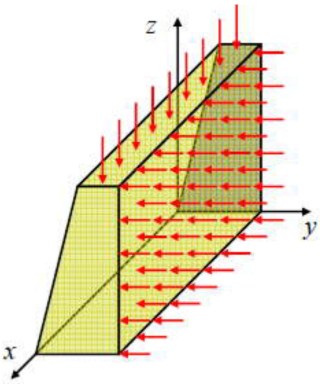

Figure 28: Plane strain state
(Kabele P., 2011)

These conditions allow eliminating strain in the transverse direction (x direction in the figure). Accordingly, stress and strain tensors can be expressed as follows:

$$\boldsymbol{\varepsilon}(y,z)=\begin{bmatrix}0 & 0 & 0\\ 0 & \varepsilon_y(y,z) & \dfrac{\gamma_{yz}(y,z)}{2}\\ 0 & \dfrac{\gamma_{yz}(y,z)}{2} & \varepsilon_z(y,z)\end{bmatrix}\quad \boldsymbol{\sigma}(y,z)=\begin{bmatrix}\sigma_x(y,z) & 0 & 0\\ 0 & \sigma_y(y,z) & \tau_{yz}(y,z)\\ 0 & \tau_{yz}(y,z) & \sigma_z(y,z)\end{bmatrix} \tag{15}$$

In the current work both, plane stress and plane strain continuum, models were adopted. On the one hand, plane strain assumption seems to be suitable for relatively thick bridge structure. It employs zero deformations in transverse direction, and is sufficient for modeling of infill material restrained by spandrel walls. On the other hand, width of the bridge is not large comparing with its length, and structure can be considered as thin. For this reason, arch barrel was modeled in plane stress state as well. This model is on the safe side and provides more conservative results due to the lack of confinement effect provided by plane strain continuum.

6.3 ATENA Software

ATENA is the software created by Cervenka Consulting Company located in Prague, Czech Republic. The software is based on the nonlinear finite element method and was initially designed to simulate concrete and reinforced concrete structures. Nevertheless, today ATENA is widely used for modeling of different materials such as masonry, steel, soil and rock. Software can be used for static, dynamic, thermal and moisture analyses. It allows for accurate assessment of new and existing structures. Load carrying capacity, fracture formation and propagation can be thoroughly studied using this package.

ATENA is applicable for two-dimensional and three-dimensional analyses. It has libraries of finite elements and offers wide range of material models. Nonlinear behavior of structures can be simulated using different solution methods such as Newton-Raphson and Arch-length. Additionally, different continuum states can be modeled, namely plane stress, plane strain and rotational symmetry, Furthermore, ATENA allows for incremental application of loads. This enables modeling of construction processes and ensures gradual settlement of the structure under its self-weight.

To conclude with, program has user-friendly interface and enables displaying of results even during the nonlinear analysis, which is very handy for complex and time-consuming tasks.

6.4 Constitutive material models

ATENA software offers several material models suitable for modeling of masonry. These models embrace wide range of aspects typical for its behavior and allow for accurate characterization of masonry structures. Brief description of models used for evaluation of Rabstejn bridge is given in the following sections. More detailed information can be found in ATENA Theory (Červenka V., Jendele L.,Červenka J., 2016).

6.4.1 Constitutive model SBETA

Constitutive model SBETA was mainly developed for concrete, but can be used for modeling of masonry as well. It employs plane stress continuum state and smeared approach for modeling of material properties.

Material model SBETA embraces following aspects typical for behavior of masonry (Červenka V., Jendele L.,Červenka J., 2016):

- nonlinear behavior in compression including hardening and softening
- fracture in tension based on the nonlinear fracture mechanics
- biaxial strength failure criterion

- reduction of compressive strength after cracking
- tension stiffening effect
- reduction of the shear stiffness after cracking (variable shear retention)
- fixed and rotated crack models.

To describe nonlinear behavior of material in the biaxial stress state, effective stress σ_c^{ef} (normally principal stress) and equivalent uniaxial strain ε^{eq} are introduced. The latter can be defined as the strain that would be produced by the stress σ_{ci} in the uniaxial test with modulus E_{ci} associated with direction *i*. This formulation allows for elimination of Poisson's effect in the plane stress state, and following relation can be expressed:

$$\sigma_{ci} = \varepsilon^{eq} \cdot E_{ci} \tag{16}$$

Corresponding equivalent uniaxial stress-strain diagram is shown in the Figure 29. It can be seen from the graph that unloading represents linear function to the origin. This takes place, when the increment of the effective strain changes the sign. If the loading is initiated anew, it follows unloading path until the point belonging to the initial loading function is reached. Onwards, loading function is resumed.

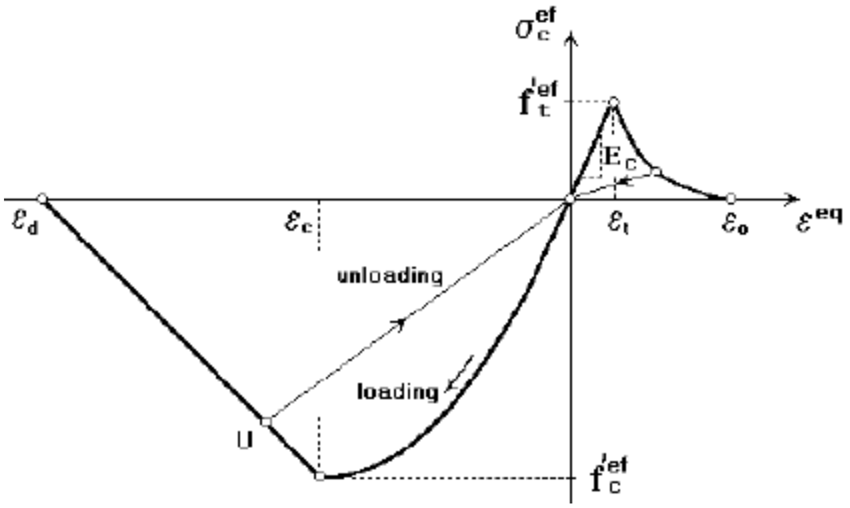

Figure 29: Uniaxial stress-strain diagram for SBETA model masonry
(Červenka V., Jendele L.,Červenka J., 2016)

This stress-strain relation allows for the definition of tangent and secant elastic modules, which are used in material stiffness matrices and serve to describe material state until the formation of first cracks. Until this moment structure behaves in the linear range, and can be described by simple constitutive equations. Material behavior in tension after cracking is based on the crack-opening law and fracture energy fictitious crack model (see Figure 30).

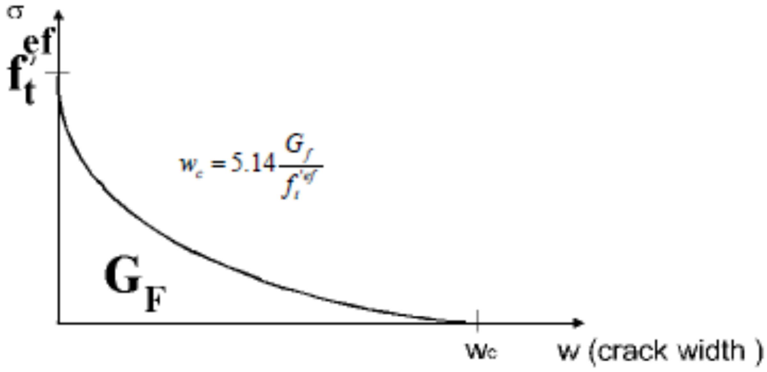

Figure 30: Exponential crack opening law in tension masonry
(Červenka V., Jendele L.,Červenka J., 2016)

Definition of crack opening w employs crack-band theory and is described by formula presented in the work of Hordijk A.D., 1991.This parameter is dependent on the fracture energy G_f, crack opening at the complete release of stress w_c and effective tensile strength f_t^{ef} derived from failure function.

In order to describe behavior of concrete in compression, following assumptions are introduced. Before reaching peak stress, relation between stress and strain is nonlinear and is numerically described according to approach given in Model Code 90 (Thomas Telford Ltd., 1993). For post-peak behavior fictitious compression plane model is adopted. It is assumed that failure occurs in a plane normal to the direction of compressive principal stress. Softening law for compression is given in the Figure 31.

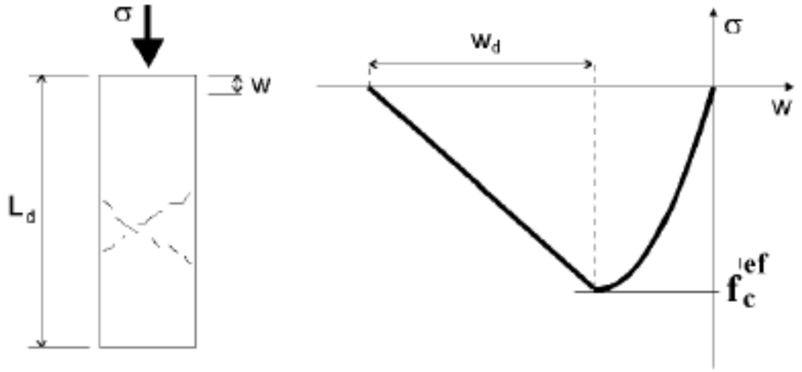

Figure 31: Softening law in compression
(Červenka V., Jendele L.,Červenka J., 2016)

In this formulation compressive fracture energy is expressed through critical compressive displacement w_d . For concrete it is recommended to be set up as 0.5 mm. In the current work, due to the lack of experimental data, the same value was adopted for historical masonry.

Effective tensile and compressive strengths f_t^{ef} and f_c^{ef} represent the limit values of stress in tension and compression. They are computed according to biaxial stress state criterion, and, thus, uniaxial stress-strain law is related with biaxial failure criterion (see Figure 32).

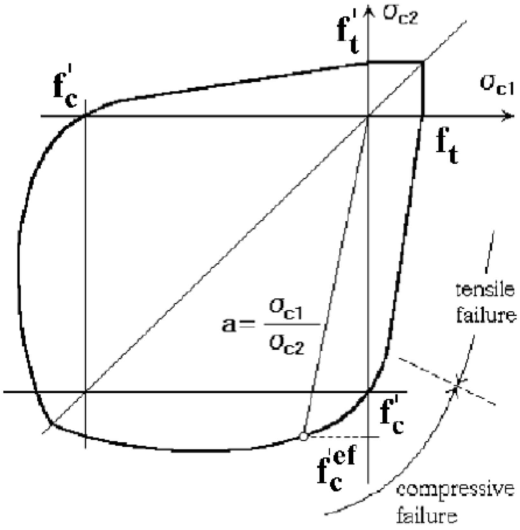

Figure 32: Biaxial failure criterion
(Červenka V., Jendele L.,Červenka J., 2016)

Compressive failure criterion adopted for SBETA model is developed in the work of Kupfer, H., Hilsdorf, H.K., Rusch, H., 1969. In the compression-compression state the function of yielding surface is expressed in terms of principal stress σ_1 and σ_2 .In tension-tension state failure takes place, once the tensile strength is reached in any direction. In tension-compression and compression-tension states tensile strength is reduced due to the compressive strength in the other direction. In these regions failure surface can be described as hyperbolic or linear function.

6.4.2 Fracture-Plastic (CC3DNonLinCementitious2) constitutive model

Fracture-Plastic constitutive model is one of the most recent material models developed by Cervenka Consulting. It combines fracturing behavior in tension and plasticity in compression. Plasticity model is based on Menétrey-Willam failure surface, whereas fracture model employs Rankine failure criterion (see Figure 33).

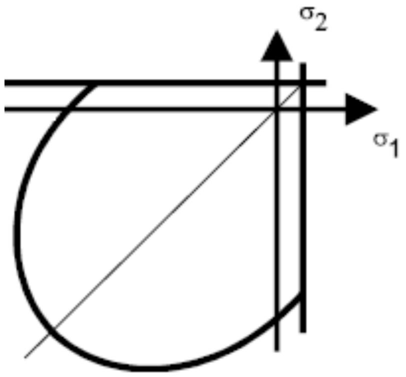

Figure 33: Failure Surface for Fracture-Plastic Constitutive model (Červenka V., Jendele L.,Červenka J., 2016)

Program algorithm is developed so that both models can be described separately, which allows for considering formation, propagation and closure of cracks as well as crushing of the material under high confinement.

Fracture model utilizes orthotropic smeared crack approach and exponential softening (see Figure 34).

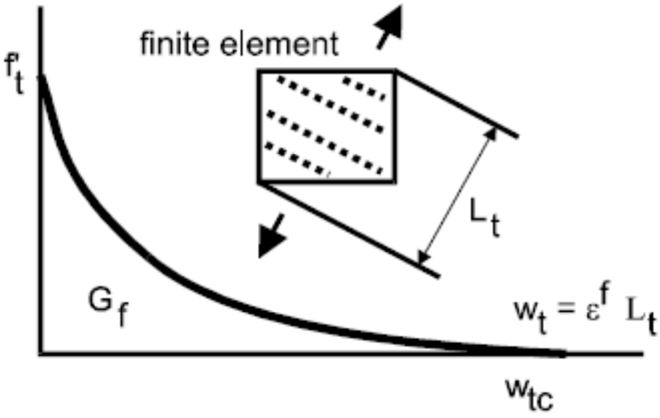

Figure 34: Fracture-plastic model. Tensile softening (Červenka V., Jendele L.,Červenka J., 2016)

Same as for SBETA model, softening is defined by fracture energy G_f, but crack opening depends on the fracturing strain ε^f and characteristic length L_t representing the crack band size proposed by Bazant Z.P and Oh B.H , 1983.

To evaluate behavior of material in compression, fracture-plastic model employs hardening and softening (see Figure 35).

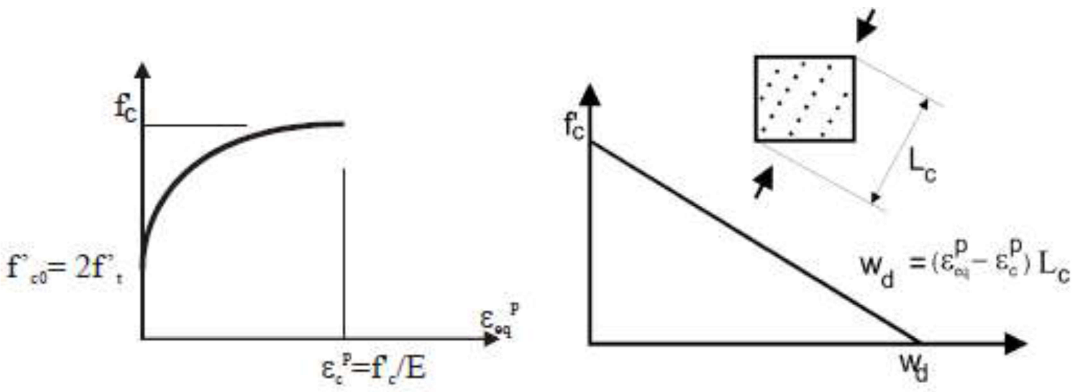

Figure 35: Hardening/softening in compression
(Červenka V., Jendele L.,Červenka J., 2016)

The onset of the nonlinear behavior is defined by the parameter $f_{c0}^{'}$, which can be determined according to ATENA theory manual (V.Červenka, L. Jendele, J.Červenka, 2016). One more input parameter is plastic strain at the compressive strength ε_c^p which can be defined as it is shown in the figure above.

In this section brief description of fracture-plastic model is given, and more detailed information on the model can be found in ATENA Theory manual (V.Červenka, L. Jendele, J.Červenka, 2016).

6.4.3 Drucker-Prager plasticity model

Drucker-Prager plasticity model is widely used for so-called pressure sensitive materials such as soils, sands, rock and concrete. These materials have internal friction, and the plane, along which slipping takes place, is rough. In other words, shear stresses needed to activate the slip are dependent on the normal stresses. Under these conditions, yielding function can be expressed as follows:

$$F_{DPt}^{p}(\sigma_{ij}) = \alpha \cdot I_1 + \sqrt{J_2} - k \tag{17}$$

Here I_1 is the first invariant of Cauchy stress, and J_2 is the second invariant of the deviatoric part of Cauchy stress. Parameters α and k define the shape of the failure surface. If Drucker-Prager yield surface represents outer cone to the Mohr-Coulomb surface, they can be derived depending on the angle of internal friction φ and cohesion c as follows:

$$\alpha = \frac{2 \cdot \sin\varphi}{\sqrt{3} \cdot (3 - \sin\varphi)} \qquad k = \frac{6 \cdot c \cdot \cos\varphi}{\sqrt{3} \cdot (3 - \sin\varphi)} \tag{18}$$

For this case, yielding surface represented in principal stresses space has the shape of ellipsoid or hyperboloid as shown in the Figure 36. Position of this failure surface can change depending on the hardening/softening law. In the ATENA software it is controlled by parameter k, and softening law can be expressed as a function of equivalent plastic strain ε_{eq}^{p} as it is shown in the Figure 37.

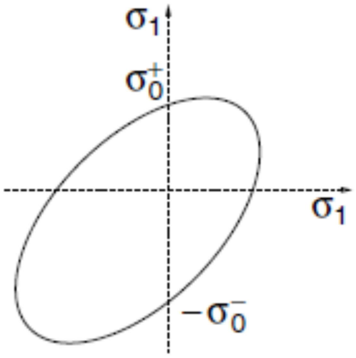

Figure 36: Drucker-Prager yield surface

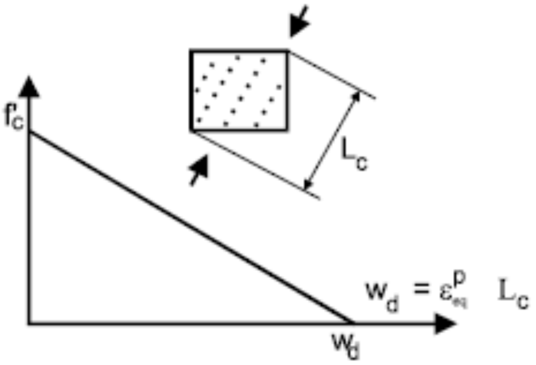

Figure 37: Linear-softening law adopted in ATENA Drucker-Prager model (Červenka V., Jendele L.,Červenka J., 2016)

6.4.4 Material model for interfaces

Material model for interfaces allows for the simulation of contact between different materials. It serves as a weakness plane and, in case of masonry structures, enables capturing tensile and shear failure of masonry. When tensile failure occurs, interface separates from the blocks due to high stresses acting normal to its plane, whereas shear failure represents sliding of stones or mortar due to high shear stresses.

Interface model is based on the Mohr-Coulomb criterion and can be described using following relations (Červenka V., Jendele L.,Červenka J., 2016):

$$|\tau| \le c - \sigma \cdot \varphi, \sigma \le 0 \qquad |\tau| = \tau_0 \sqrt{1 - \frac{(\sigma - \sigma_c)^2}{(f_t - \sigma_c)^2}}$$

$$\tau_0 = \frac{c}{\sqrt{1 - \frac{\sigma_c^2}{(f_t - \sigma_c)^2}}} \qquad \sigma_c = -\frac{f_t^2 \cdot \varphi}{c - 2 \cdot f_t \cdot \varphi} \qquad 0 < \sigma < f_t \tag{19}$$

Graphic representation of failure criterion is given in the Figure 38. In tension failure surface represents ellipsoid crossing the axes of normal and shear stresses at the values of tensile strength f_t and cohesion c. Tangent to surface line corresponds to the angle of internal friction φ. The state, when Mohr-Coulomb criterion is violated, corresponds to a dry friction, and initial surface collapses to residual one.

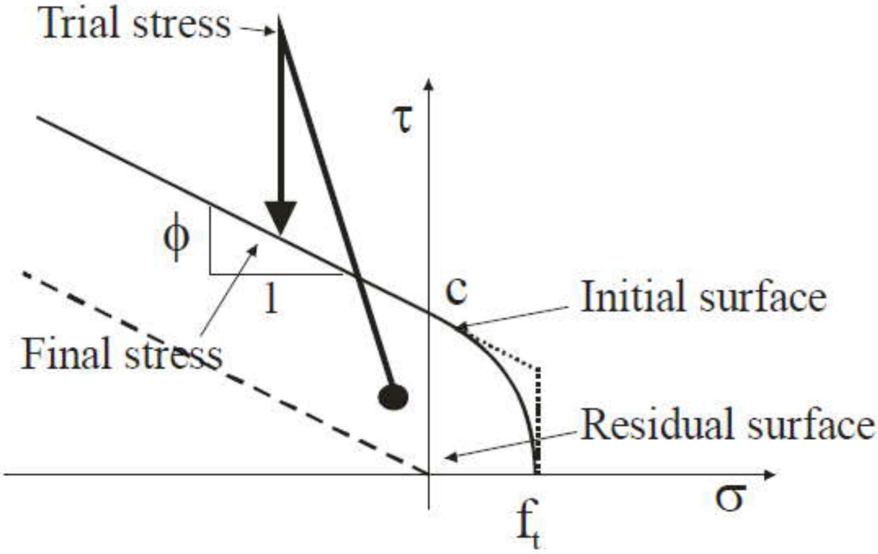

Figure 38: Failure surface of interface elements (Červenka V., Jendele L.,Červenka J., 2016)

Description of interface model requires denoting of normal and tangent stiffnesses K_{nn} and K_{tt} defining behavior of interface in tension (see Figure 39) and friction (see Figure 40). Here $K_{nn}^{\min}$ are $K_{tt}^{\min}$ parameters introduced for numerical reasons in order to preserve positive definiteness of an overall structure, once the failure of some element occurs. According to ATENA package recommendations, these values should be assigned as 0.1% of K_{nn} and K_{tt} respectively.

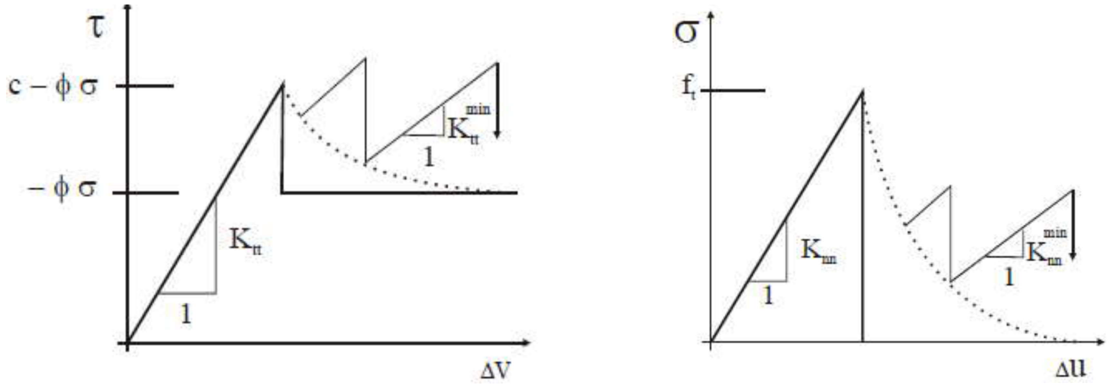

Figure 39: Behavior of interface in friction (Červenka V., Jendele L.,Červenka J., 2016)

Figure 40: Behavior of interface in tension (Červenka V., Jendele L.,Červenka J., 2016)

7. NONLINEAR FINITE ELEMENT MODELING OF THE RABSTEJN BRIDGE

7.1 Modeling of geometry

For the nonlinear FEA geometrical model created for simplified numerical analysis was adopted. As it was mentioned in the section 2.2, Rabstejn bridge has inclined plane, and thickness of infill material is different along the structure. The height of the infill is minimum above the crown of the left arch. It is only equal to 80 cm, and such a minor value does not allow for sufficient live load distribution and results in high stress and strain concentration within the arch barrel. For this reason, capacity of the bridge was defined as the capacity of the left arch implying that bearing strength of the right arch is guaranteed, once it is assured for the left arch. To this end, to simplify the analysis and make it less time consuming, only left arch was modeled as it is shown in the Figure 41. Accordingly, additional boundary conditions in horizontal direction were introduced to substitute right part of the bridge.

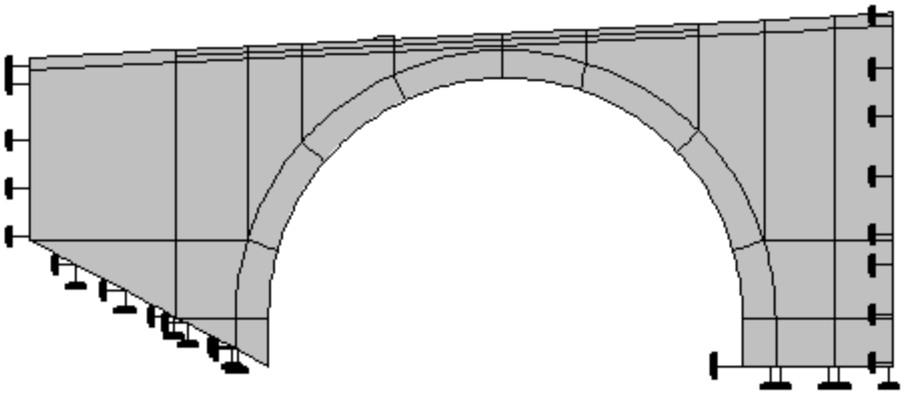

Figure 41: Geometry and boundary conditions of adopted model

7.2 Modeling approaches

In the current work different modeling strategies and continuum configurations were adopted for thorough study on the structural behavior of the bridge. One geometrical model with homogenized arch barrel and two simplified micro-models (one with stone units and mortar strips and another with stone units and interfaces within arch barrel) were created. Each of three models was tested assuming plane stress and plane strain continuum states for arch barrel, as discussed in the section 6.4. Consequently, six models were adopted and tested, as it is shown in the Table 7.

Table 7: Models for nonlinear FEA

Model 1	Macro-model + Plane stress	Model 2	Macro-model + Plane strain
Model 3	Micro-model with mortar strips + Plane stress	Model 4	Micro-model with mortar strips + Plane strain
Model 5	Micro-model with interfaces + Plane stress	Model 6	Micro-model with interfaces + Plane strain

7.2.1 Macro-model

To begin with, macro-model was created, and arch masonry was modeled as homogenized material. This technique is suitable only for large-scale modeling, since it does not capture local failure of material. Nevertheless, homogenized approach is suitable for the definition of load-bearing capacity, and it is easy and fast to compute. Model adopted for Rabstejn Bridge is shown in the Figure 42. Quadrilateral elements were used for meshing, and four elements per thickness of the barrel were assigned, in order to ensure gradual formation and propagation of cracks.

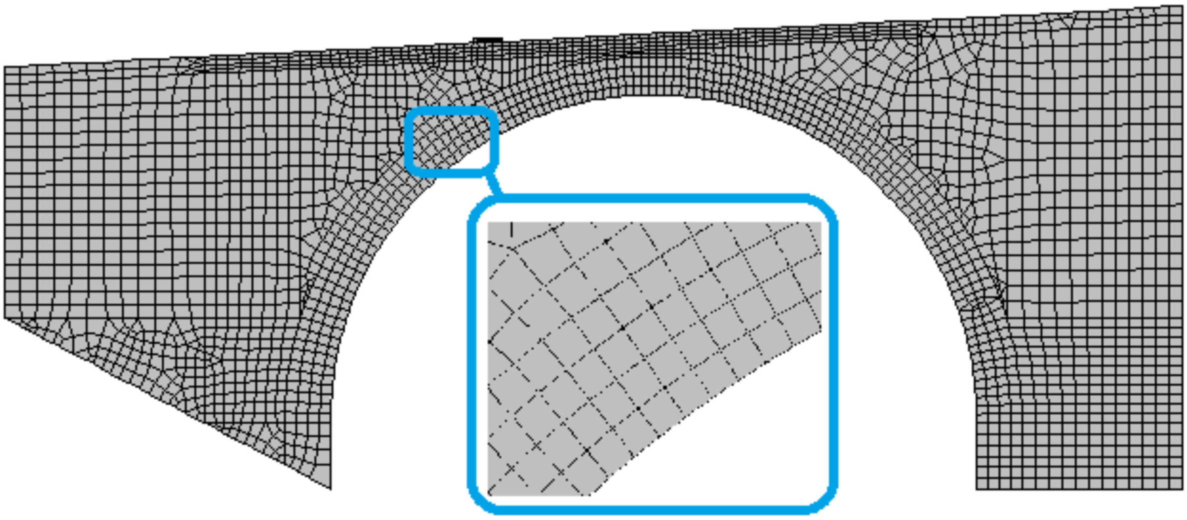

Figure 42: Macro-model

7.2.2 Micro-model with stone units and mortar strips

Next model created in the current work was model with stone units and mortar joints within the arch barrel (see Figure 43). Comparing with homogenized model, this approach allows to capture local failure and to get realistic collapse mechanism.

According to surveying results, phyllite stones composing the arch are very thin, and modeling them in real scale would be extremely time-consuming and difficult to calculate. For this reason, stone blocks were modeled with a width of 15 cm, and the ratio between stone and mortar thicknesses was preserved. From the photographic survey carried out by Pudis a.s., the latter was assessed as 3:1(see Figure 6), and thickness of mortar was set up as 5 cm. Same as in homogenized model, quadrilateral elements were used, and six elements per barrel thickness were created. Furthermore, despite low thickness of mortar blocks, two elements per block width were assigned.

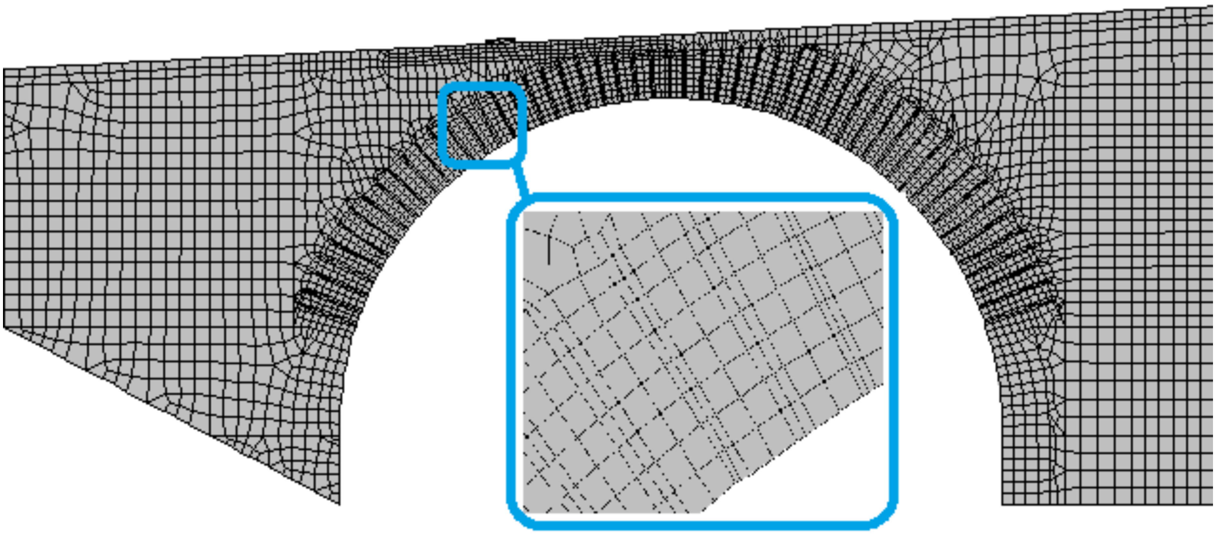

Figure 43: Micro-model with stone units and mortar strips

7.2.3 Micro-model with interfaces

In the micro-model with interfaces mortar strips were substituted with two-dimensional interfaces, and stones were extended to preserve the geometry. For more accurate modeling, dimensions of stones were reduced to 10 cm. Comparing with the previous model, micro-model with interfaces cannot capture crushing of mortar in compression, but, still, allows for consideration of realistic collapse mechanism related with tensile or shear failure.

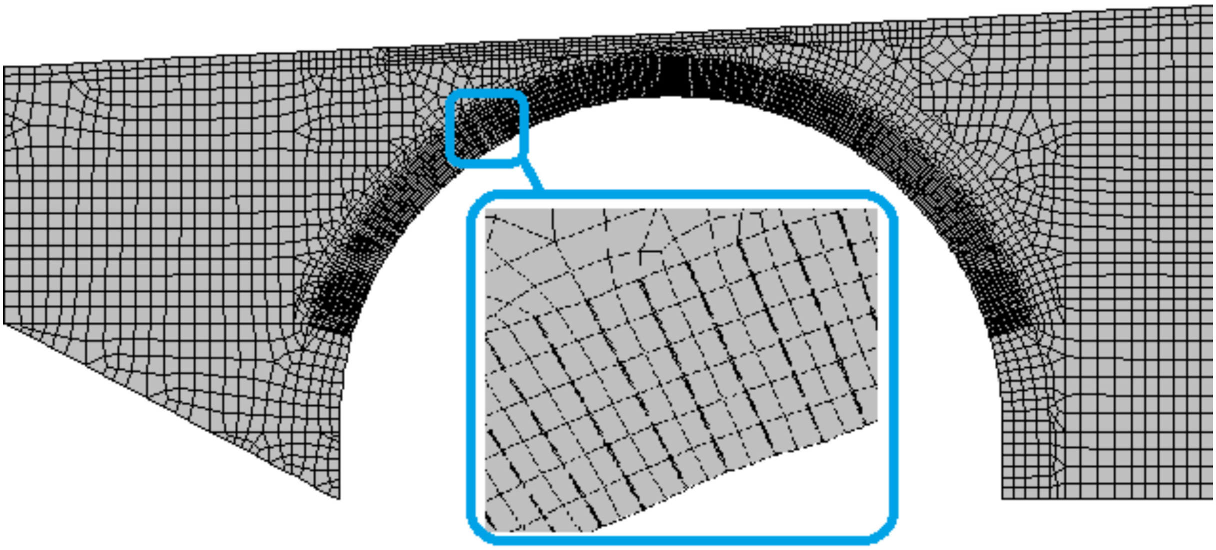

Figure 44: Micro-model with stone units interfaces

7.3 Modeling of materials

Correct definition of materials is essential to describe behavior of structure in the nonlinear range. In most cases this turns to be challenging due to the lack of experimental and historical data. Under these conditions, required parameters can be derived from literature: from scientific works, conducted experiments and historical records. Despite the availability of all these sources, parameters that can be obtained from them are quite variable. For this reason, material modeling turns to be a very complex task, involving addressing and combining different sources and approaches.

In the current work experimental outcomes from tests carried out on Rabstejn Bridge by Pudis a.s. were employed. This was not enough for thorough modeling, and scientific literature was addressed in order to derive missing data. Additionally, to obtain properties of homogenized material, numerical approach employing formulas from Eurocode 6 (European committee for standardisation, 2005) was used.

7.3.1 Phyllite masonry

Homogenized model was used to create arch and piers in the macro-model as also piers in the micro-model. To define the material in plane stress state, constitutive model SBETA was used. For plane strain continuum modeling, Fracture-Plastic constitutive model was employed. Basic parameters required for the description of these material models are uniform, and procedure of their derivation is given below.

Data obtained from experimental tests was limited by the properties of stones and mortar, and no information on the properties of composite masonry was available. For this reason, numerical approach from Eurocode 6 (European committee for standardisation, 2005) was adopted. In compliance with code requirement, in the absence of experimental data, characteristic compressive strength f_k of masonry made with general purpose mortar can be derived from the following formula:

$$f_k = K \cdot f^{0.7}{}_b \cdot f_m{}^{0.3} \tag{20}$$

Here f_b and f_m are characteristic compressive strengths of stone units and mortar joints accordingly, and K is constant, which is equal to 0.45 for natural dimensioned stone, according to standard requirements.

Compressive strength of mortar was assigned in compliance with experimental data. This value was assessed to be in the range between 0.4 and 1 MPa, and the lowest value of 0.4 MPa was employed. No experimental data was available on the compressive strength of stone units, and several papers were addressed to assign this parameter.

Several tests on phyllite samples with different direction of laminates were carried out by Ramamurthy T. et al, 1993. Due to the laminated structure of phyllite, it can be characterized as anisotropic material with strength variable in different directions. Properties of plyllite stone vary depending on the angle between major loading direction and direction of laminates (see Figure 45).

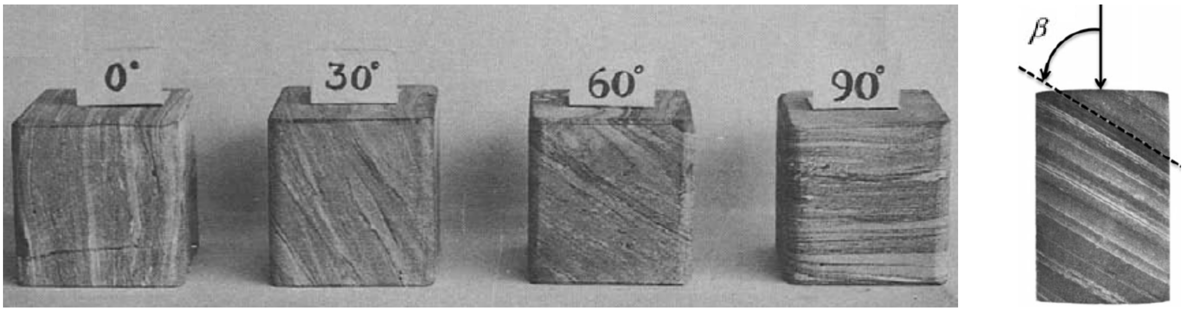

a. Samples with different laminate angles

b. Angle between major direction and laminates

Figure 45: Direction of laminates in phyllite samples (Ramamurthy T. et al, 1993)

In the current case study stone units within the arch are placed so that laminate direction coincides with the arch radius. Since these stones mainly work in the perpendicular to radius direction, outputs for angle β equal to 90 degrees were employed (see Figure 45). This value was the highest among others. For the sake of safety, and due to the absence of data on the nature of materials, lower value of 50 MPa was introduced. In this wise, compressive strength of masonry was computed to be equal to 5.3 MPa. Tensile strength of masonry was computed as a fraction of compressive strength. It was set up as 5% of compressive strength and drew up the value of 0.265 MPa.

To evaluate elasticity modulus, Eurocode 6 was employed. This standard recommends defining the Young's modulus for new masonry as $1000 \cdot f_k$, if the required data is absent. For existing masonry multiplying factor varies in the wide range from 200 to 2000 as it stated in the work of Tomazevich M., 1999. For historical structures this value is recommended to be closer to lower boundary. Accordingly, the multiplying factor equal to 600 was chosen for the current task, and the Young's modulus was defined to be equal to 3170 MPa.

One more important parameter required to model masonry in the nonlinear range is tensile fracture energy G_f. This value reflects the energy required to create unit area of stress-free crack. It can be obtained experimentally, but no explicit correlations for its definition exist for historical masonry. This is due variety of materials that can be met in historical constructions and their anisotropic nature. According to experimental data obtained by Pluijm R., 1999, fracture energy for different types of masonries varies over a wide range, depending on the thickness of material components and their nature. Under these conditions, no specific value could be obtained, and tensile fracture energy was defined according to the relations available for concrete structures. Model Code 90 (Thomas Telford Ltd., 1993) was addressed. Standard recommends defining tensile fracture energy for the material with grain size up to 8 mm as follows:

$$G_f = 0.025 \cdot \left(\frac{f_c [MPa]}{10} \right)^{0.7} \quad [KN/m] \tag{21}$$

Accordingly, tensile fracture energy was computed to be equal to 0.016 kN/m.

Properties assigned to SBETA and CC3DNonLinCementitious2 material models of phyllite masonry are presented in the Table 8.

Table 8: Properties assigned to phyllite masonry

Material type 1	SBETA	Tensile strength f_t, [Mpa]	0.265
Continuum state 1	Plane stress	Young's modulus E, [Mpa]	3170
Material type 2	CC3DNonLinCementitious2	Poisson's ratio υ	0.20
Continuum state 2	Plane strain	Fracture energy G_f, [kN/m]	0.016
Compressive strength f_c, [Mpa]	5.30	Material weight γ, [kN/m^3]	24.00

7.3.2 Phyllite stones

Following the idea of micro-modeling, material model for phyllite units was introduced. This material was only used for stones within arch barrel. Constitutive model SBETA for plane stress state and CC3DNonLinCementitious2 model for plane strain state were employed.

As stated in the previous section, compressive strength of phyllite stones was assessed to be equal to 50 MPa, and the angle between laminates and major working direction was set up as 90 degrees. In this wise, tensile strength of phyllite stones can be assessed as 2 MPa (Ramamurthy T. et al, 1993).

Modulus of elasticity was defined as consistent with outcomes of several works such as of Saeidi O. et al, 2013 and Lubo M. et al, 2012. Eventually, the value of 40 000 MPa was employed. Following the procedure described in the Model code 90, fracture energy was computed according to formula (21) and the value 0.075 kN/m was derived. Resulting properties for modeling of phyllite stones are given in the Table 9.

Table 9: Properties assigned to phyllite stones

Material type 1	SBETA	Tensile strength f_t, [Mpa]	2.00
Continuum state 1	Plane stress	Young's modulus E, [Mpa]	40000
Material type 2	CC3DNonLinCementitious2	Poisson's ratio υ	0.34
Continuum state 2	Plane strain	Fracture energy G_f, [kN/m]	0.075
Compressive strength f_c, [Mpa]	50.00	Material weight γ, [kN/m^3]	24.00

7.3.3 Mortar joints

Mortar joints represent planes of weakness in composite masonry and accumulate the highest level of damage causing formation of hinges, sliding and crushing in compression. For this reason, analysis can be quite sensitive to input parameters assigned to mortar joints, and accurate estimation of these values is required. According to surveying results, compressive strength of mortar was defined as 0.40 MPa. Tensile strength of such a weak composition should be almost zero. On the other hand, even a very weak mortar can carry some minor tensile stresses (Pippard A.J.S., Ashby R.J. 1993). In this wise, minor value equal to 5% of compressive strength was assigned to tensile capacity of mortar, and it was set up as 0.02 MPa. In order to relate micro-model to homogenized one, Young's modulus of mortar was computed employing following approach. Homogenized block and composite with stones and mortar were considered (see Figure 46).

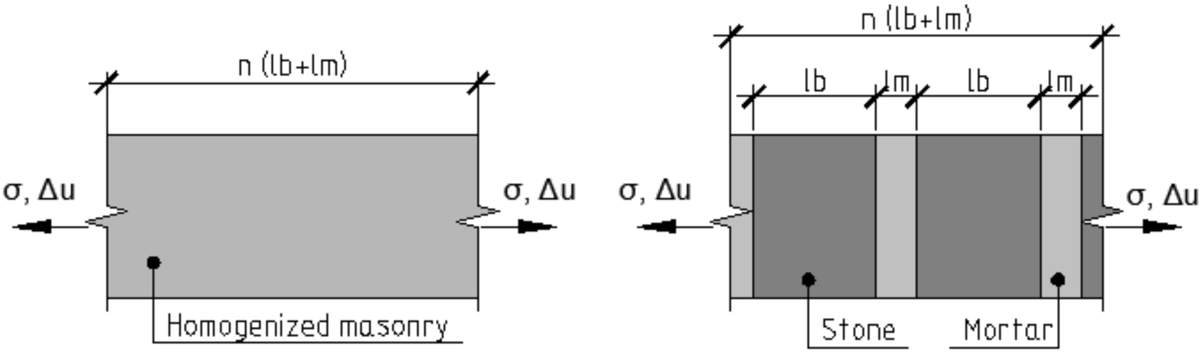

Figure 46: Scheme for defining Young's modulus of mortar

Dimensions of blocks, stress state and relative displacement Δu were set up as uniform for both models. Linear-elastic behavior of blocks was assumed, and Young's modulus of mortar E_m was computed as a function of elasticity modulus of homogenized masonry E_h and of stone units E_s :

$$\frac{l_m}{E_m} = \frac{1_b + l_m}{E_h} - \frac{l_b}{E_s} \tag{22}$$

Given that stone units in micro-model were created with a width of 15 cm and mortar strips with a width of 5 cm, Young's modulus of mortar was computed to be equal to 840 MPa. Accordingly, parameters for modeling of mortar are presented in the Table 10.

Table 10: Material properties assigned to mortar

Material type 1	SBETA	Tensile strength f_t, [Mpa]	0.02
Continuum state 1	Plane stress	Young's modulus E, [Mpa]	840
Material type 2	CC3DNonLinCementitious2	Poisson's ratio υ	0.20
Continuum state 2	Plane strain	Fracture energy G_f, [kN/m]	0.003
Compressive strength f_c, [Mpa]	0.40	Material weight γ, [kN/m^3]	18.00

7.3.4 Sandstone masonry

Base of the bridge is composed of sandstone masonry. To model this material SBETA model was employed for plane stress continuum state and CC3DNonLinCementitious2 for plane strain continuum state.

Compressive strength of sandstone blocks was defined experimentally. According to surveying results it was assessed to be up to 40 MPa. For the sake of safety, a shade less value of 30 MPa was assigned.

The procedure of deriving remaining input parameters is the same as described in the section 7.3.1, and results of calculations are presented in the Table 11.

Table 11: Material properties assigned to sandstone masonry

Material type 1	SBETA	Tensile strength f_t, [Mpa]	0.19
Continuum state 1	Plane stress	Young's modulus E, [Mpa]	2218
Material type 2	CC3DNonLinCementitious2	Poisson's ratio υ	0.34
Continuum state 2	Plane strain	Fracture energy G_f, [kN/m]	0.012
Compressive strength f_c, [Mpa]	3.70	Material weight γ, [kN/m^3]	23.20

7.3.5 Interfaces

Interface model was used to create joints in simplified micro-model. Description of interfaces requires definition of tensile strength and cohesion. Additionally, normal and tangential stiffnesses are to be computed. To determine these parameters, approach used in the section 7.3.3 was employed. Homogenized block and block composed of stones and interfaces with zero-thickness were considered (see Figure 47).

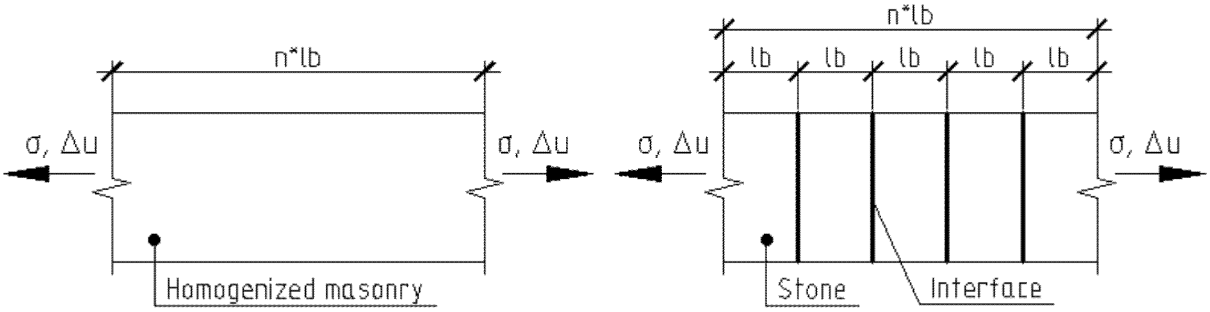

Figure 47: Scheme for defining normal stiffness for interface

Dimensions of blocks, stress state and relative displacement Δu were set up as uniform for both models. Materials were considered to behave in the linear-elastic range, and normal stiffness of interface K_n was defined depending on Young's modulus of homogenized masonry E_h and Young's modulus of stone units E_s :

$$\frac{1}{K_{nn}} = \frac{1_b}{E_h} - \frac{l_b}{E_s} \tag{23}$$

Then tangential stiffness was defined as follows:

$$K_{tt} = \frac{K_{nn}}{2 \cdot (1 + \upsilon)} \tag{24}$$

Parameters computed for the definition of interface model are presented in Table 12.

Table 12: Properties assigned to interfaces

Material type 1	2D Interface	Tensile strength f_t, [MPa]	0.02
Normal stiffness K_{nn}, [kN/m^3]	0.0345	Cohesion c, [MPa]	0.02
Tangential stiffness K_{tt}, [kN/m^3]	0.0140	Friction coefficient	0.57

7.3.6 Infill material

According to surveying results, infill material represents clay sand with mechanical properties stated in the section 2.3. Since it is restraint by spandrel walls, it was modeled in plane strain continuum state adopting Drucker-Prager failure criterion model.

Young's modulus, specific material weight, cohesion and angle of internal friction required for the definition of this model were taken from the report of Pudis a.s., 2015. Input parameters α_{DP} and

K were computed as described in the section 6.4.3. The only parameter derived from literature was Poisson's ratio, which according to Bowles J., 1996 was set up as 0.30.

Table 13: Material properties assigned to infill material

Material type	Drucker-Prager	Drucker-Prager criterion parameter α_{DP}	0.214
Continuum state	Plane strain		
Young's modulus E, [Mpa]	20.00	Drucker-Prager parameter K, [Mpa]	0.006
Poisson's ratio υ	0.30	Material weight γ, [kN/m^3]	20.00

7.3.7 Material for roadway base

To begin with, roadway concrete base was created adopting SBETA constitutive model. Accordingly tensile and compressive strength limits were assigned. This resulted to the failure of model due to high level of damage accumulated in the roadway base, whereas strength limit of masonry arch was not reached. To avoid this type of failure, roadway base was modeled as linear-elastic. This allowed for better distribution of live load applied at the quarter of a span. This assumption is reasonable to some extent, since in reality the load induced by the moving vehicle is distributed along the cover material, and no pin load exists. In this wise, characteristics presented in the Table 14 were assigned to the roadway material.

Table 14: Material properties assigned to roadway base

Material type	Plane stress elastic isotropic	Poisson's ratio υ	0.20
Young's modulus E, [Mpa]	17000	Material weight γ, [kN/m^3]	23.50

7.4 Modeling of loads

For nonlinear FEA load pattern discussed in the section 4.2 was adopted. Self-weight was automatically applied to the modeled geometry, and roadway structure above concrete base was substituted with uniformly distributed load, as consistent with section 5.2.3. Resultant dead load was gradually applied in ten uniform steps, in order to account for construction process and ensure stable settlement of the structure under applied self-weight.

As distinct from simplified numerical analysis, live load was applied not as the force but as prescribed vertical displacement. To derive value of corresponding force, reaction in the point of load application was measured in each step. For that, monitoring point 1 was introduced (see Figure 48). In this wise, small displacement increment was imposed to the roadway base at the left quarter span of the arch. It was equal to 1 mm and was increased in each step by means of multiplying factor f_0. This approach was chosen in order to obtain stable convergence of calculations and observe post-peak behavior of the studied structure.

Additionally, to observe how the structure was deforming throughout the loading process, monitoring point 2 was introduced at the arch intrados. It was used to control vertical displacement in each step (see Figure 48) and was located at the left quarter span of the arch, where maximum deformations were expected to occur.

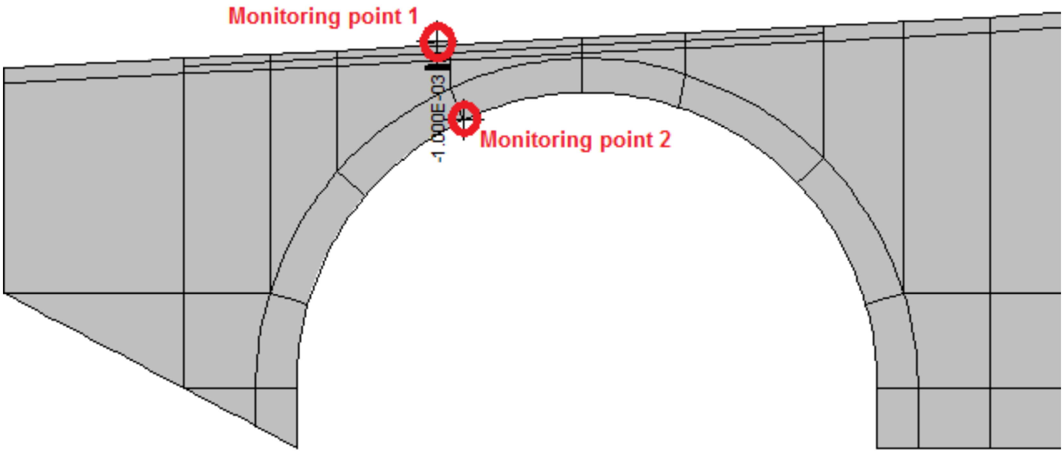

Figure 48: Live load increment imposed to the bridge and monitoring points

In this wise, two-dimensional structural model was subjected to dead and then live loads applied in a step-wise fashion. Live load was gradually increased until the peak value of load was reached. This peak load was taken as the maximum axial load F_a, which could be carried by one meter width of the bridge. Then, the capacity of the structure was defined using formula ((12) as consistent with standard TP 199.

8. RESULTS OF NONLINEAR FINITE ELEMENT ANALYSIS

8.1 Model 1: Macro-model with homogenized material within arch barrel modeled in plane stress continuum state

To begin with, model with homogenized material within arch barrel modeled in plane stress continuum state was tested. Structure was loaded by the self-weight and prescribed vertical translations in the monitoring point 1, as consistent with section 7.4. In this point vertical reaction was measured in each step. Vertical translation in the arch intrados was controlled in the monitoring point 2.

No significant damages and translations were observed in the structure, when the self-weight was applied. First cracks appeared in the arch barrel, when the live load was equivalent to 0.203 MN. Cracking took place in the arch portion underlying the point of live load application. Cracks had perpendicular to the arch intrados direction (see Figure 49) and width up to 0.01 mm. In reality it would be impossible to observe such a minor cracks, but process of their formation was initiated, and they continued to grow in the following steps.

Next, under the load equivalent to 0.440 MN set of cracks up to 0.02 mm width developed within the right quarter span of the arch as well as in the vicinity of right support (see Figure 50). Finally, when reaction in the monitoring point reached the value of 0.657 MN, cracks, normal to arch extrados, appeared in the left side of the arch (see Figure 51). At this point, cracks at the left quarter span grew up to 1.6 mm and up to 0.2 mm in the remaining structure.

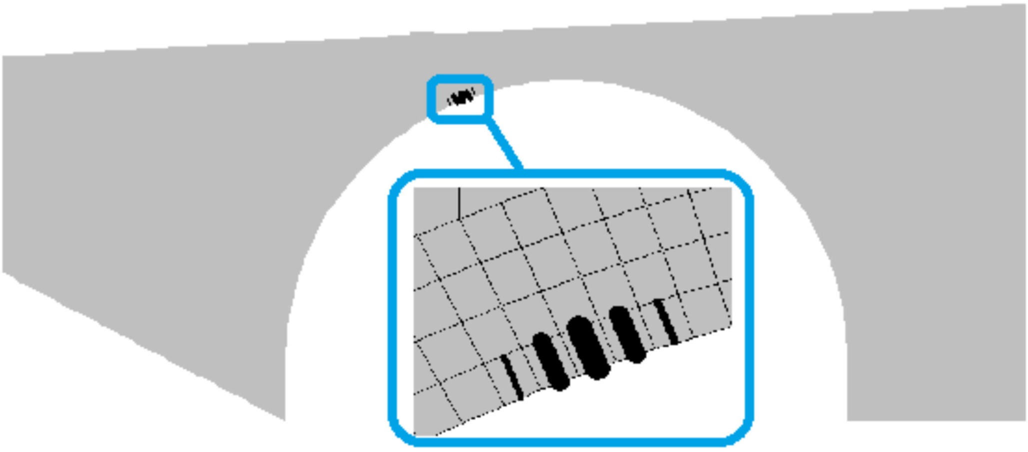

Figure 49: Crack pattern corresponding to the load of 0.203 MN

Initially, they formed in the direction perpendicular to the arch extrados/ intrados. This is reasonable due to high tensile stresses in the arch tangent direction. Nevertheless, when the live load reached the value of 0.935 MN, cracks developed in tangent, normal and perpendicular to arch intrados/extrados directions (see Figure 52).

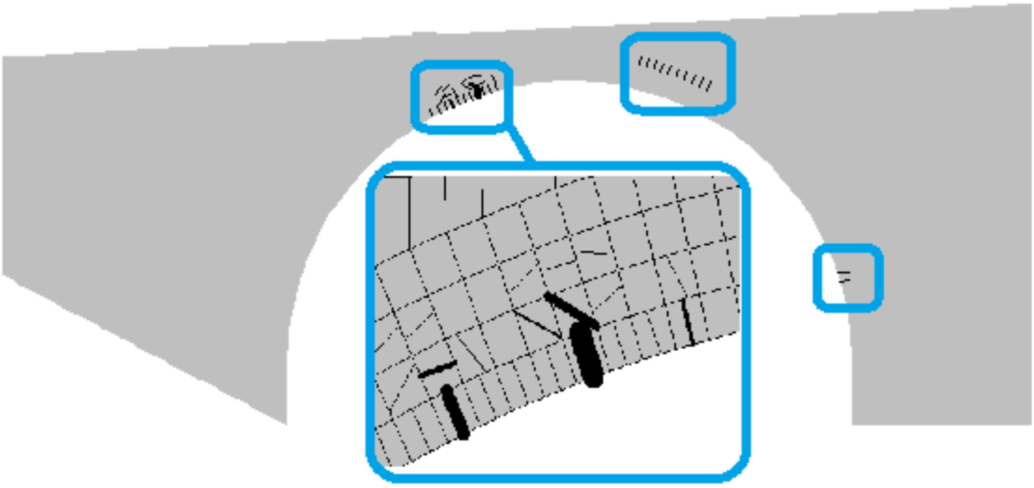

Figure 50: Crack pattern corresponding to the load of 0.440 MN

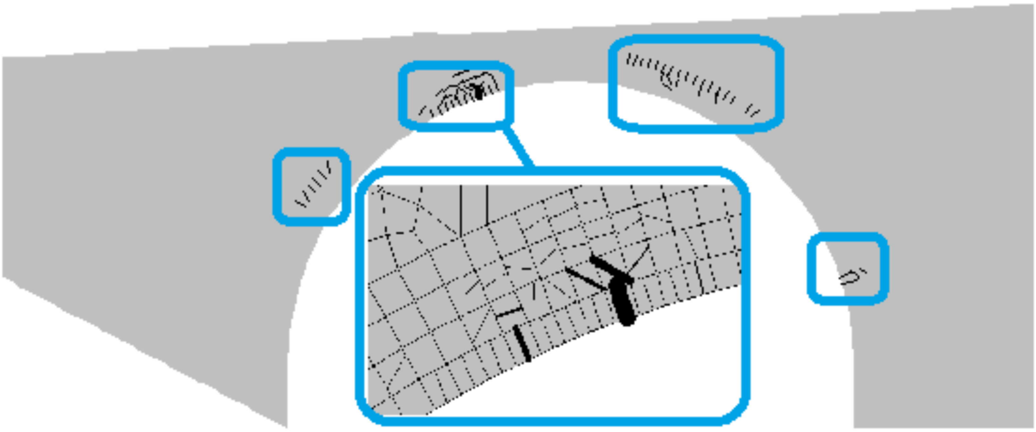

Figure 51: Crack pattern corresponding to the load of 0.657 MN

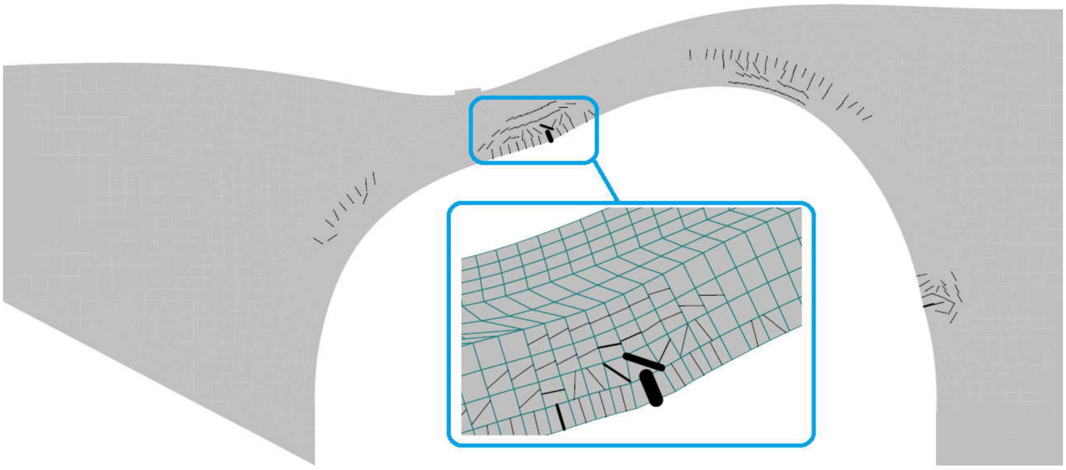

Figure 52: Deformed shape (Scale 1:30) and crack pattern under the load of 0.935 MN

Figure 53 shows load-displacement diagram obtained from monitoring points of Model 1. Monitoring point 2, in which vertical translation was measured, was chosen before the analysis and does not coincide with the point, in which vertical displacement was the highest. Nevertheless, it is possible to observe that live load equivalent to 0.935 MN corresponds to the onset of softening. Accordingly, this value was considered as the peak load or maximum value of vertical axial force, which could be carried by the one meter width of the bridge.

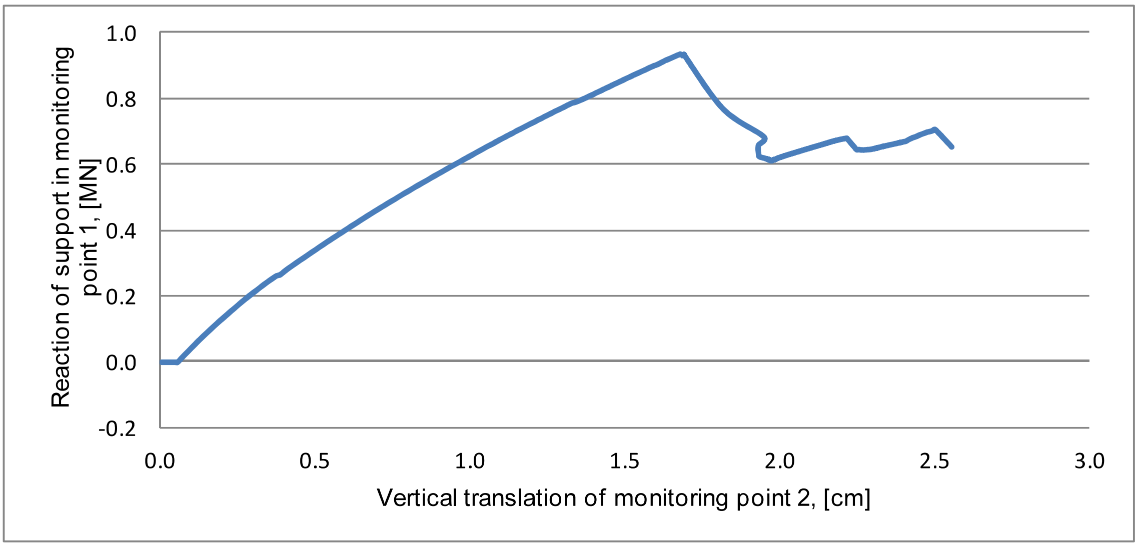

Figure 53: Load-displacement diagram for Model 1

Figure 54 shows distribution of maximum principal stress under the live load equivalent to 0.935 MN. It is important to note, that ATENA software considers tensile stresses and strains as positive values, whereas compressive stresses and strains are shown as negative. The highest stresses were observed in the roadway material due to its elastic nature. They were much higher than stresses within the arch barrel, and observation of latter in a given scale was inconvenient for this reason. Accordingly, in the Figure 54 high stress values are filtered so that only stresses within arch barrel are shown.

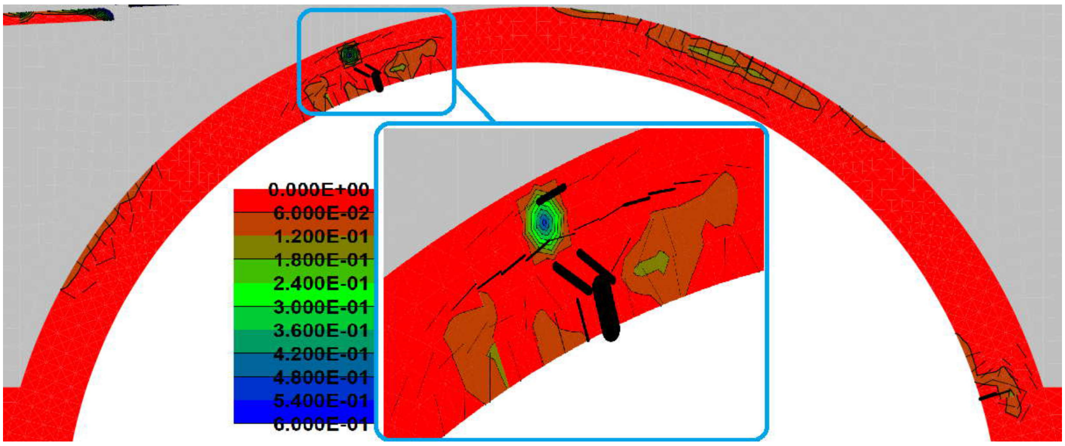

Figure 54: Maximum principal stresses in [MPa] in the arch under the peak load

It can be seen that in the sound parts of the arch, where cracks have not appeared, tensile stresses are low. This means that material is still working in elastic range. In significantly damaged regions of the arch tensile stress are also low. This is due to the softening effect turning tensile stresses into zero, once the crack is fully opened. Region with concentration of high tensile stresses can be observed at the left quarter span of the arch (see Figure 54). This corresponds to the onset of cracking, and fully formed cracks can be seen in the following step (see Figure 55). Tangential crack in the above mentioned region has grown from 0.02 mm to 1 mm within one step. Accordingly, cracks perpendicular to the arch intrados underwent closing from 3.7 mm to 2.9 mm.

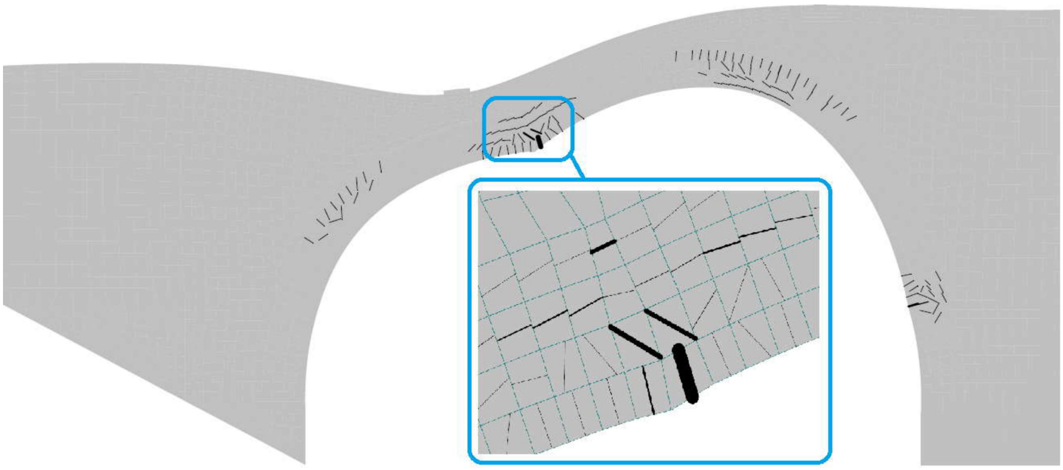

Figure 55: Deformed shape of the model (Scale 1:30) and
crack pattern in the first post-peak step

It is of importance that occurrence and growth of cracks in tangential and diagonal to arch extrados/ intrados direction does not reflect real behavior of masonry. The reason for this kind of damage is adoption of homogenized approach implying material isotropy. Under these conditions, typical for masonry arches cracks along mortar strips cannot be observed. Tensile strength is equally low along all axes, and cracks can form in any direction, perpendicular to which maximum principal stresses reach tensile strength.

Figure 56 and Figure 57 show distribution of normal strains ε_y in the peak and first post-peak steps. ATENA software considers horizontal axis as “x” and vertical axis as “y”, whereas “z” axis is oriented in transverse direction. It can be seen that vertical normal strains increased significantly in the post-peak step. On the basis of that, it is possible to conclude that extensive deformation in the vertical direction caused the drop of the reaction in the point, where prescribed displacement was applied. Failure of the model is associated with local failure of the material in left quarter span of the arch. Maximum vertical displacement measured in this position was equal to 2.18 cm in the peak. In the last converged step this value increased up to 5.57 cm. The width of the major crack, which was equal to 2.96 mm in the peak step, increased in the last converged step up to 8.10 mm. Tangential to arch extrados crack grew from 1 mm to 5.9 mm. Following divergence of the model was probably associated with the high level of damage in single elements, for which equilibrium of internal and external forces could not be reached anymore. Divergence of the model can also be attributed to high plastic strains and distortion of finite elements within infill material. Due to adoption of fracture-based SBETA model, plasticity can only be observed within infill material. Figure 58 shows distribution of maximum principal plastic strains in the last converged step. Extensive deformations can be observed within the plastic band formed in the infill material. The highest plastic deformations took place along infill-arch interface and were mainly caused by rigid connection assigned between these materials.

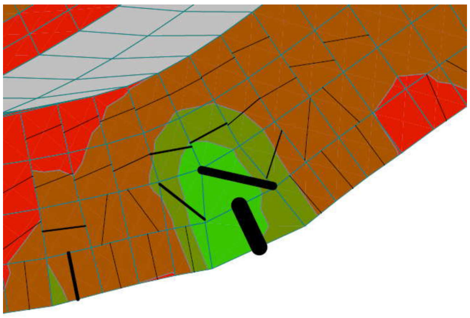

Figure 56: Normal strains ε_y in the peak step

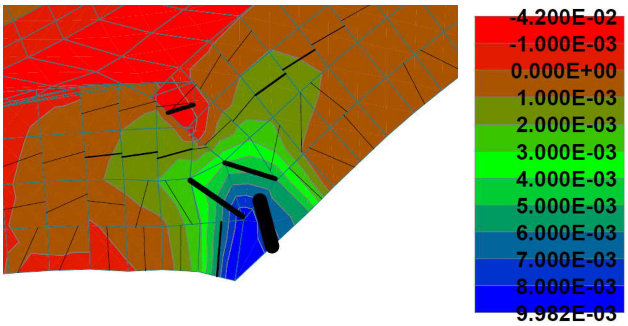

Figure 57: Normal strains ε_y in the first post-peak step

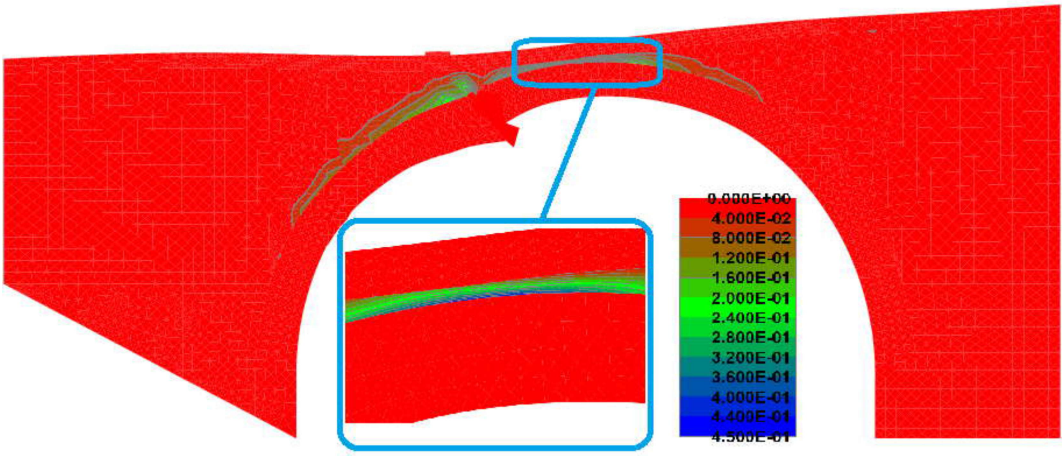

Figure 58: Maximum principal plastic strain in the last converged step

8.2 Model 2: Macro-model with homogenized material within arch barrel modeled in plane strain continuum state

For model with homogenized material within arch barrel analyzed in plane strain continuum state process of crack formation in the beginning of the loading was similar to Model 1 (see section 8.1). First cracks in the arch appeared, when the live load was equivalent to 0.208 MN. Pattern and width of these cracks coincides with the one shown in the Figure 49. Next, cracks appeared at the right side of the arch (see Figure 50) under the live load equivalent to 0.451 MN and at the left side of the arch (see Figure 51), when the live load corresponding to 0.597 MN was applied. At this point, width of a major crack in the left quarter span of the arch (see Figure 51) reached the value of 1.7 mm, and cracks in the remaining structure opened up to 0.3 mm.

Despite similar structural behavior of Model 1 and Model 2 in the beginning of the loading process, peak load for Model 2 was measured to be higher than for Model 1. This is due to plane strain assumption for the arch barrel resulted in the absence of deformations in transverse direction. In this wise, arch barrel turned out to be confined during loading process. This stiffened the structure and delayed its collapse. Figure 59 shows load-displacement diagram obtained for Model 2. Maximum vertical axial load, which could be carried by the bridge, was measured to be equal to 1.66 MN.

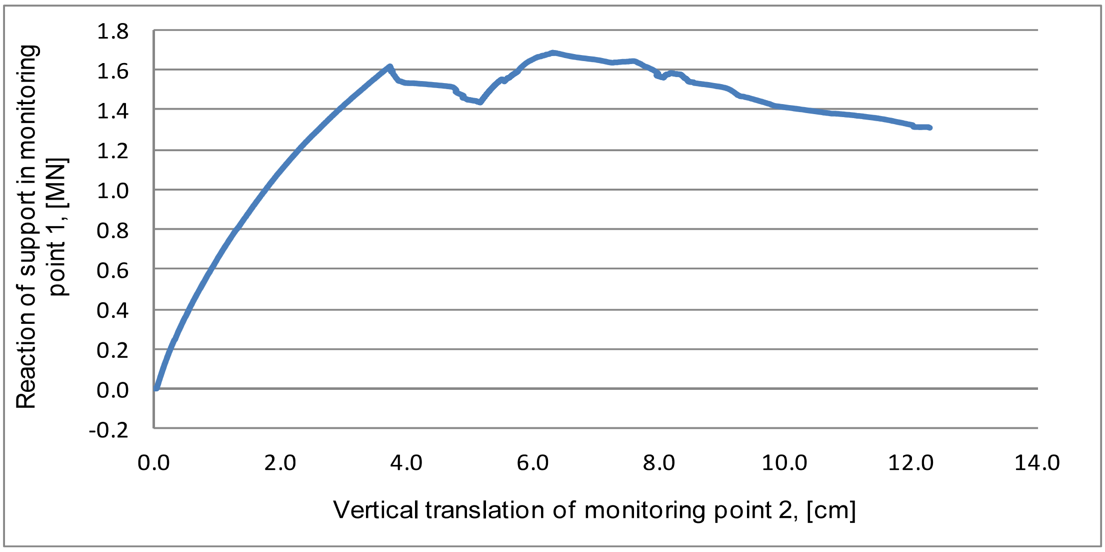

Figure 59: Load-displacement diagram for Model 2

It can be seen that once the peak value of live load was reached, deformations within the structure kept on increasing relatively fast, whereas decrease of live load was very slow. Process of softening was very gradual, and structure accumulated significant amount of damage in the post-peak range. Deformed shape of the bridge as well as distribution of maximum principal strains in the peak and last converged steps is shown in Figure 60 and Figure 61. It can be seen that, similar to Model 1, set of cracks formed in tangential and diagonal to arch extrados directions. As discussed in the previous section, it is not realistic and is caused by isotropic nature of material within the arch barrel.

It can be also noticed that level of damage accumulated by Model 2 in the post-peak is much higher than for Model 1. Maximum vertical displacement, measured at the arch intrados (see Figure 60) increased from 8.50 cm in the peak step till 11.65 cm in the last converged step (see Figure 61). Width of the major crack in this region increased from 1.3 cm to 3.8 cm. After that, model started to diverge, most likely due to high amount of damage and deformations accumulated within single elements.

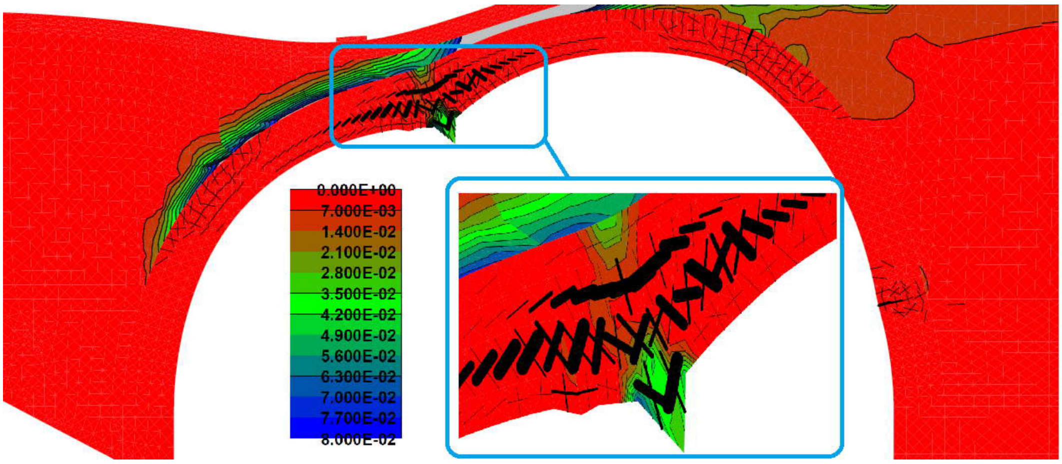

Figure 60: Maximum principal strains in the arch barrel under the peak load
(Deformed shape is shown in the scale of 1:10)

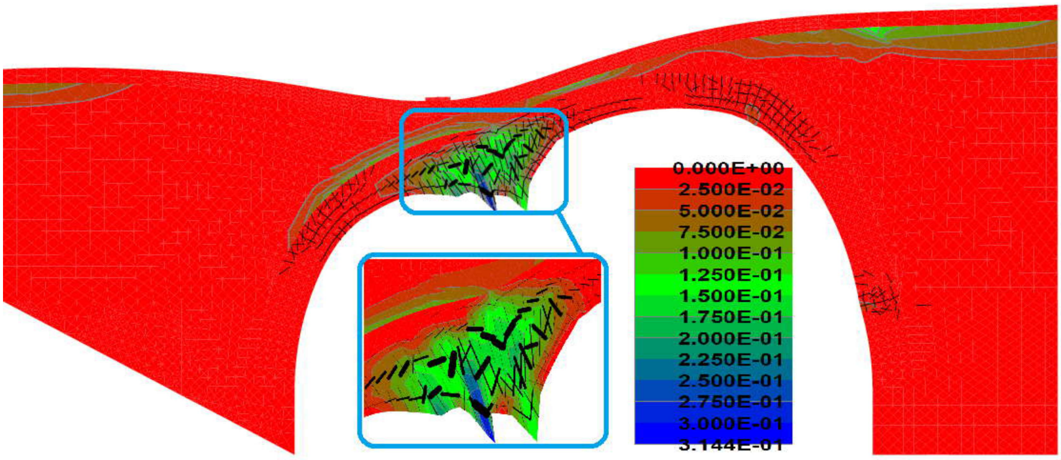

Figure 61: Maximum principal strains in the arch barrel in the last converged step
(Deformed shape is shown in the scale of 1:10)

Figure 62 and Figure 63 show distribution of maximum principal stresses in the peak and last converged step. It can be seen that, due to high level of damage, principal stresses are low in the peak step but decrease even more in the last converged step. Accordingly, it can be concluded that in spite of the fact, that structure did not reach apparent peak (see Figure 59), it undergoes gradual softening, and further increase of bearing strength is impossible.

In this wise, it can be concluded that failure of the model is associated with extensive deformations and collapse of material within the left quarter span of the arch. This can be explicitly seen from Figure 60 and Figure 61: material in this region deforms significantly, whereas maximum principal strains in remaining structure are very low.

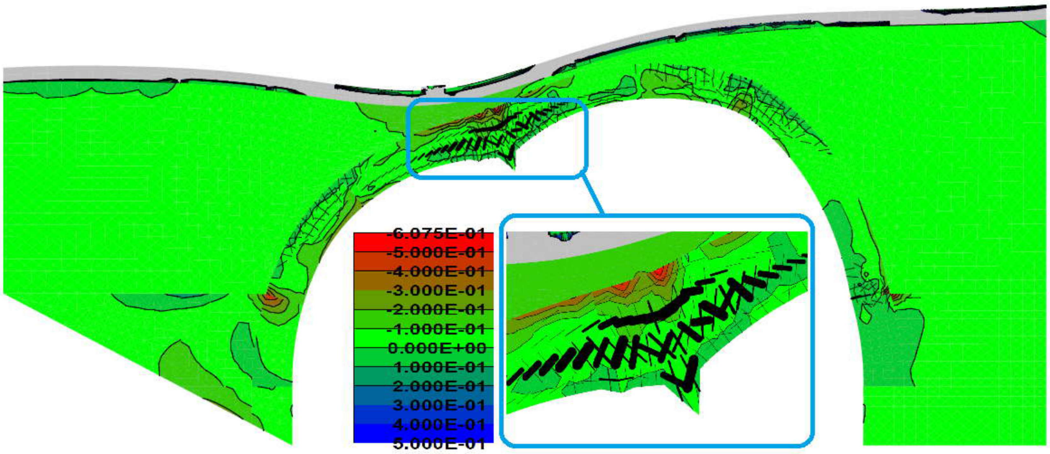

Figure 62: Maximum principal stresses in [MPa] in the arch barrel under the peak load. (Deformed shape is shown in the scale of 1:10)

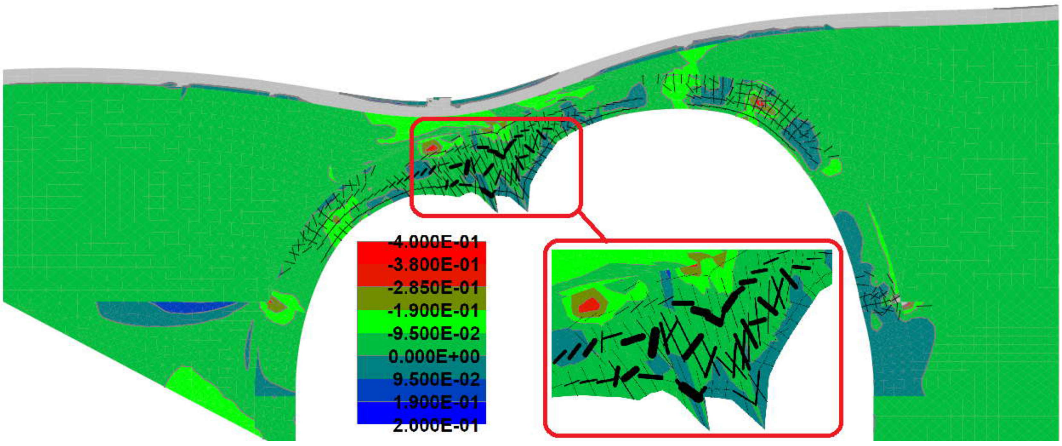

Figure 63: Maximum principal stresses in [MPa] in the arch barrel in the last converged step. (Deformed shape is shown in the scale of 1:10)

8.3 Model 3: Micro-model with stone units and mortar strips within arch barrel modeled in plane stress continuum state

Next model analyzed under the scope of current thesis was micro-model with distinct stone units and mortar strips as also adopted plane stress continuum state for arch barrel. First, structure was loaded with the self-weight. When 80% of the dead load was applied, model started to diverge. Figure 64 shows distribution of normal strains ε_y at this load level. It can be seen from the diagram that mortar strip in the vicinity of right support underwent significant vertical deformations. In other words, it crushed under the self-weight of the structure due to very low strength. This caused divergence of model, and calculations did not proceed further.

Apparently, observed phenomenon is unlikely to happen in reality, due to collaborative work of materials within composite masonry. Indeed, being confined, mortar has higher strength than assigned in the FEA. This was not reflected in the current model, because stone units and mortar strips were modeled separately. To reflect reality, strength of mortar should be increased. Experimental work required for this adjustment could not have been done under the scope of current work due to time constraints. Alternatively, created model was tested in plane strain continuum state, in which sufficient strength of mortar was ensured due to confinement effect.

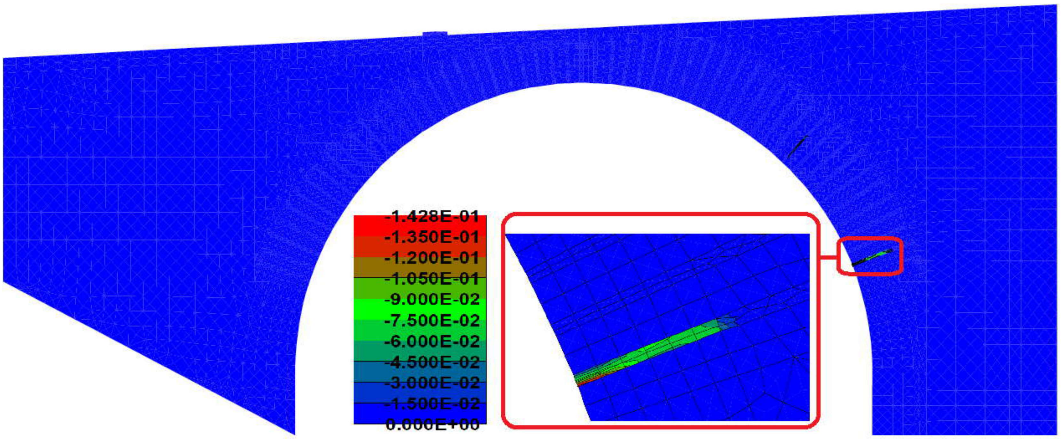

Figure 64: Minimum principal strains in the structure after application of 80% of dead load

8.4 Model 4: Micro-model with stone units and mortar strips within arch barrel, modeled in plane strain continuum state

Deficiency related with extensive deformations of mortar strip was eliminated in the current model. Plane strain assumption for the arch barrel resulted in the absence of transverse deformations and provided confinement effect preventing crushing of mortar in compression. Figure 65 shows load-displacement diagram obtained for Model 4.

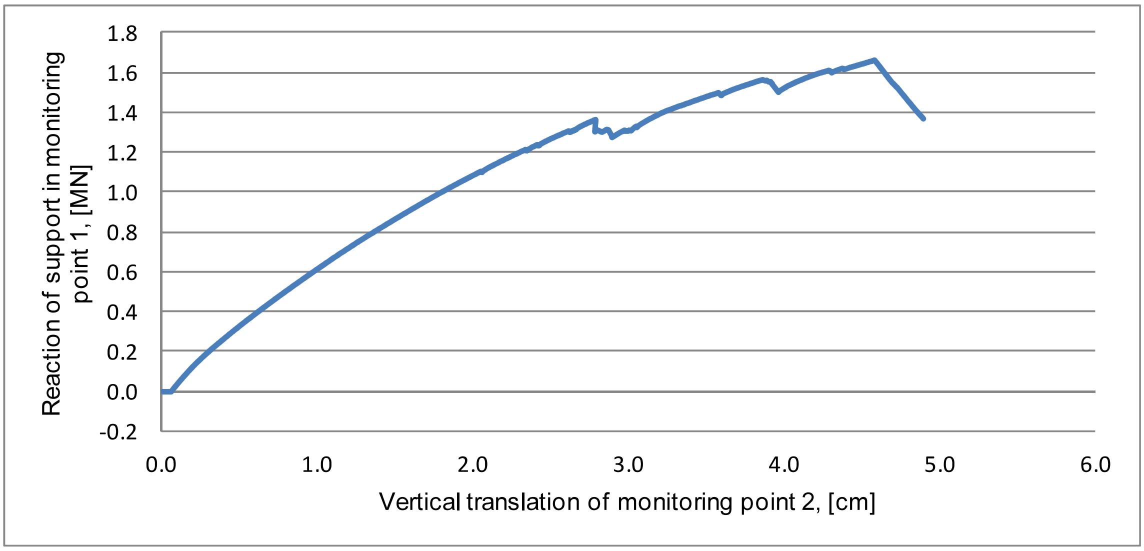

Figure 65: Load-displacement diagram for Model 4

Maximum reaction in the monitoring point 1 measured throughout loading process is equal to 1.69 MN. Nevertheless, several drops of the load can be observed prior to the peak. They are related to development of local damages, which do not imply collapse of an overall structure.

It can be seen that due to the presence of weak mortar strips, structure started behaving in the nonlinear range under relatively low loads. First cracks with a minor thickness appeared at a quarter span of the arch at a load level equivalent to 0.105 MN (see Figure 66). Almost zero tensile strength assigned to mortar material was exceeded in the tangential to arch intrados direction, and cracks formed perpendicularly to arch intrados. Next, at a load level of 0.271 MN set of cracks formed at the right quarter span of the arch and in the vicinity of right support (see Figure 67).

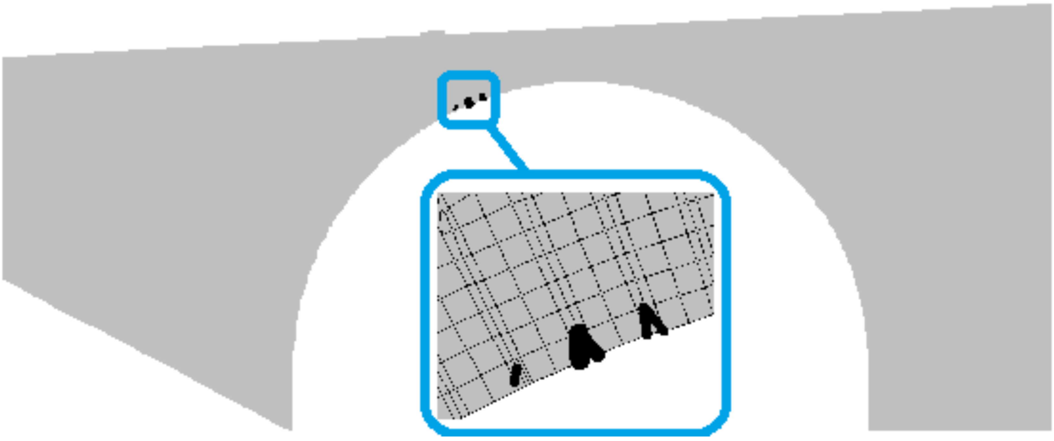

Figure 66: Crack pattern corresponding to the load of 0.105 MN

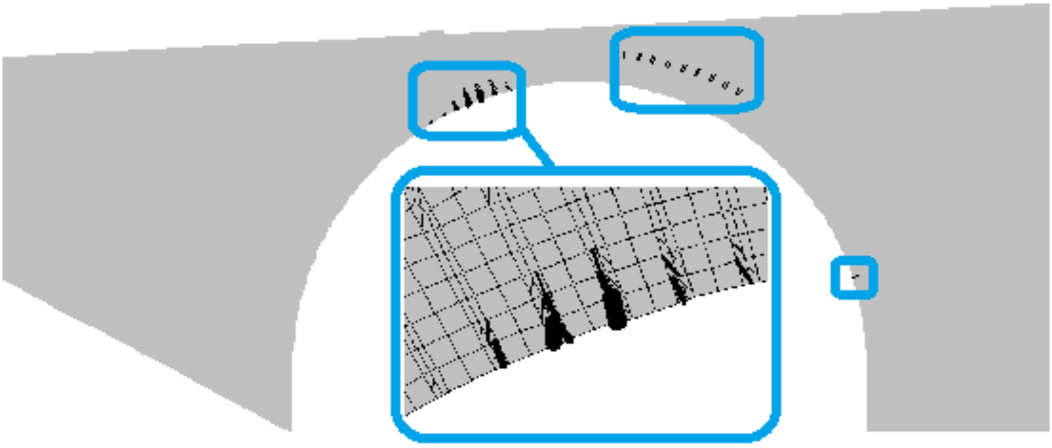

Figure 67: Crack pattern corresponding to the load of 0.271 MN

Finally, when the live load reached the value of 0.417 MN, cracks appeared at the left extrados of the arch (see Figure 68). At this point, cracks appeared only in the weak mortar and had thickness up to 0.2 mm. Direction of major cracks was observed to be perpendicular to the intrados and extrados of the arch.

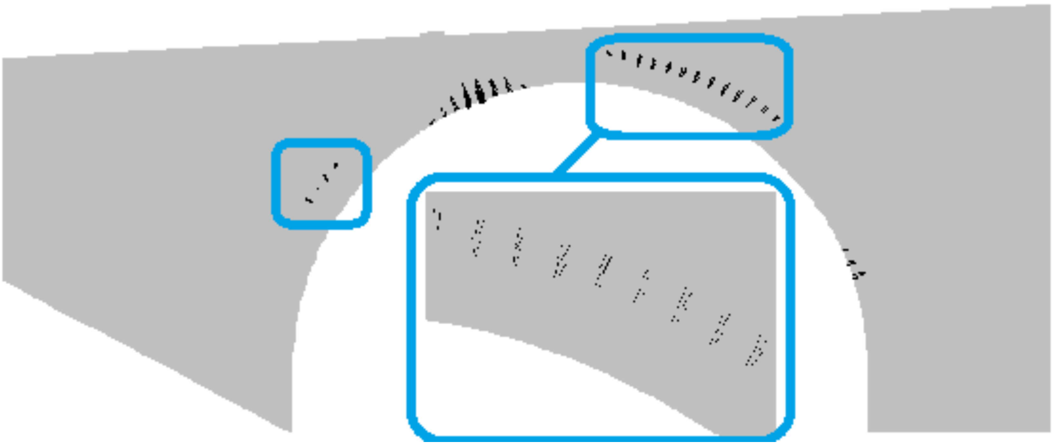

Figure 68: Crack pattern corresponding to the load of 0.417 MN

First drop of the live load, which can be seen from Figure 65, took place at the live load equivalent to 1.36 MN. In the next step this value decreased up to 1.31 MN. This drop was caused by sharp growth of deformations in the left quarter span of the arch. Figure 69 and Figure 70 show distribution of maximum principal strains in this position under the load level of 1.36 MN and 1.31 MN. It can be seen that decrease in the reaction measured in the monitoring point 1 is caused by progressive development of cracks in the above mentioned region. Major cracks in the mortar strip increased from 5.3 mm to 7.8 mm within one step. Also, cracks tangential to arch extrados opened dramatically in stone units till 1.3 mm width. This local phenomenon did not signify an overall failure, and loading was renewed.

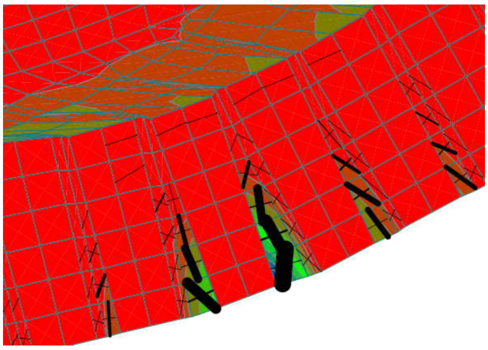

Figure 69: Maximum principal strains in the left quarter span of the arch under the live load of 1.36 MN

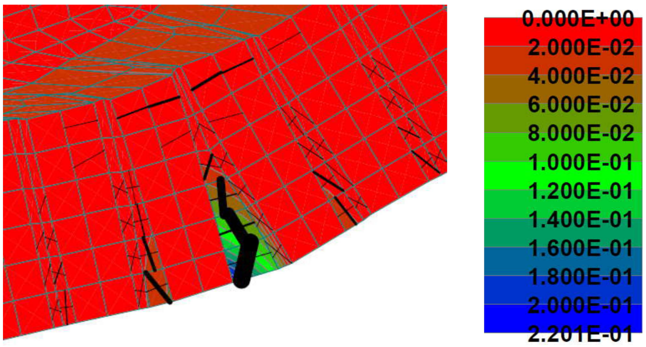

Figure 70: Maximum principal strains in the left quarter span of the arch under the load of 1.31 MN

Next drop of reaction was observed at the level of live load equivalent to1.54 MN. In the next step this value decreased to 1.51 MN. Same as in the previous case, this was related with development of local deformations at the left quarter span of the bridge (see Figure 71). At this point, considerable cracks formed not only in the mortar but also in stone units. Nevertheless, it was not crucial for the stability of the bridge, and further calculations processed.

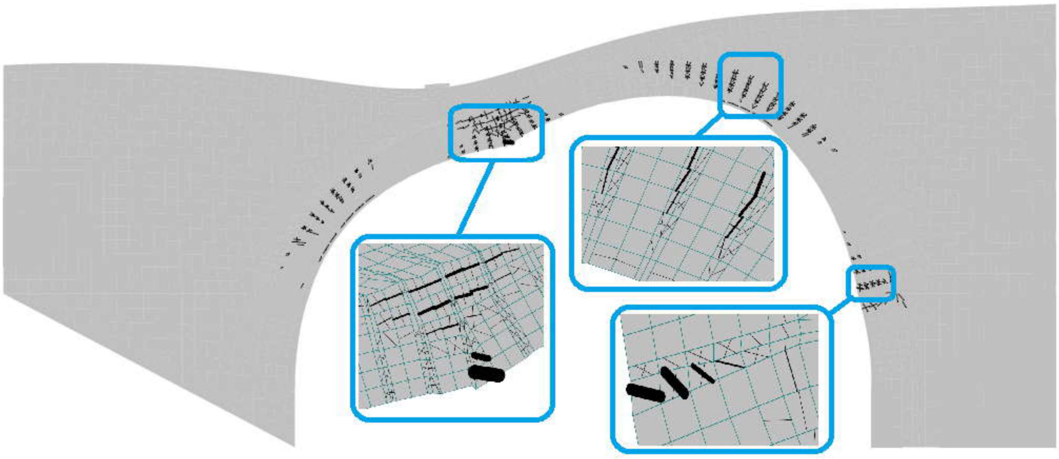

Figure 71: Deformed shape (Scale 1:30) and crack pattern under the load of 1.54 MN

In the peak step live load was equivalent to 1.69 MN. At this step, excessive deformations developed in the vicinity of the left support. Distribution of maximum principal strains for this region in the peak and first post-peak steps is given in the Figure 72 and Figure 73. It can be seen that significant increase of strains is caused by the development of tangential to arch intrados cracks within stone units. This can be explained by low deformability and high stiffness of stone units comparing with mortar joints. Being compressed during loading process, more deformable and less stiff mortar tend to expand across arch barrel. Deformations within adjacent stone units in the same direction are lower, and due to rigid connection assigned between two materials, deformation of mortar is limited by deformation of stone. In this wise, mortar strip turns out to be compressed, whereas stone unit can work in tension and crack, once tensile strength is reached.

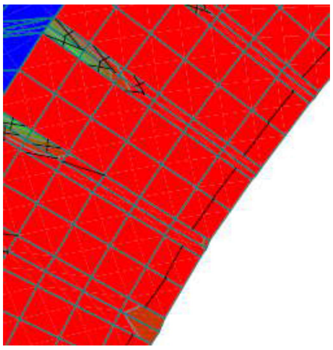

Figure 72: Maximum principal strains in the left support of the arch under the peak live load

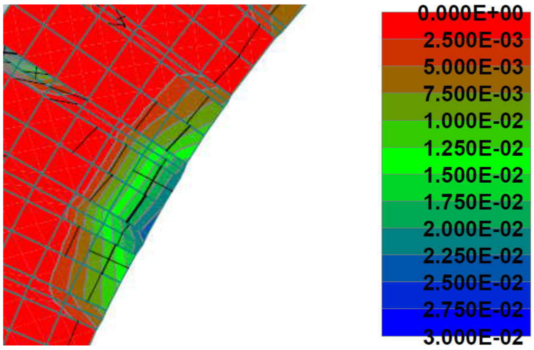

Figure 73: Maximum principal strains in the left support of the arch in the first post-peak step

Deformed shape of the bridge in a scale of 1:10 as well distribution of maximum principal plastic strains in the peak step can be seen in the Figure 74. At this point, width of cracks at the left quarter span of the arch reached the value of 1.86 cm. Maximum vertical displacement of element nodes in this region drew up the value of 6.1 cm. After this step model started diverging. Accordingly, collapse of the model was associated with local failure of the material at the left quarter span of the arch.

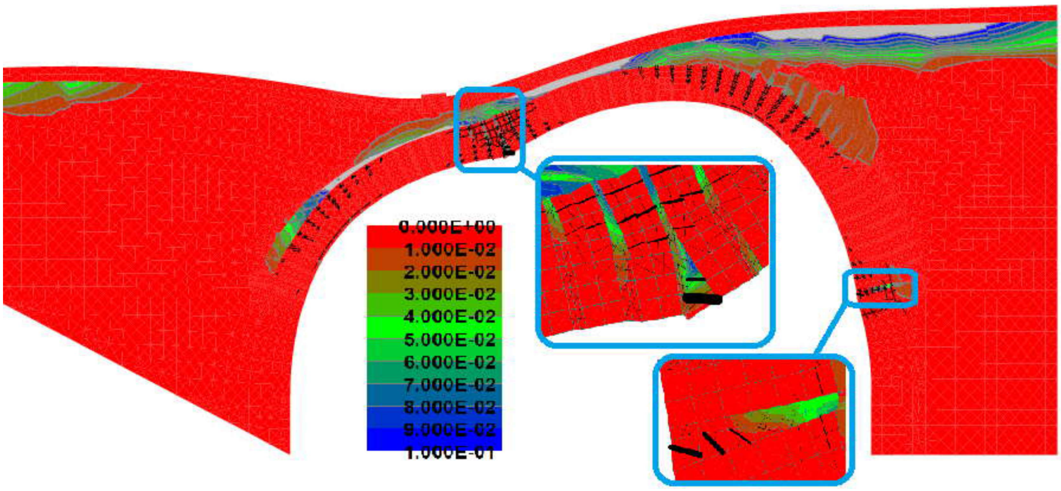

Figure 74: Maximum principal plastic strains under to the load of 1.69 MN

8.5 Model 5 and Model 6: Micro-models with stone units and interfaces

In Model 5 and Model 6 mortar strips were substituted with interfaces representing planes of slipping and cracking. In this wise, typical for composite masonry sliding and cracking of mortar across arch barrel is accounted for. Stone units were created with relatively high strength parameters, and nonlinear behavior occurred mainly within interfaces. Since continuum configuration does not affect interfaces, Model 5 tested in plane stress continuum yielded the same results as Model 6 tested in plane strain continuum. Bearing capacities obtained for these models had variation less than 7% from their average, whereas discrepancy computed for homogenized models drew up the value of 29%. For this reason, only results from Model 6 are presented. Load-displacement diagram for this case is shown in the Figure 75.

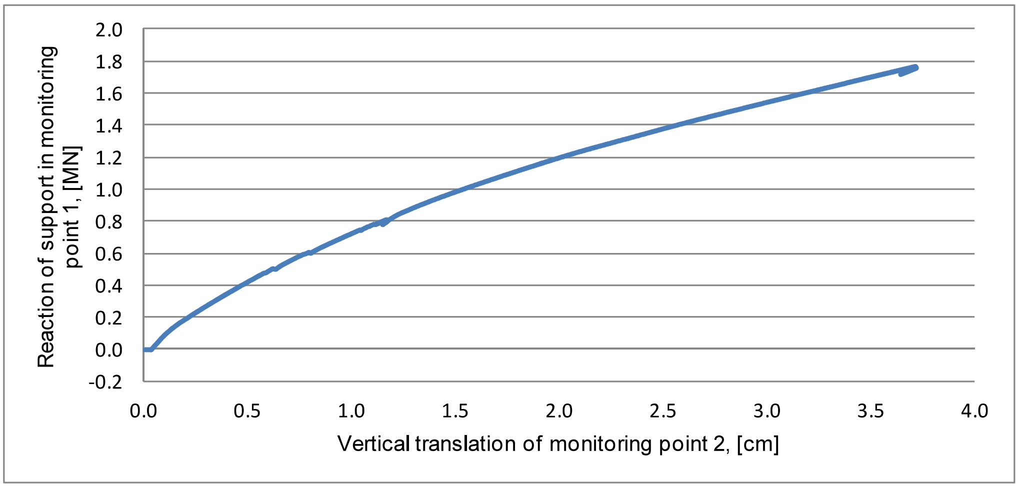

Figure 75: Load-displacement diagram for Model 6

It is important to note that monitoring point 2 does not coincide with the point, where maximum displacement was observed. Nevertheless, from the diagram it is possible to conclude that peak load equivalent to 1.76 MN was reached.

First significant damage observed within the bridge was related to tensile failure of interface at the left quarter span, when the live load was equivalent to 0.211 MN. This corresponds to the formation of hinge or crack going through the entire thickness of adjacent stones (see Figure 76). Colored lines in the magnified part show distribution of normal stresses in the interfaces, and zero values can be observed between split stones. It can be also seen that interfaces in adjacent units partially released of normal stresses. Thus, development of cracks across arch barrel was initiated. Also, set of cracks can be observed in the vicinity of the arch extrados. This phenomenon is not realistic, and can be related to rigid connection assigned between stone units and infill material.

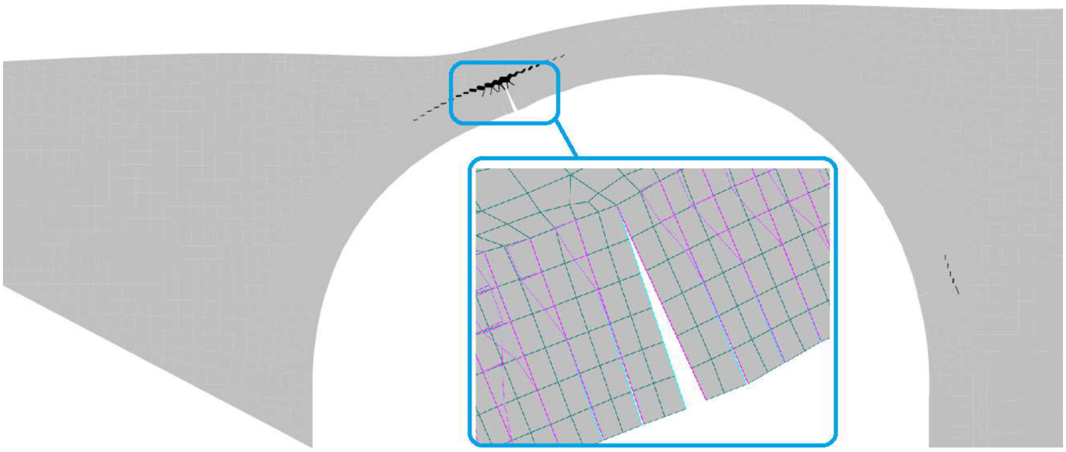

Figure 76: Deformed shape (Scale 1:50) and crack pattern under the load of 0.291 MN

Next hinge appeared at the right support, when live load was equivalent to 0.721 MN. At this step, separation of stones due to failure of interfaces and cracking of units was initiated at the right quarter span of the bridge (see Figure 77).

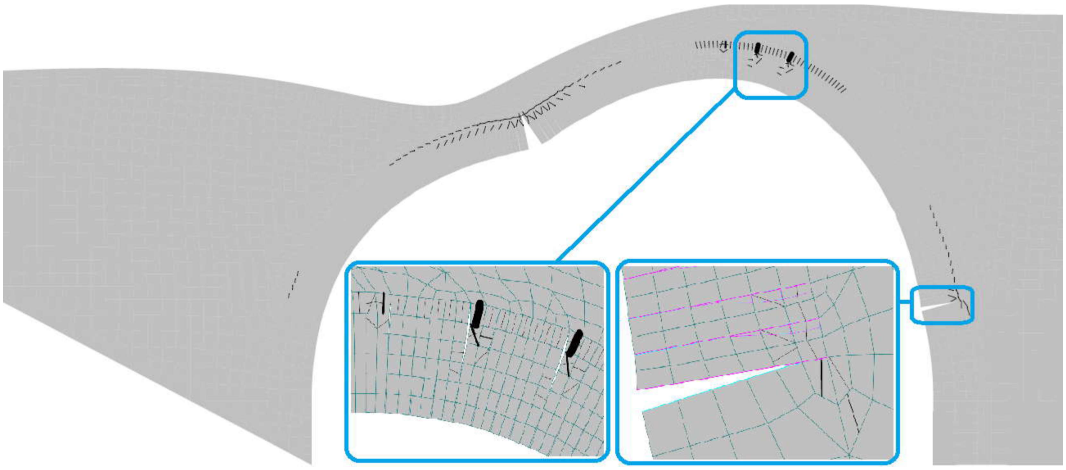

Figure 77: Deformed shape (Scale 1:50) and crack pattern under the load of 0.721 MN

At the load level equivalent to 0.861 extensive growth of cracks at the left quarter span of the arch was initiated (see Figure 78). Width of cracks increased from 0.04 mm till 2.63 mm within one step. This resulted in significant deformations within stone unit.

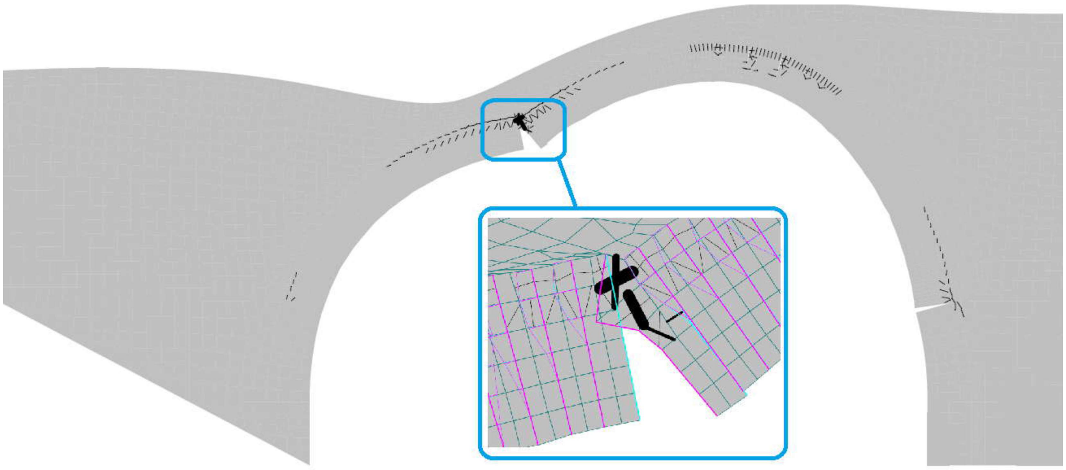

Figure 78: Deformed shape Scale 1:50) and crack pattern under the load of 0.861 MN

Figure 79 and Figure 80 show distribution of maximum principal strains in the step preceding to those, where fast growth of cracks took place, and corresponding to it. Extensive cracking resulted in high deformations within single stone. Nevertheless, in the following steps convergence was stable, and loading processed. Observed local failure did not mean collapse of an overall structure, and peak load was not still reached. When the live load was equivalent to 1.76 MN, model started to diverge. Deformed shape of the structure at this load step is shown in the Figure 81.

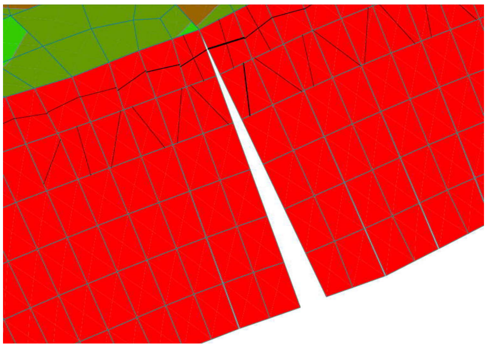

Figure 79: Maximum principal strains in the step before initiation of extensive cracking

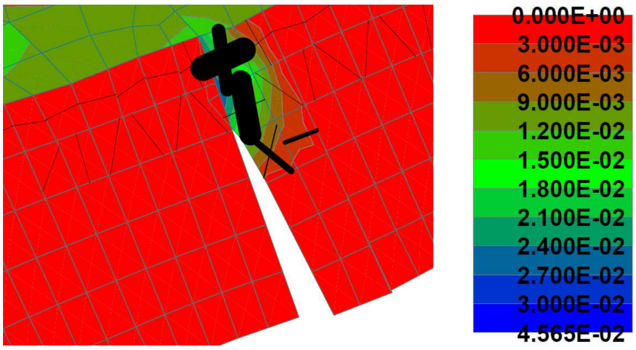

Figure 80: Maximum principal strains in the step corresponding to initiation of extensive cracking

It can be seen that appeared in previous steps cracks interconnected, and, due to failure of interfaces, stone turned out to be isolated from the entire structure. In this wise, local failure of stone unit took place.

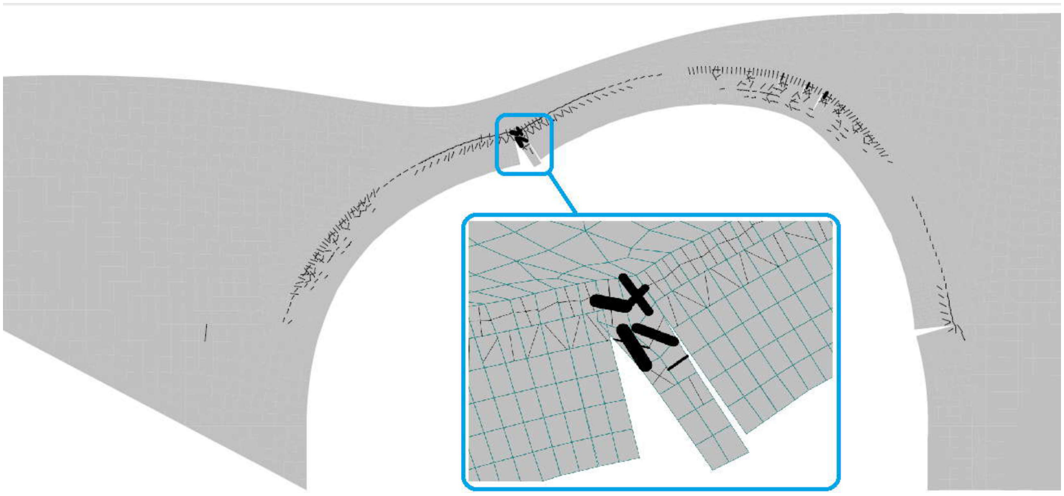

Figure 81: Deformed shape (Scale 1:10) and crack pattern under the load of to 1.67 MN

It is also interesting to note that formation of hinges was initiated in the positions characteristic for four-hinge failure mechanism, namely in the vicinity of right support (see Figure 82), at the right quarter span (see Figure 83) and in the left part of the arch(see Figure 84). Nevertheless, it was not sufficient to turn the structure into the mechanism. This is mainly due to rigid connection assigned between arch barrel and infill materials. Stone units turned out to be connected in the point between arch barrel and infill material, and opening of the hinge was restrained.

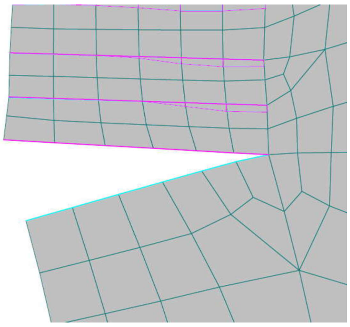

Figure 82: Distribution of normal interface stresses in the right support

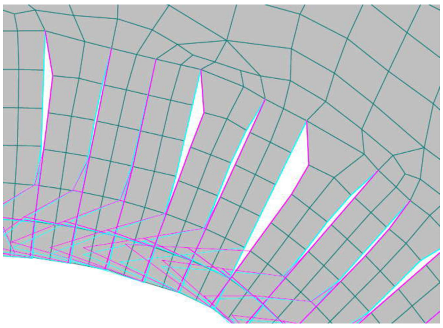

Figure 83: Distribution of normal interface stresses in the right quarter span

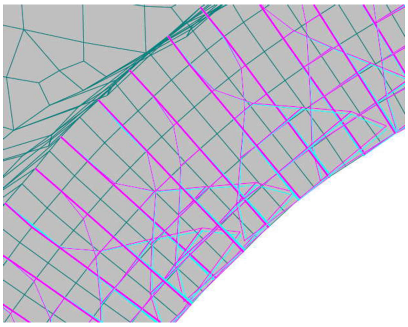

Figure 84: Distribution of normal interface stresses in the left part of the arch

Figure 85 shows distribution of minimum principal stresses under the load equivalent to 1.76 MN. It can be seen that compressive stresses in some portions of the arch reach the value of 21 MPa. On the one hand, it is lower than compressive strength of stone units, which is equal to 50 MPa. On the other hand, in reality arch barrel is consistent of stone units and mortar strips. This composite masonry has much lower compressive strength, and would have crushed in compression under established load level. Accordingly, it is possible to conclude that created model is unable to capture compressive failure. Indeed, arch barrel is consistent of stone units with high compressive strength and interfaces, which can only fail in tension or shear. In this wise, structure is capable to accumulate significant compressive stresses, which does not reflect the reality.

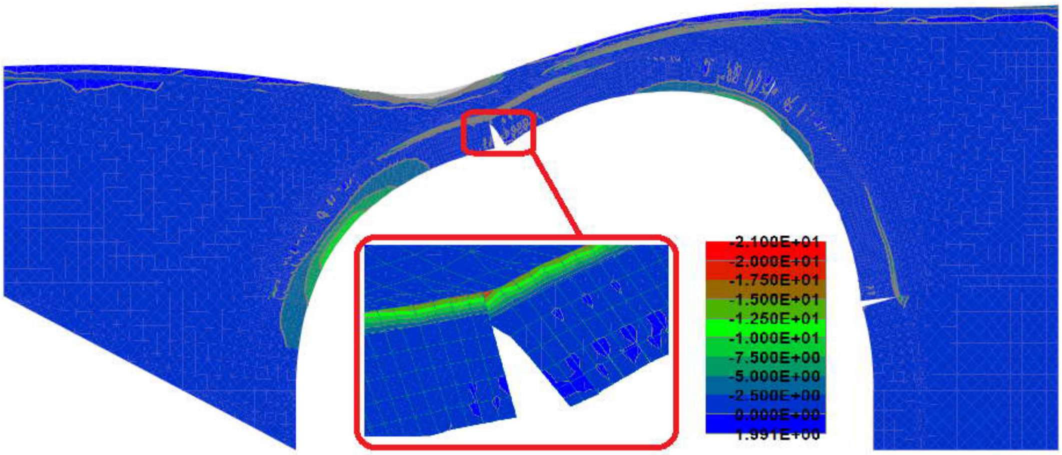

Figure 85: Distribution of minimum principal stresses in [MPa] the arch under the load level of 1.76 MN

Eventually, it can be concluded that created with stone units and interfaces models were insufficient for the goals of current analysis. They could not capture failure of material in compression and provided unrealistic damage pattern.

8.6 Discussion on the results of Finite Element Analysis

Models analyzed under the scope of current work provided with different results in terms of bearing capacity and developed damage patterns of the bridge. Nevertheless, it is possible to conclude that the main reason for models to fail was localized damage in the portion of the arch underlying the position of live load application. For homogenized models this was reflected by extensive deformations and progressive cracking of isotropic material at the left quarter span of the arch, whereas for micro-model with stone units and mortar strips local failure of mortar in the above mentioned region took place. Eventually, micro-models with interfaces failed due to formation of hinge and subsequent cracking of adjacent stone.

Primarily tested macro-models could not provide realistic damage pattern, but, as the least demanding in terms of input data and computational efforts, they can be considered as the most optimal for capacity assessment. It can be also concluded that micro-models with interfaces did not reflect real behavior of the structure. They were unable to capture crushing of masonry in compression and could not provide realistic damage pattern due to rigid connection assigned between stone units and infill material. In this wise, these models cannot be used for the definition of load-bearing capacity and will not be discussed further. As against to micro-models with interfaces, micro-model with stone units and mortar strips was able to capture compressive, tensile and shear failure of mortar, but, due to adoption of rigid connection between materials within arch barrel, observation of cracking and slipping along stone-mortar interfaces was impossible. Creation of interfaces between these materials as also between arch barrel and infill could result in more realistic damage pattern and collapse mechanism, but was not done in the current work due to time constraints. Nevertheless, outcomes of implemented analysis gave adequate results and were sufficient to assess load bearing capacity of the bridge.

Figure 86 shows load-displacement diagrams, obtained for Model 1, Model 2 and Model 4. It can be seen from the diagram that capacity curves coincide in the beginning of loading process, and discrepancy, caused by continuum state and modeling approach (micro or macro), can be explicitly observed only close to the peak.

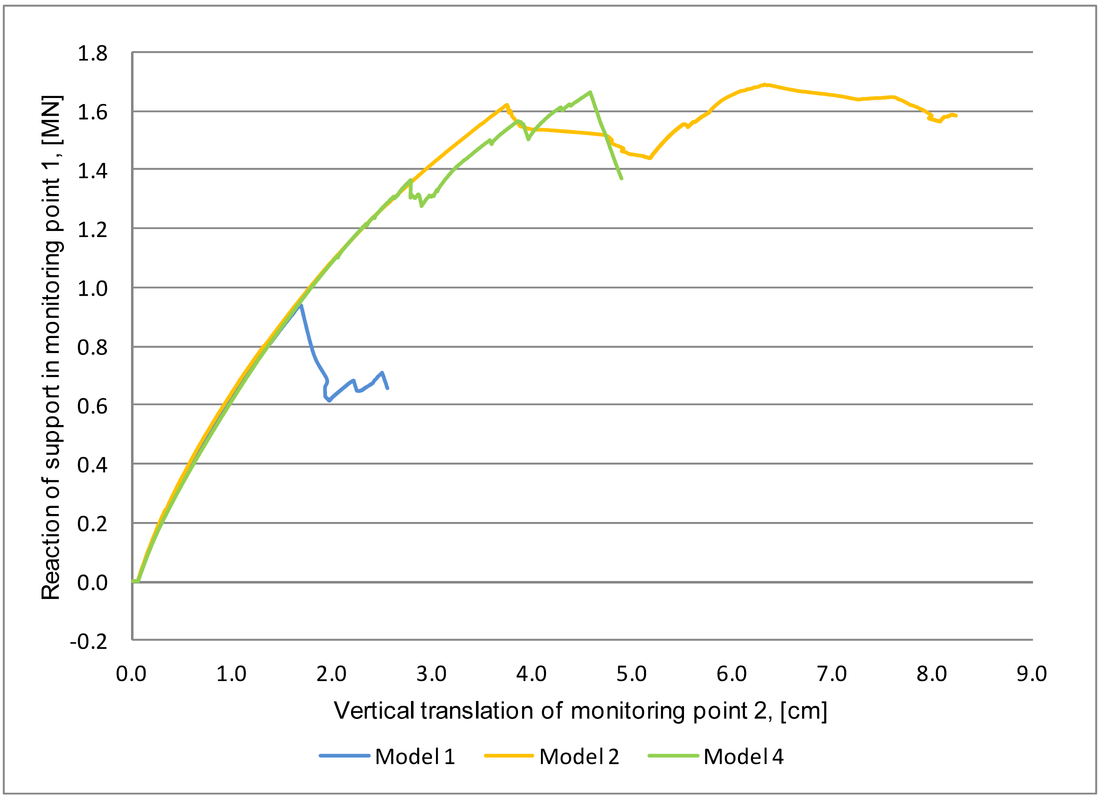

Figure 86: Load-displacement diagrams for Models 1, 2 and 4

Table 15 shows the values of load bearing capacity per meter width of the bridge derived from the discussed models.

Table 15: Maximum axial load obtained from analyzed models

	Model 1	Model 2	Model 4
Maximum axial force per meter width, [MN]	0.935	1.66	1.69

It can be noticed that Model 2 and Model 4 yielded similar values of nominal axial load with variation less than 1% from their average. These models were tested in plane strain state and gave higher results in terms of bearing capacity than model analyzed in plane stress state. Indeed, adoption of plane strain continuum implies that the bridge does not deform in the transverse direction, but it is not actually true for the current structure. On the other hand, structure modeled in plane stress state is considered as planar and thin, which does not reflect the reality as well. In this wise, bearing strength of the bridge should be falling inside values obtained for models tested in plane stress and plane strain continuum states. Nevertheless, to compute load bearing capacity of the Rabstejn bridge, model with homogenized arch barrel tested in plane stress continuum state (Model 1) was used. This model provided the most conservative results and was chosen in order to account for adopted in experimental model simplifications related to geometry and materials.

As consistent with requirements of TP 199 (MD ČR, 2008), normal capacity of the bridge was computed according to formula (12). Ultimate load per meter width F_a defined for Model 1 is equal to 0.935 MN. To account for the entire thickness of the structure this value was multiplied by the width of the roadway equal to 3.8 meters. In this wise, nominal axial load was defined as:

$$F_a = 0.935 \cdot 3.8 = 3.57 \quad [MN] \tag{25}$$

Following the idea of TP 199, permissible service load was defined as the fraction of this value, and reduction factor of 3.4 was applied:

$$F_s = 3.57 / 3.4 = 1.05 \quad [MN] \tag{26}$$

Accordingly, capacity of the bridge under normal service conditions computed using Formula (12) was defined to be equal to 107.7 tons. This is almost 4 times higher than the capacity obtained from direct simplified approach (see Section 5.1) and 3 times higher than outcomes of simplified numerical analysis (see Section 5.2). Permissible capacity defined by engineers from Pudis a.s. is equal to 24 tons (Pudis a.s., 2016), which is 4.5 times lower than the value computed according to results of nonlinear FEA.

Even though the most conservative FE model was chosen for comparison, assigned by Pudis a.s. capacity provided the bridge with great reserve in strength. Deformations, which can take place under corresponding load level, should be negligible for an overall structure. To verify this and characterize damage state of the bridge, when the load corresponding to the capacity defined by Pudis a.s. is applied, numerical nonlinear FEA was implemented.

Point live load corresponding to the capacity of 24 tons was derived from Formula (12) and was expressed as follows:

$$F_a = \frac{V_n[t] \cdot 3 \cdot g \cdot \delta}{4} \quad [kN] \tag{27}$$

From this relation, live load was computed to be equal to 252 kN. This value represents the load per entire thickness of the bridge. For numerical model with one meter thickness, force equivalent to 67 kN was imposed at the left quarter span of the bridge. Model 3 provided the most realistic damage pattern was chosen for the analysis.

It was observed that under the live load equivalent to 67kN bridge does not have any cracks. Figure 87 shows distribution of maximum principal stresses under assigned load. It can be seen that highest values of principal stresses take place in the elastic cover, whereas arch barrel mainly works in compression. It can be also noticed that maximum principal stresses in mortar strips are negative, implying that material works in compression, and development of tensile cracks is impossible.

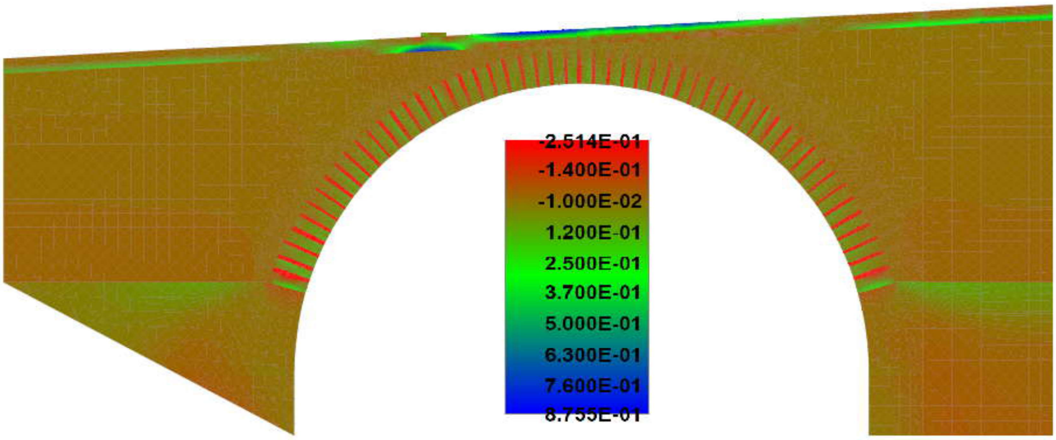

Figure 87: Distribution of maximum principal stresses in [MPa] in Model 3 under the load of 67 kN

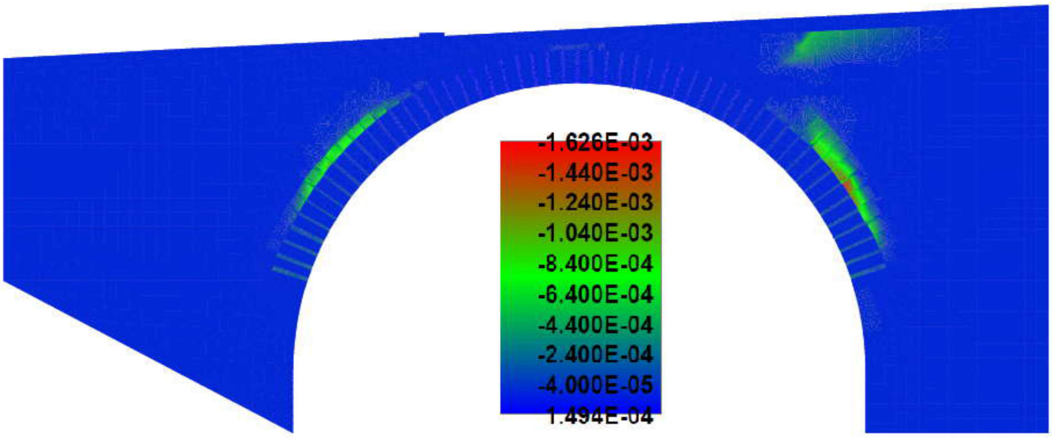

Figure 88: Distribution of plastic strains ε_y in Model 3 under the load of 67 kN

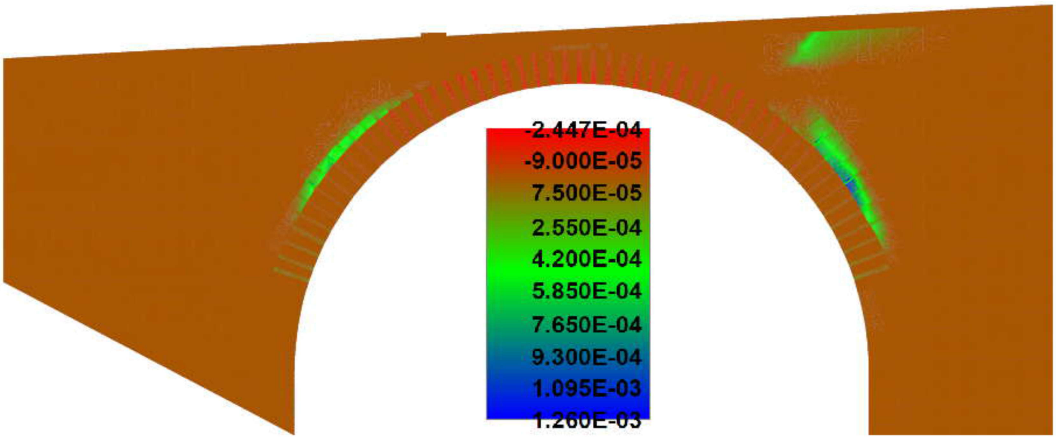

Figure 89: Distribution of plastic strains ε_x in Model 3 under the load of 67 kN

Being compressed under assigned load level, mortar strips accumulated plastic deformations. Figure 88 and Figure 89 show distribution of plastic strains in vertical ε_y and horizontal ε_x directions. It can be seen that mortar strips underwent plastic compressive deformations in vertical direction and expanded across arch barrel in the vicinities of supports. Nevertheless, these deformations are relatively low and do not exceed 0.1%.

Figure 90 shows distribution of vertical displacements within the structure under assigned load level. It can be seen that maximum vertical translation is equal to 6.5 mm. It takes place in the elastic cover and infill material, whereas vertical translation within arch barrel does not exceed 1 mm. Figure 91 shows vertical displacement in the structure after application of the dead load. It can be seen that values from two diagrams vary just by 0.2 mm. On the basis of that, it is possible to conclude that vertical displacements within the model are mostly related to the settlement of the structure under its self-weight, and will not take place in the existing bridge. Accordingly, only minor displacements up to 0.1 mm in the arch barrel and up to 0.2 mm within the entire structure will take place under assigned load level. Analogically, taking into account settlement under the self-weight, horizontal deformations, which can be seen in the Figure 92, do not exceed 0.3 mm, which is low for an overall structure.

Normal and shear stresses within the structure were observed to be relatively low, which can be seen from the Figure 93, Figure 94 and Figure 95.

Eventually, it can be concluded that under assigned by Pudis a. s. operating conditions, bridge does not present any significant damages or deformations. Nevertheless, it is important to note that nonlinear FEA was implemented for the structure, which did not have significant damages. Accordingly, to ensure safety of the bridge, remediation works proposed by Pudis a.s. should be implemented. First of all, repairing of arch barrel with substitution of fallen bricks and repointing of mortar is required. Furthermore, remediation of waterproofing system should be carried out in order to protect bridge components of moisture induced damage. Also, roadway structure should be renovated, in order to ensure sufficient distribution of load transferred from the vehicle to bridge components.

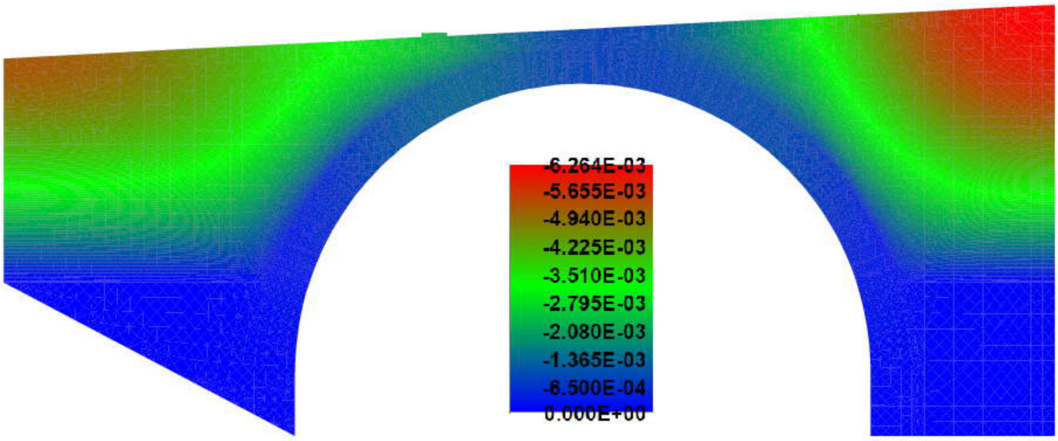

Figure 90: Vertical displacements in [m] in Model 3 under the load of 67 kN

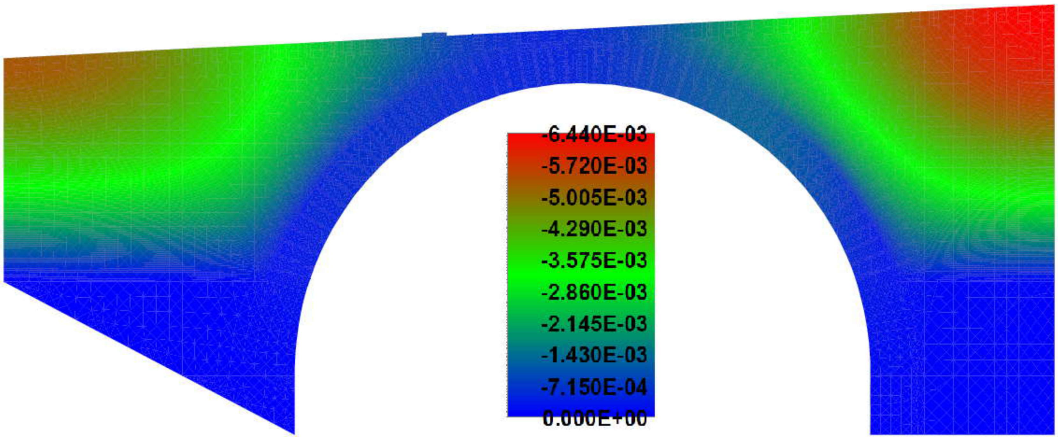

Figure 91: Vertical displacements in [m] in Model 3 after application of the dead load

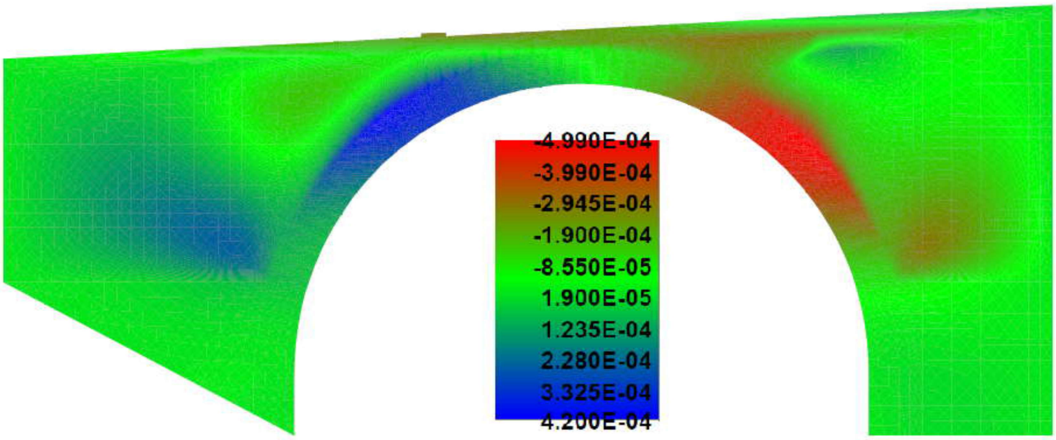

Figure 92: Horizontal displacements in [m] in Model 3 under the load of 67 kN

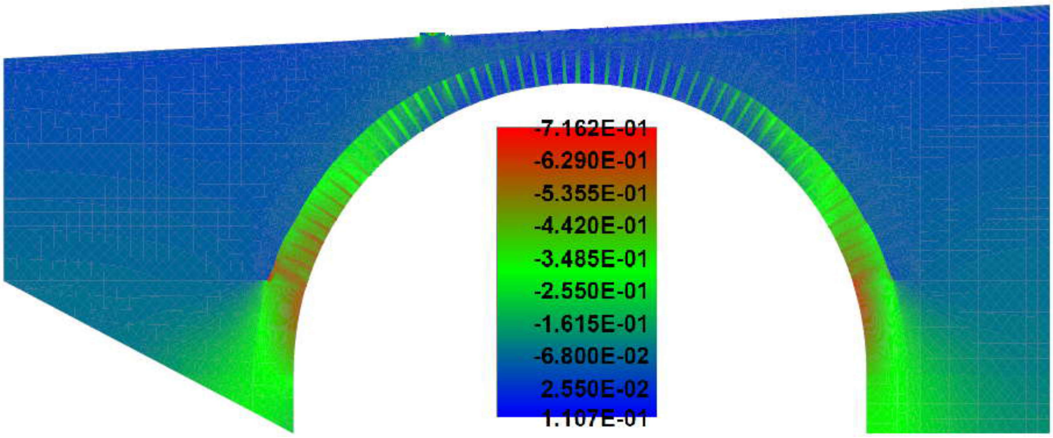

Figure 93: Distribution of normal σy stresses in [MPa] in Model 3 under the load of 67 kN

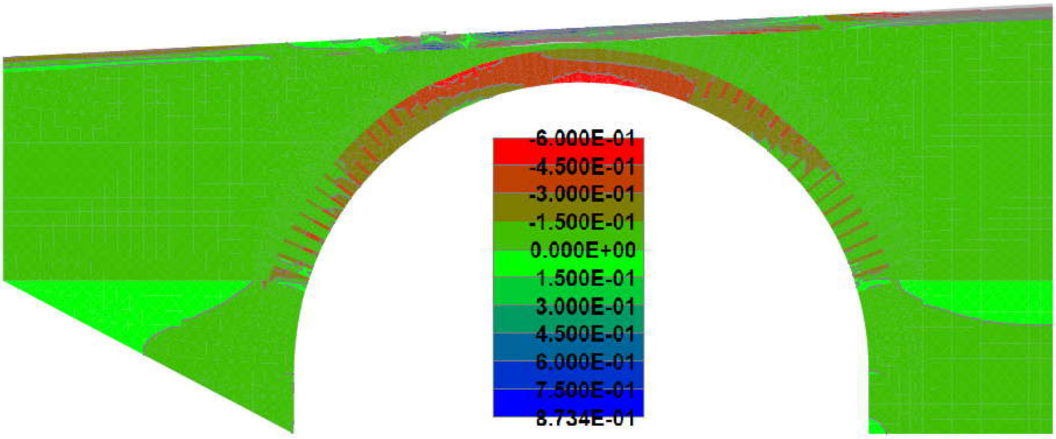

Figure 94: Distribution of normal σx stresses in [MPa] in Model 3 under the load of 67 kN

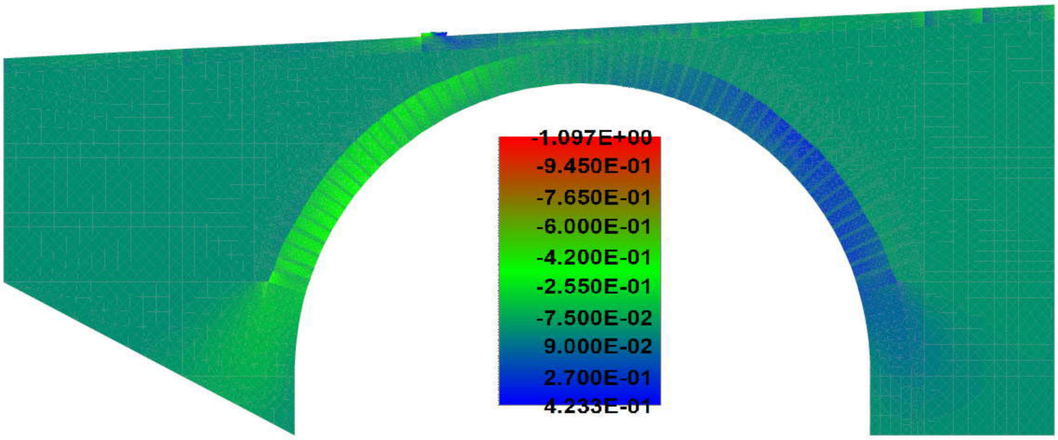

Figure 95: Distribution of shearτ_{xy} stresses in [MPa] in Model 3 under the load of 67 Kn

9. CONCLUSIONS

In the current work historical arch stone bridge situated in Rabstejn, Czech Republic, was analyzed. Numerical evaluation of the bridge, which is originally from 14th century, was required in order to verify its safety under established operating conditions. For this purpose, simplified geometry based techniques as also nonlinear Finite Element Analysis (FEA) were used.

It was demonstrated that simplified methods employ very rough idealizations with respect to geometry of examined structure and do not take into account material properties. Nevertheless, these methods provide conservative results and can be successfully used for evaluation of arch stone bridges, if experimental data is absent, structure does not have significant damages and satisfies specific for each method requirements. Simplified techniques allow for fast and straightforward evaluation of the bridge but are inapplicable in many cases. If the level of accuracy provided with these techniques is not sufficient or extensive data on the structural behavior of the bridge is required, nonlinear FEA is to be implemented. This kind of analysis is also indispensible, if the structure underwent significant deformations and accumulated considerable amount of damage as also if computed from simplified methods capacity is not sufficient for proposed use of the bridge.

Calculations implemented in the current work have shown that, even though geometry of the Rabstejn bridge was not in line with requirements set up by the relevant standard, simplified techniques could be employed, and high level of conservatism was provided. Bearing capacity obtained from direct and simplified numerical methods was equal to 27.7 and 37.8 tons accordingly. This is much lower than bearing strength derived from nonlinear FEA, under the scope of which six models with variable input parameters were tested. Adoption of different models allowed for thorough investigation of the structural behavior of the bridge and gave insight on the advantages and disadvantages of each approach. It was concluded that micro-model with stone units and interfaces could not reflect real behavior of composite masonry and was unable to provide with realistic collapse mechanism due to simplifications employed in the model. The most precise in terms of geometry representation micro-model with stone units and mortar strips could only be tested in plane strain continuum. It accounted for compressive, tensile and shear modes of failure, but observing of sliding and cracking along stone-mortar interface was impossible due to rigid connection assigned between these materials. This model reflected realistic damage pattern but required additional input data and high computational efforts. For these reasons, it can be concluded that the least demanding and the most stable macro-models can be successfully employed when the main goal of the analysis is capacity assessment.

In this wise, for the definition of load-bearing capacity of the Rabstejn bridge, model with homogenized material within arch barrel tested in plane stress state was used. Capacity obtained from this model was the lowest among other finite element models, but, even though, was much higher than values obtained from simplified techniques.

Load bearing capacity of the Rabstejn bridge derived from FEA outcomes was equal to 107.7 tons. This is 4.5 times higher than the value of 24 tons assigned to the bridge by Pudis a.s. engineers. To study structural behavior of the bridge under the live load corresponding to the capacity of 24 tons, numerical model with stone units and mortar strips was analyzed. It was demonstrated that structure did not have any damages and underwent very minor deformations. On the basis of that, it is possible to conclude that Rabstejn bridge has great reserve in strength and can be successfully used under established operating conditions. These outcomes met the purposes of current work, but for more thorough investigation on Rabstejn bridge, additional procedures can be implemented.

Development of models created in the current work was limited due to time constraints and lack of experimental data. Accordingly, for further investigations more advanced models can be recommended. First of all, full micro-model of arch barrel, including stone units, mortar strips and interfaces between these material as also between arch barrel and infill material can be created. Also, three-dimensional analysis including modeling of spandrel walls and parapets can be implemented. This will allow assessing bearing strength of all bridge components and accounting for non-uniform distribution of load along the width of the bridge. These models may require additional laboratory and in-situ tests to investigate geometry and material properties of the structure more thoroughly. Additionally, stochastic analysis accounting for material variation within the structure can be implemented.

10. REFERENCES

1. Angelillo M. Lourenço P. B. , Milani G. Masonry behavior and modeling / CISM International Centre for Mechanical Sciences. - 2014. - pp. 1-26.

2. Barbat A.H. Yepez F., Canas J.A. Damage scenarios simulation for seismic risk assessment in urban zones / Eartquake Spectra, 12(3). - 1996. - pp. 371-394.

3. Bazant Z.P, Oh B.H Crack Band Theory for Fracture of Concrete, Materials and Structures: RILEM, Vol. 16, 155-177., 1983.

4. Bazant Z.P. Oh B.H. Crack Band Theory for Fracture of Concrete / Material and structures, RILEM. - 1983. - pp. 155-177.

5. Bowles J.E. Foundation Analysis and Design : McGraw-Hill, 1996.

6. Cavicchi A., Gambarotta L. Collapse analysis of masonry bridges taking into account arch–fill interaction / Engineering structures, 27: 2005. - pp. 605-615.

7. Červenka J. ATENA Program Documentation. Part 4-1.Tutorial for Program ATENA 2D - Prague : 2016.

8. Červenka V. Červenka J. Atena program documentation. Part 2-1. User's Manual for ATENA 2D [Book]. - Prague : 2016.

9. Červenka V., Jendele L.,Červenka J. ATENA Program Documentation. Part 1. Theory , Prague : 2016.

10. Český normalizační institut ČSN 73 6220: Evidence mostních objektů pozemních komunikací - 1996.

11. Department of Transport The Assessment of Highway Bridges and Structures, Design Manual for Roads and Bridges, Volume 3, Section 4, Part 3. - London : 2001.

12. European committee for standardisation Eurocode 1: Actions on structures - Part 1-1: General actions -Densities, self-weight, imposed loads for buildings - 2002.

13. European committee for standardisation Eurocode 6: Design of masonry structures. - 2005.

14. Gibbons N., Fanning P.J. Progressive cracking and assessed capacities of masonry arch bridges : Department of Engineering, University of Cambridge, 2015.

15. Heyman J. The masonry arch. Chichester : Ellis Harwood, 1982.

16. Hogg V. Effects of repeated loading on masonry arch bridges and implications for the seviceability limit state. The University of Nottingham, School of Civil Engineering, 1997.

17. Hordijk A.D. Local approach to fatigue of concrete. Technische Universiteit of Delft, 1991.

18. Kabele P. Structural Analysis Techniques: Governing Equations of Solid Mechanics. 2011.

19. Kooharian A. Limit analysis of voussoir (segmental) and concrete arches/ American Concrete Institute, 24 (4). 1952. - pp. 317-328.

20. Kupfer, H., Hilsdorf, H.K., Rusch, H. Behavior of Concrete under Biaxial Stress . Journal ACI, Proc. V.66,No.8, Aug., pp.656-666, 1969.

21. Lourenço P.B. Recent advances in masonry modelling: Micromodelling and homogenisation / Multiscale Modeling in Solid Mechanics: Computational Approaches,3. 2009. - pp. 251-293.

22. Lubo M., Tianbin LI , XU Jin,Guoqing C. , Hongming M. , Hongyu Y. Deformation and Failure Mechanism of Phyllite under the Effects of THM Coupling and Unloading / J. Mt. Sci, 9. - 2012. - pp. 788-797.

23. MD ČR TP 199 Zatížitelnost zděných klenbových mostů - 2008.

24. Page J. State-of-the-art review: masonry arch bridges . London : Transport Research Laboratory, Department of Transport, Her Majesty's Stationery Office, 1993.

25. Pippard A.J.S. Ashby R.J. An Experimental Study of the Voussoir Arch / Journal of the Institution of Civil Engineers, 10. - 1993. - pp. 383-405.

26. Pluijm R. Out of plane bending of masonry . 1999.

27. Pudis a.s. Rabštejn nad Střelou Projektová dokumentace pro provádění stavby (PDPS). 2016.

28. Pudis a.s. Restaurátorský průzkum a záměr - Pohledové kamenné prvky historického mostu, Rabštejn n/Střelou. 2015.

29. Pudis a.s. Stavebně-technický průzkum (diagnostika) technického stavu mostu. PROJEKT PRŮZKUMNÝCH PRACÍ. 2014.

30. Pudis a.s. Velká oprava historického mostu ev. č. 206-004, Rabštejn nad Střelou. Stavebně-technický průzkum technického stavu mostu. 2015.

31. Ramamurthy T. Venkatappa Rao G. , Singh J. Engineering behavior of phyllites / Engineering Geology, 33 . - 1993. - pp. 209-225.

32. Rericha P., Posch M. Load rating of masonry arch bridges - semiempirical formulas: Czech Technical University in Prague, Faculty of Civil Engineering, 2012.

33. Roca P. Ancient rules and classical approaches. Part 4: Kynematic approach . 2007.

34. Saeidi O., Geranmayeh Vaneghi R. , Rasouli V. , Gholami R. A modified empirical criterion for strength of transversely anisotropic rocks with metamorphic origin / Bull Eng Geol Environ,72. - 2013. - pp. 257-269.

35. Thomas Telford Ltd. CEB-FIP Model Code 90. 1993.

36. Tomazevic M. Earthquake-resistant design of masonry buildings . London : Imperial College Press, 1999.

ANNEX A. TECHNICAL DRAWINGS ON RABSTEJN BRIDGE PREPARED BY PUDIS A.S.

VYTYČOVACÍ SCHÉMA KONSTRUKCE

M1:100

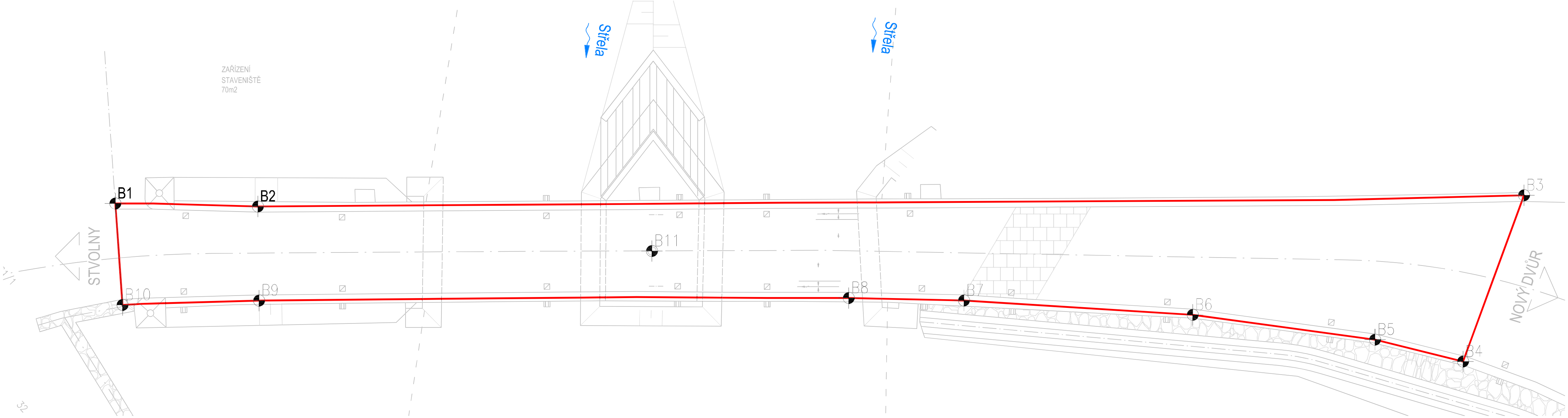

Číslo bodu	Poloha -Y	Poloha -X
B1	-823268,792	-1035950,929
B10	-823265,306	-1035953,778
B11	-823250,982	-1035935,094
B12	-823206,473	-1035908,765
B13	-823203,462	-1035900,973
B2	-823264,370	-1035946,427
B3	-823226,316	-1035905,326
B4	-823222,812	-1035912,332
B5	-823226,183	-1035914,503
B6	-823232,516	-1035919,619
B7	-823239,919	-1035926,550
B8	-823243,493	-1035930,182
B9	-823261,305	-1035949,248

VYTYČOVACÍ SCHÉMA NENAHRAZUJE VYTYČOVACÍ VÝKRES ZHOTOVENÝ AUTORIZOVANÝM GEODETEM

PŘEDMĚTEM VYTYČENÍ JE ŽB DESKA.

Souřadnicový systém JTSK

Výškový systém Bpv

PUDIS
projektová, průzkumná a konzultační společnost
PUDIS a.s., Nad Vodovodem 2/3258, 100 31 Praha 10
tel.: +420 274 776 645, fax: +420 274 778 656, www.pudis.cz, info@pudis.cz

Vypracoval:	Hlavní inženýr projektu:	Investor:
Ing. Dušan Drahoš	Ing. Dušan Drahoš	Správa a údržba silnic Plzeňského kraje, příspěvková organizace Škroupova 18, 306 13 Plzeň IČ: 720 53 119 DIČ: CZ72053119
	Výrobní ředitel: Ing. Jan Vlček	
Odpovědný projektant: Ing. Zdeněk Podráský	Ředitel společnosti: Ing. Martin Höfler	
Číslo zakázky: 1–9948–0001–02	Datum: 03/2016	

Akce:	Měřítko:	Formát:
Velká oprava historického mostu ev.č. 206–004, Rabštejn nad Střelou	1:100	8 x A4
	Stupeň: PDPS	Souprava:
Příloha: VYTYČOVACÍ SCHÉMA KONSTRUKCE	Číslo přílohy: C.2.2	

PODÉLNÝ ŘEZ
M 1:100

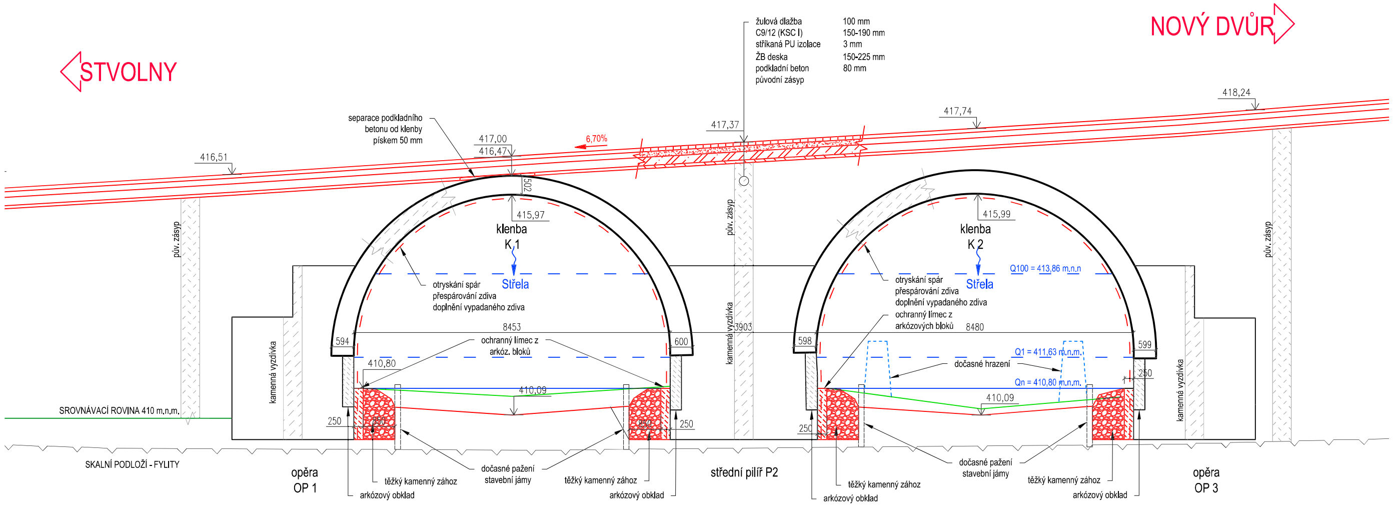

MATERIÁLY

BETON:

C16/20 X0	podkladní beton
C30/37 XC4 XA2	betonové límce
C30/37 XF1	ŽB deska

LEGENDA

▬	hrany konstrukce – klenby	▨	původní zásyp
─	hrany konstrukce – opěry a pilíř	🟥	nový zásyp
─	nové konstrukce	▨	původní kámen – břidlice
- - - -	dočasné hrazení vodoteče	▨	původní kámen – pískovec
– – –	rozsah sanace zdiva		

Souřadnicový systém JTSK
Výškový systém Bpv

PUDIS
projektová, průzkumná a konzultační společnost
PUDIS a.s., Nad Vodovodem 2/3258, 100 31 Praha 10
tel.: +420 274 776 645, fax: +420 274 778 656, www.pudis.cz, info@pudis.cz

Vypracoval: Ing. Dušan Drahoš	Hlavní inženýr projektu: Ing. Dušan Drahoš	Investor: Správa a údržba silnic Plzeňského kraje, příspěvková organizace Škroupova 18, 306 13 Plzeň IČ: 720 53 119 DIČ: CZ72053119
	Výrobní ředitel: Ing. Jan Vlček	
Odpovědný projektant: Ing. Zdeněk Podrásky, CSc.	Ředitel společnosti: Ing. Martin Höfler	
Číslo zakázky: 1–9948–0001–02	Datum: 03/2016	

Akce: Velká oprava historického mostu ev.č. 206–004, Rabštejn nad Střelou	Měřítko: 1:100	Formát: 3 x A4
	Stupeň: PDPS	Souprava:
Příloha: PODÉLNÝ ŘEZ	Číslo přílohy: C.2.6	

VZOROVÉ PŘÍČNÉ ŘEZY - SOUČASNÝ STAV - BOURANÉ KONSTRUKCE

PŘÍČNÝ ŘEZ KLENBOU K2

M 1:50

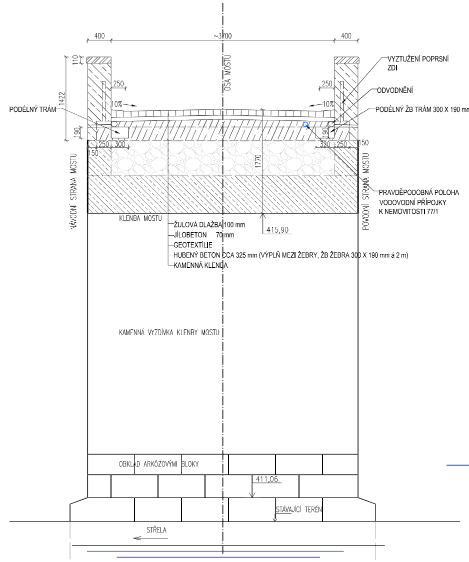

ŘEZ PILÍŘEM P2

M 1:50

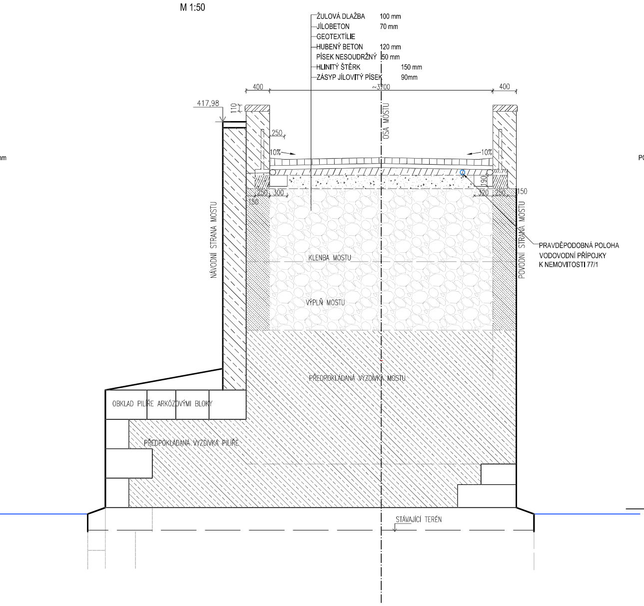

ŘEZ KLENBOU K1

M 1:50

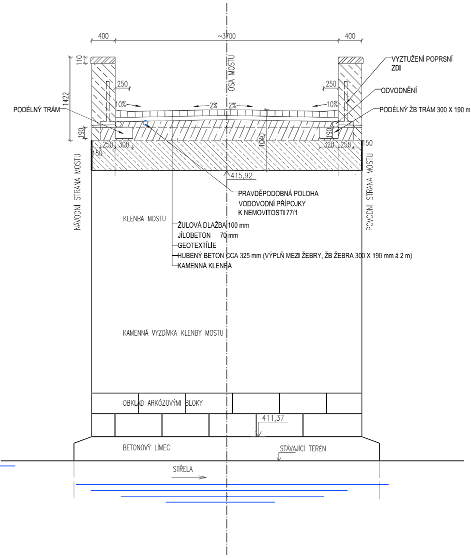

VYZNAČENÍ ŘEZŮ

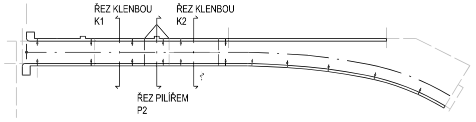

LEGENDA:

- BOURANÉ KONSTRUKCE
- NOVÉ KONSTRUKCE

POZNÁMKY

- NOVÉ POPRSNÍ ZDI VYZDÍT STEJNOU TECHNOLOGIÍ JAKO BYLA POUŽITA PŮVODNĚ TAK, ABY NEBYL PATRNÝ PŘECHOD NOVÉHO A PŮVODNÍHO ZDIVA

VZOROVÉ PŘÍČNÉ ŘEZY - NAVRHOVANÝ STAV

PŘÍČNÝ ŘEZ KLENBOU K2

M 1:50

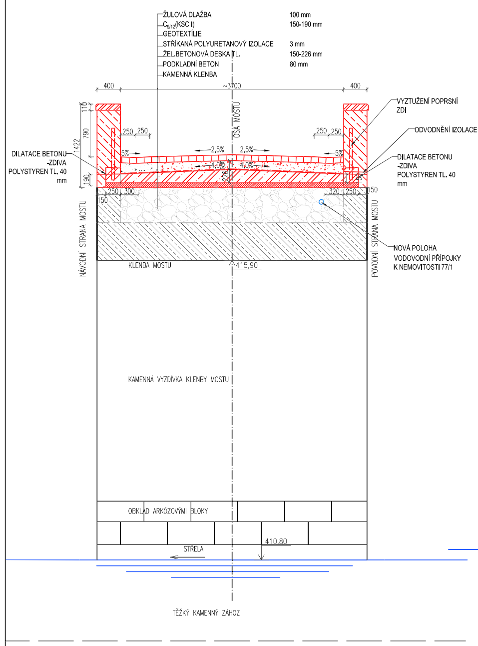

ŘEZ PILÍŘEM P2

M 1:50

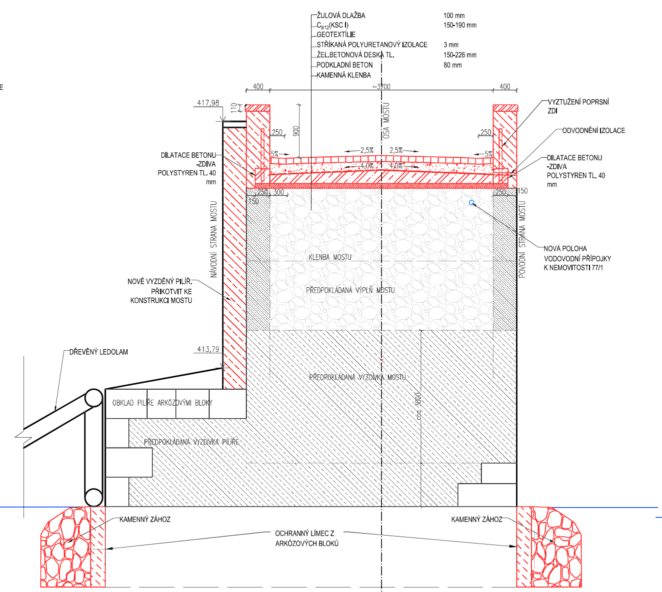

ŘEZ KLENBOU K1

M 1:50

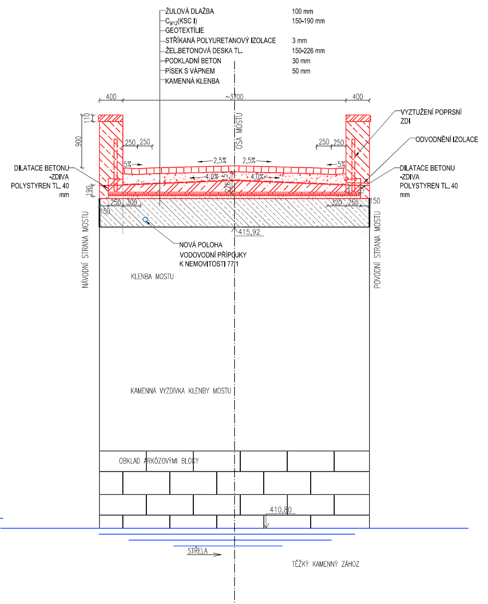

Souřadnicový systém JTSK

Výškový systém Bpv

PUDIS

projektová, průzkumná a konzultační společnost

PUDIS a.s., Nad Vodovodem 2/3258, 100 31 Praha 10
tel.: +420 274 776 645, fax: +420 274 778 656, www.pudis.cz, info@pudis.cz

Vypracoval: Ing. Dušan Drahoš	Hlavní inženýr projektu: Ing. Dušan Drahoš Výrobní ředitel: Ing. Jan Vlček	Investor: Správa a údržba silnic Plzeňského kraje, příspěvková organizace Škroupova 18, 306 13 Plzeň IČ: 720 53 119 DIČ: CZ72053119
Odpovědný projektant: Ing. Zdeněk Podráský, CSc.	Ředitel společnosti: Ing. Martin Höfler	
Číslo zakázky: 1-9948-0001-02	Datum: 03/2016	

Akce: Velká oprava historického mostu ev.č. 206-004, Rabštejn nad Střelou	Měřítko: 1:50	Formát: 8 x A4
	Stupeň: PDPS	Souprava:
Příloha: VZOROVÉ PŘÍČNÉ ŘEZY	Číslo přílohy: C.2.5	